Void Evolution during Processing of Out-of-Autoclave Prepreg Laminates

by

Leyla Farhang

B.Sc., Sharif University of Technology, 2004

M.Sc., Sharif University of Technology, 2006

A THESIS SUBMITTED IN PARTIAL FULFILLMENT OF

THE REQUIREMENTS FOR THE DEGREE OF

DOCTOR OF PHILOSOPHY

in

THE FACULTY OF GRADUATE AND POSTDOCTORAL STUDIES

(Materials Engineering)

THE UNIVERSITY OF BRITISH COLUMBIA

(Vancouver)

October 2014

© Leyla Farhang, 2014

Abstract

Out-of-Autoclave (OOA) prepreg processing is a promising candidate for replacement of autoclave (AC) processing, which is the current standard for manufacturing primary structural parts in the aerospace industry. However, its success is dependent on the ability to produce high quality parts with low porosity. This thesis develops an understanding of porosity in this process by studying the evolution of the voids during processing.

Characterization of voids in partially cured laminates is challenging due to the soft nature of the prepreg matrix. A method for preparation of partially cured samples for optical microscopy and porosity measurement is developed and validated by comparison with results from the ASTM standard density method. It is also shown that thickness can be used to estimate porosity for the no-bleed prepreg system used in this study but that the accuracy is lower than microscopy and density methods.

The evolution of voids during different processing cycles and process conditions was studied using the aforementioned optical microscopy on partially cured laminates made of MTM 45-1/5HS carbon/epoxy prepreg. Fiber tow geometry and gas permeability were also measured to determine fibre tow compaction and the gas transport capability throughout the cure process. It is shown that gas transport, fiber bed compaction and resin infiltration govern void evolution during the process.

Porosity is governed by multiple chemical and transport phenomena, among which gas transport through vacuum evacuation plays a crucial role. An understanding of gas transport in OOA prepreg processing is developed by examining the time scales for gas transport by Darcy flow and molecular diffusion and comparing those to experimental gas permeability and porosity data. Darcy flow is shown to be the primary means of gas removal during the process. The study shows that the dominant direction of gas transport is dependent on the aspect ratio of the laminate, the prepreg material and the processing history as both in-plane and through-thickness permeability vary throughout the cure cycle. Based on these observations, a simple debulk map that gives the minimum recommended room temperature debulk time for OOA laminates as a function of in-plane and through-thickness dimensions is presented.

Preface

This thesis presents research conducted by Leyla Farhang. The research was supervised by Dr. Göran Fernlund at The University of British Columbia.

The majority of the work presented in this thesis is conducted by the author and was supervised by Dr. Göran Fernlund. Gabriel Fortin, a co-op student, assisted with permeability measurement (Appendix B.1) and resin infiltration test (section 6.3.3) under the candidate's supervision. Jeremy Wells, a co-op student, assisted with a few TGA measurements under the candidate's supervision.

A manuscript based on Appendix B has been published. [Leyla Farhang] and G. Fernlund, (2014) *Gas Permeability Measurements: Effect of Measurement Technique*, 10th Canada-Japan Workshop on Composites, Vancouver, Canada. The candidate conducted all of the testing and wrote the manuscript.

A manuscript based on sections of Chapter 5 has been published. [Leyla Farhang], E. Quinlan, G. Fernlund & et al., (2014) *Evaluation of Laminate Quality for Out of Autoclave Manufacturing for a Complex Shaped Crew Door*, AHS 70th Annual Forum and Technology Display, Montreal, Canada. The candidate helped with fabrication of the helicopter crew door and writing of the manuscript.

Portions of chapter 4, 5 and Appendix B have been published. [Leyla Farhang], G. Fernlund, (2011) *Void Morphology, Void Evolution and Gas Transport in Out-of-Autoclave Prepregs*, 2nd Joint ASC-CANCOM Conference, Montreal, Canada and [Leyla Farhang], G. Fernlund, (2011) *Void Evolution and Gas Transport during Cure in Out-of-Autoclave Prepreg Laminates*, International SAMPE Symposium, Long Beach, CA. The candidate conducted most of the testing and wrote all of the manuscript. The section on "Permeability Measurement" was partly performed by Gabriel Fortin, a co-op student under the candidate's supervision.

Other portions of chapter 4, 5 and Appendix B have been published. [Leyla Farhang], J. Kay, K. Hsiao, G. Fernlund, (2011) *Effect of Process Conditions on Porosity in Out-of-Autoclave Prepreg Laminates*, 18th International Conference on Composite Materials, Jeju Island, Korea. The candidate wrote the manuscript jointly with Dr. Göran Fernlund. Half of the presented results (porosity and permeability evolution) was based on the tests performed by the candidate. The section on "Permeability Measurement" was partly performed by Gabriel Fortin, a co-op student under the candidate's supervision. The other half of the results (effect of moisture and vacuum level on porosity) was provided by James Kay, a PhD student.

A manuscript based on a version of chapter 5 is submitted for publication. All the work in this manuscript is performed by the author of this thesis and supervised by Dr. Göran Fernlund.

Two manuscripts based on chapters 4 and 7 are submitted for publication. All the work in this manuscript is performed by the author of this thesis and supervised by Dr. Göran Fernlund.

Table of Contents

Abstract ..... **ii**

Preface ..... **iv**

Table of Contents ..... **vi**

List of Tables ..... **xii**

List of Figures ..... **xiv**

Glossary ..... **xxii**

Acknowledgements ..... **xxiv**

Dedication ..... **xxvi**

Chapter 1: Introduction **1**

1.1 Porosity in Out of Autoclave Processing of Prepregs 2

Chapter 2: Literature Review **4**

2.1 Out of Autoclave Processing of Prepregs 4

2.1.1 Prepreg 4

2.1.2 Prepreg Processing 5

2.1.2.1 Out-of Autoclave versus Autoclave Processing 9

2.2 Porosity in Out of Autoclave Processing of Prepregs 11

2.2.1 Porosity 11

2.2.2 Gas Transport in Out of Autoclave Processing of the Prepregs 14

2.2.2.1 Diffusion 14

2.2.2.2 Advection 15

2.2.2.2.1 Permeability 17

2.2.3 Void Characterization 18

Chapter 3: Thesis Objectives 22

3.1.1 Objectives 23

Chapter 4: Void and Porosity Characterization of Uncured and Partially-cured Prepregs 26

4.1 Introduction 26

4.2 Methods 27

4.2.1 Materials 27

4.2.2 Sample Preparation 28

4.2.3 Optical Microscopy 31

4.2.4 Density Measurements 34

4.2.5 Thickness Measurements 36

4.3 Results and Discussion 36

4.3.1 Optical Microscopy and Density Methods 36

4.3.1.1 Fully Cured Samples 37

4.3.1.2 Partially Cured Samples 40

4.3.2 Thickness as a Proxy for Porosity 42

4.4 Summary 47

Chapter 5: Experimental Study of Void Evolution in Out-of-Autoclave Processing of MTM45-1/5HS Prepreg 49

5.1 Introduction 49

5.2 Methods 51

5.2.1 Materials 51

5.2.2 Sample Preparation and Partial Cycle Tests 51

5.2.3 Sample Preparation for Directional Breathing Tests 54
5.2.4 Void Characterization 57
5.2.5 Gas Permeability 59
5.2.6 Flow Measurement 62
5.2.7 Thermogravimetric Analysis (TGA) 63
5.3 Results and Discussion 65
5.3.1 Void Evolution Studies 65
5.3.1.1 Void Morphology before Processing 65
5.3.1.2 Porosity Evolution during a Long Room Temperature Debulk 68
5.3.1.3 Porosity Evolution during Heat-Up and Cure 70
5.3.1.4 Void Distribution during Heat up and Cure 71
5.3.1.5 Effect of Temperature and Humidity on Porosity Evolution 72
5.3.1.5.1 Off-Gassing during the Cure Cycle 76
5.3.1.6 Effect of Gas Evacuation Direction on Porosity Evolution 79
5.3.2 Gas Flow Rate and Permeability Studies 81
5.3.2.1 Gas Flow during Long Room Temperature Debulk 81
5.3.2.2 Gas Permeability during Heat-Up and Cure 83
5.3.2.2.1 Through Thickness Permeability of Bagging Materials (Brick and Release Film)… 90
5.3.3 Fiber Bed Compaction and Resin Infiltration 91
5.4 Summary 95
Chapter 6: Effect of Vacuum Release Time on Final Porosity during Heated Cycle.....98
6.1 Introduction 98

6.2 Methods 98
6.2.1 Materials 98
6.2.2 Sample Preparation 98
6.2.3 Void Characterization 100
6.2.4 In-Plane Permeability Measurement and Resin Infiltration 101
6.3 Results and Discussion 103
6.3.1 Effect of Vacuum Release Time on Porosity 103
6.3.2 Effect of Vacuum Release Time on Void and Tow Geometry 104
6.3.3 Effect of Vacuum Release Time on Permeability 105
6.4 Summary 107
Chapter 7: Time Scales for Gas Transport and Vacuum Debulk in Out of Autoclave Processing of Prepregs 108
7.1 Introduction 108
7.2 Methods 110
7.2.1 Materials 110
7.2.2 Laminate Preparation 111
7.2.3 Characterization of Voids and Porosity 112
7.2.4 Permeability Measurements 112
7.3 Results and Discussion 113
7.3.1 Effect of Breathing Direction on Final Porosity 113
7.3.2 Time Scales for Gas Transport during Processing of Small Flat Laminates 115
7.3.3 Effect of Size on Time Scales for Gas Transport 126
7.3.4 Guidelines for the Required Debulk Time to Achieve a Defined Porosity Level 130

7.4 Summary 134

Chapter 8: Summary, Conclusions, Contributions and Future Work 136

8.1 Summary 136

8.2 Conclusions and Contributions 142

8.3 Future Work 147

8.4 Broader Implications 148

References 150

Appendices 159

Appendix A Gas Permeability Measurements 159

A.1 Introduction 159

A.2 Methods 160

A.3 Results and Discussion 161

A.4 Summary 169

Appendix B Modified Through-Thickness Permeability Test Set-up and Comparison of MTM45-1/5HS Thin and Thick Prepregs Permeability 171

B.1 Modified Through-Thickness Permeability Test Set-up 171

B.2 Results and Discussion 172

Appendix C Prepreg Surface Morphology 175

Appendix D Autoclave Prepreg vs. Out-of-Autoclave Prepreg 179

D.1 Introduction 179

D.2 Methods 179

D.3 Results and Discussion 180

Appendix E Theoretical Estimation of Laminate Permeability 182

Appendix F Mass Flow Sensor Calibration and Detection Limit 184
F.1 Mass Flow Sensor Calibration 184
F.2 Mass Flow Sensor: Minimum Detectable Flow Rate 187
F.3 Summary 188
Appendix G Comparison of the Gas Removed during Debulk Test with the Expected Gas in the Laminate 189
Appendix H Void Area Fraction Measurement: Effect of Surface Preparation and Image Acquisition Equipment 191
H.1 Void Characterization Method 191
H.2 Results 192
Appendix I Thickness Rebound of Un-cured and Partially Cured Laminates 194

List of Tables

Table 3-1 Overview of the scientific literature on porosity in prepreg processing. 22

Table 3-2 Summary of performed tests and analyses in the thesis. 25

Table 4-1 Specifications of the MTM 45-1 (ACG) prepregs used in this study..... 28

Table 4-2 Required parameters for calculation of composite theoretical density 34

Table 4-3 Density of fully cured laminates and the required weight measurements for their calculation. 38

Table 4-4 Density of partially cured laminates and the required weight measurements for their calculation. 41

Table 4-5 Advantages and disadvantages of three methods used for porosity determination in this study 47

Table 5-1 Thickness of brick and release film samples used in through-thickness permeability test 61

Table 5-2 Temperature-time cycles used in TGA test 63

Table 5-3 Temperature and relative humidity of conditioning containers. 64

Table 5-4 Tow impregnation model parameters [9] 92

Table 6-1 Permeability measurements of the laminates vented after 2.23, 4.23 and 22.23 hours 105

Table 7-1 Specifications of the MTM 45-1 (ACG) prepreg forms used in this study..... 111

Table 7-2 Input parameters for calculation of the Reynolds number and time scales for Darcy flow and diffusion. 117

Table 7-3 In-plane and through thickness permeability of MTM45-1/5HS – Thick during the process..... 119

Table 7-4 Time scale approximations with respect to laminate size (L: half of total in-plane length, T: thickness)..... 127

Table 7-5 Average input parameters for each processing stage used in the scale up study 127

Table 7-6 Prepreg permeabilities after room temperature debulk[1] 134

Table 8-1 Summary of porosity reduction mechanisms in Figure 8-2. Note: Pressure state is assumed, not measured. 140

Table A-1 Porosity and permeability of as laid up, continuous, interrupted and MRCC samples 167

Table D-1 3900-2/T800H cure cycle [111] 180

Table D-2 Laminate thickness before and after cure 181

Table E-1 Input parameters used for $K_{IP\text{-}LAM}$ estimation 183

Table F-1 Mass flow sensor minimum flow readings 187

Table G-1 Input parameters used in estimation of gas mass in an as laid-up laminate……..….190

Table G-2 Mass of gas in as laid-up laminate versus gas mass measured by flow sensor during long debulk……...……...190

Table H-1 Image analysis procedures used for creation of binary images using the Image J software……192

List of Figures

Figure 1-1 Schematic of prepreg microstructure before and after cure. 2

Figure 2-1 Prepreg a) roll, b) surface (woven fabric) and c) micrograph of a laminate cross-section made from a prepreg with 5HS woven carbon fiber embedded in epoxy matrix. 5

Figure 2-2 Schematic of Prepreg Processing a) Prepreg roll, b) Laminate Lay-up, c) Vacuum bagging, d) Curing, e) Cured laminate..... 7

Figure 2-3 Typical cure cycle for a carbon fiber reinforced prepreg [19]. 8

Figure 2-4 µCT of porous CFRP laminate, a) two-dimensional slice, b) three-dimensional microstructure. 20

Figure 2-5 Optical microscopy image of CFRP laminate (voids are black). 21

Figure 4-1 Vacuum bagging steps. 29

Figure 4-2 a) Processing cycle for “partially cured” laminate: In this test, both temperature and compaction pressure are stopped at time t and the sample is removed for further analysis. b) Processing cycle for “fully cured” laminate: In this test, compaction pressure is released at time t, while temperature cycle is continued to the end of the cycle. Then the sample is removed for further analysis..... 31

Figure 4-3 Preparation of partially cured samples for optical microscopy. 32

Figure 4-4 Part of an OM mosaic image (Vent time: 0 hour). 33

Figure 4-5 Use of Epo-color mounting resin for distinguishing the resin filled voids from the resin matrix by comparison of bright-field and dark-field images, a) Bright field, b) Dark field. 33

Figure 4-6 Part of a mosaic OM image of a laminate fully cured without vacuum (vacuum release time = zero hour)..... 37

Figure 4-7 Comparison of measured porosity of fully cured laminates (MTM45-1/5HS-Thin) obtained from optical microscopy (OM) and density methods. Optical microscopy (OM) porosity at 22.23 hrs is 0.3% and not visible in the figure. 39

Figure 4-8 Part of a mosaic OM image of an as laid-up, uncured laminate (processing time = zero hour). 40

Figure 4-9 Porosity of partially cured samples obtained from OM and density methods (MTM45-1/5HS-Thin). 41

Figure 4-10 Porosity estimated from the thickness method compared with porosity from optical microscopy and density methods, a) fully cured laminates (MTM45-1/5HS-Thin), b) partially cured laminates (MTM45-1/5HS-Thin) and c) partially cured laminates (MTM45-1/5HS-Thick). 44

Figure 4-11 Correlation between porosity from thickness method versus optical microscopy and density methods. Thickness based porosity is above the line of equality for fully cured laminates and below it for partially cured laminates. A plausible explanation is that the thickness measurements of fully cured samples over estimates the actual thickness as the samples used in this study had a rough bag surface (Figure 4-6) and the caliper sits on the rigid protrusions on the surface during measurements. Thickness measurements of partially cured samples may underestimate the actual thickness because these samples are soft and can elastically deform under moderate caliper pressure. 46

Figure 5-1 Sealing configurations: a) surface and edge breathing, b) edge breathing only, c) surface breathing only. 54
Figure 5-2 Laminate preparation steps in edge breathing and surface breathing tests. 56
Figure 5-3 Permeability test set-up, a) in-plane b) through-thickness. 60
Figure 5-4 Through-thickness permeability test bagging sequence for laminate, brick and release film permeability measurements (top view). 62
Figure 5-5 Humidity conditioning containers, a) ambient condition, b) $NaCl/H_2O$ salt solution (RH = 75%). 64
Figure 5-6 Initial state of an undebulked and uncured laminate. Stereo microscopy images of a) laminate and b) prepreg surface, c) Three-dimensional µCT image of laminate, d) Optical microscopy image of a laminate cross section. 67
Figure 5-7 Void Evolution during a) Long room temperature debulk and b) Heated 80°C cure cycle. Note that the data for 0 and 0.23 hours are the same for the two cycles (Error bars denote +/- one standard deviation). φ_T: Total porosity; φ_R: Resin porosity; φ_I: Inter-laminar porosity; φ_F: Fiber tow porosity. 68
Figure 5-8 Evolution of porosity distribution during 80 ˚C cure cycle, a) Through-Thickness, b) In-Plane (Error bars denote +/- one standard deviation). 72
Figure 5-9 a to c) Effect of cure cycle hold temperature (120 ˚C vs. 80 ˚C) on the evolution of different types of porosity. d to f) Effect of relative humidity on the evolution of different types of porosity in a 120 °C cycle (Error bars denote +/- one standard deviation). 73
Figure 5-10 Effect of humidity on porosity of fully cured samples. a) RH = 75% (zero porosity), b) RH = 98% (5.7% porosity). 75

Figure 5-11 a) Temperature-time cycles; Weight loss during different cycles, b) at RH = 31% (ambient) and c) at RH = 75%. 77

Figure 5-12 a) Effect of relative humidity (23% vs. 75%) on porosity evolution in a 120˚ C cycle, b) effect of relative humidity (31% vs. 75%) on the weight loss in 120˚C cycle and 200 ˚C ramp. 78

Figure 5-13 Effect of breathing direction on void evolution during an 80 °C cure cycle. a) total porosity, b) fiber tow porosity, c) inter-laminar porosity, d) tow minor dimension. . 80

Figure 5-14 a) Flow rate measured during a 10 hour room temperature debulk. b) magnification of early hours of debulk (The flow rate plateau (0.0093 L/min) is indicated on the magnified graph). The red color shows the area under the graph. The black color shows the fluctuating data points due to the noisy signal in this low flow regime..... 82

Figure 5-15 a) MTM45-1 resin viscosity, b) In-plane and through thickness gas permeability and c) Calculated gas flow ratio throughout an 80˚C cure cycle. Flow and permeability values below detectable limit (Q ≈ 0.006 L/min, K (In-Plane) ≈ 10^{-15} m^2, K (Through-Thickness) ≈ 10^{-17} m^2) are assumed to be effectively zero. (Error bars denote +/- one standard deviation). 84

Figure 5-16 Pin holes formed at warp/weft intersections when prepreg is subject to permeability testing when resin viscosity is low..... 86

Figure 5-17 Relationship between fiber tow porosity and a) in-plane permeability, b) through-thickness permeability. 88

Figure 5-18 Through thickness permeability of laminate, brick and release film during 80 °C cure cycle. 90

Figure 5-19 Evolution of fiber tow porosity (Φ_F), tow compaction (ε_T) and resin infiltration (β) during a) long debulk and b) 80˚C cure cycle. Error bars denote +/- one standard deviation..... 93

Figure 5-20 Comparison of fiber tow porosity (Φ_F) and tow compaction (ε_T), evolution at different temperature cure cycles and relative humidity levels. Error bars denote +/- one standard deviation. 94

Figure 6-1 Processing cycle; Vacuum is released at time t, while the temperature cycle is continued to the end of the cycle. 99

Figure 6-2 Image analysis steps for inter-laminar voids, a) original image, b) binary image, c) binary image after noise removal (ready for measurement). 101

Figure 6-3 Set up used for resin infiltration test. 102

Figure 6-4 a) Thickness and porosity vs. vent time, b) Porosity Type vs. vent time. Porosity is less than 0.3% at 6.23 hours and not visible on the graph. 103

Figure 6-5 Optical microscopy image a) vent time: 0 hour, b) vent time: 8 hours..... 104

Figure 6-6 Void and tow geometry, a) void aspect ratio, b) tow minor and major. 105

Figure 6-7 a) Resin infiltrated network of interconnected inter-laminar voids (vent time: 4 hours). High magnification images b) bright field image, c) dark-field image. 106

Figure 7-1 Schematic of gas removal and porosity (φ) evolution in processing of OOA prepregs (section 5.3.1)..... 109

Figure 7-2 Effect of sealing configuration and breathing direction on porosity (φ) (Error bars denote +/- one standard deviation)..... 114

Figure 7-3 Cross sectional optical microscopy images of samples presented in Figure 7-2: (a) 5HS-Thin – Surface and Edge Breathing (no porosity gradient); (b) 5HS-Thin –

Surface Breathing Only (porosity gradient); (c) UD – Surface and Edge Breathing (no porosity gradient); (d) UD – Surface Breathing Only (porosity gradient)..... 115

Figure 7-4 Geometry, flow distance, pressure and concentration boundary conditions used in the time scale study..... 120

Figure 7-5 Time scales for gas transport via Darcy flow and diffusion during a) Long room temperature debulk; b) 80 °C cure cycle. The calculations were made for laminates with L ≈ 64 mm, T ≈ 4 mm (Figure 7-4). The red line represents a reference time of one hour. TT = Through-Thickness, IP = In-Plane..... 123

Figure 7-6 Effect of laminate geometry, length L and thickness T, on time scales for gas transport at different stages of the process a, b) debulk, b, d) ramp and e, f) early temperature hold. IP = In-Plane, TT = Through-Thickness. 129

Figure 7-7 Debulk maps showing the maximum part size (L^*, T^*) for achieving a porosity level of less than 2% for a specific debulk time based on eq. (7-14). 133

Figure 8-1 Void sources and sinks in a vacuum bagged laminate. Void morphology of a laminate before processing, 1) fiber tow voids, 2) inter-laminar voids and 3) resin voids. Note that void morphology changes during the process..... 137

Figure 8-2 Relative porosity at different points in the cure cycle. This graph is created based on the data in Figure 5-7 from the void evolution study on MTM45-1/5HS laminates (127 mm × 127 mm × 8 layers). 139

Figure A-1 a) Resin viscosity profile in 80 °C cure cycle, b) Continuous and interrupted permeability in in-plane and through-thickness directions. Flow and permeability values below detectable limit (Q ≈ 0.006 L/min, K (In-Plane) ≈ 10^{-15} m^2, K (Through-Thickness) ≈ 10^{-17} m^2) are considered to be zero……..163

Figure A-2 Comparison of porosity of samples that have undergone interrupted and continuous permeability measurements with as laid-up and MRCC cured samples. The as laid-up sample is not cured whereas the other three samples are fully cured. 164
Figure A-3 Cross sectional optical micrograph of through-thickness permeability sample under "continuous" and "interrupted" measurement methods. Cross sections perpendicular and parallel to flow are considered. 165
Figure A-4 Cross sectional optical micrograph of in-plane permeability sample under "continuous" and "interrupted" measurement methods. Cross sections perpendicular and parallel to flow are considered. 166
Figure A-5 Comparison of sample porosity in perpendicular and parallel directions to the gas flow for samples subjected to permeability testing..... 169
Figure B-1 Through-thickness permeability test set-up. a to c) original set-up, d to f) modified set-up. 172
Figure B-2 Permeability of 5HS–Thick and 5HS–Thin prepregs during 80 °C cure cycle..... 173
Figure B-3 Pinholes in a) 5HS-Thick prepreg, b) 5HS-Thin prepreg. Pinholes are marked with green border. 174
Figure C-1 Surface morphology of prepregs used in this study, a to f) MTM45-1/5HS – Thick, g to l) MTM45-1/5HS – Thin, m to r) MTM45-1/UD. Top and bottom surface of prepregs before and after roller application (a - d, g – j, m – p). Prepreg layer under light reflection and transmission modes (e – f, k – l, q – r). 176
Figure D-1 Optical micrograph of a 3900-2/T800H laminate after debulk (a, b: bright-field and c, d: dark-field) and after cure (e, f: bright-field). 181
Figure E-1 Schematic of laminate cross-section. 182

Figure F-1 Digital mass flow sensor calibration curve provided by Convergent. 184

Figure F-2 Flow rate measurement set-up. 185

Figure F-3 Rotameter calibration curve (Omega engineering company). 186

Figure F-4 Flow rate: mass flow sensor versus rotameter. 186

Figure H-1 Part of cross-section image (vent time = 0 hour), a) original image, b) binary image. 191

Figure H-2 a) Porosity from camera and OM images, b) original camera image, c) binary camera image, d) original OM image, e) binary OM image. 193

Figure I-1 Thickness rebound of uncured and partially cured laminates..... 194

Figure I-2 Effect of thickness rebound of uncured and partially cured laminates on their porosity (porosity is estimated based on the thickness of the laminates (for calculation details refer to section 4.3.2)). 195

Glossary

Prepreg: Prepreg is a form of raw composite material in which the fibers (woven or uni-directional) are pre-impregnated with an uncured but catalyzed thermoset resin which will cure at elevated temperatures. Prepreg can also use thermoplastics as a matrix, but it is less common.

Laminate: A laminate consists of several layers of prepreg laid-up and stacked on top of each other.

Cure: Cure refers to a thermo-chemical reaction that thermoset polymers go through during processing. Thermosets change from low viscosity polymers to rigid polymeric structures during the cure process. The cure reaction gradually advances during the process under a pre-determined temperature cycle. The laminates are partially cured during the cure process and become fully cured by the end of the cure process. A part has to be fully cured to obtain the properties that are required for service conditions.

Five Harness Satin (5HS) weave pattern fabric: 5HS refers to a weave pattern in which the warp thread runs under four weft threads in a repeated pattern. In this thesis each thread is a fiber tow.

Fiber tow: Fiber tow consists of a large number of fibers expressed by fiber count (1k (1000 fibers), 2k (2000 fibers), etc). The fibers used in this thesis are carbon fiber and their diameter is about 7 μm.

Matrix: In this study refers to the continuous polymeric phase (resin) that embeds the reinforcement fibers in a composite material.

Resin: An organic polymer or pre-polymer which serves as a matrix to embed the reinforcement fibers in a composite material. The matrix may be a thermoplastic or a thermoset, and may contain a wide range of additives or components.

Void: A laminate consists of three phases: fibers, resin and voids. Void refers to a space filled with gas or vacuum.

Porosity: Porosity refers to the volume fraction of voids or the void content.

Autoclave (AC) processing of prepregs: In this method laminates are made through prepreg layup, vacuum bagging and autoclave curing. An autoclave is a pressurized vessel in which vacuum bagged laminates can be cured under high pressure (~ 6 atm) and temperatures (~ 200 °C).

Out of Autoclave (OOA) processing of prepregs: OOA processing of prepregs is similar to AC processing of prepregs. The difference is that in this process vacuum bagged laminates are cured in an oven under atmospheric pressure (~ 1 atm). Temperature and vacuum conditions are similar to AC processing.

Vacuum Bag Only (VBO) process: VBO process is another name for Out-of-Autoclave processing of Prepregs.

Acknowledgements

This work would not have been possible without the support of my colleagues, friends and family and I owe all of them my most heartfelt thanks.

I am sincerely grateful to my supervisor, Dr. Göran Fernlund, for his invaluable support, encouragement and guidance during these years. Your knowledge and insight truly helped this effort to be more meaningful.

It has been a privilege to be a member of the UBC Composites Group and the Composites Research Network and I would like to thank Dr. Anoush Poursartip, Dr. Reza Vaziri and my supervisor, Dr. Göran Fernlund for giving me the opportunity to join this dynamic group. I appreciate all the support and friendships with current and past members of the group. I owe special thanks to Bryan Louis, Nathan Avery Slesinger, Kevin Hsiao, James Kay, Kamyar Gordnian, Ryan Thorpe, Gabriel Fortin, Sanjukta Chatterjee, Navid Zobeiry, Mehdi Haghshenas, Sardar Malekmohammadi, Alireza Forghani, Christophe Mobuchon and Roger Bennett for their valuable assistance, feedback, and discussions.

I would like to thank Dr. Mike Thompson from Boeing Company for the constructive discussions and feedbacks. I also would like to thank Dr. Abdul Arafath and Malcolm Lane of Convergent technologies for use of mass flow sensor equipment and technical support.

This work was conducted as part of a Consortium for Research and Innovation in Aerospace in Quebec (CRIAQ) collaborative project (COMP-1). I would like to thank the industrial and academic partners for their financial and intellectual support: Bell Helicopter Textron Canada, Bombardier Aerospace, Delastek, The Institute of Aerospace Research, The Aerospace Manufacturing Technologies Center, the National Research Council Canada, and The Center for Development of Composites in Quebec (CDCQ), McGill University, Concordia University and the University of British Columbia.

And last but not least, I would like to thank my family without whom; this would not have been possible. I would like to thank my dear parents and sister, Shahin, Mahmoud and Nazila for their unconditional love and support throughout my life. I would like to thank my dear husband, Ardavan, for standing by my side and helping me to always see the bright side.

Dedication

To the light of my life “Ardavan”

Chapter 1: Introduction

The use of polymer matrix composites in the aerospace industry is increasing. It began in non-critical, secondary, applications but now critical primary structural components such as fuselages and wings are made of carbon fiber composites in large civil aircrafts [1]. The use of composites in structural aerospace parts is reliant on cost-efficient manufacturing. Composite structures can be expensive compared to aluminum, however their manufacturing methods reduces the need for joining by allowing manufacturing of larger monolithic structures which offers significant cost savings. Currently, autoclave (AC) processing of prepreg laminates is the main processing method for production of structural composite parts in the aerospace industry. Autoclave processing is a robust method that gives high quality parts that meet industry specifications in a fairly reproducible manner. However AC processing may not be able to meet the production rates in a cost effective way as market demand increases. The demand for composite aero structures is expected to increase for the next few years. The continued increase in production of the Boeing 787 and Airbus A350XWB dominates the growth and is the driving force for an accelerated demand over the next three years [2]. Limitations of autoclave processing include large initial capital investment, high operating costs and part size limitations. Consequently there is an interest in aerospace to replace AC processing with lower cost out of autoclave (OOA) processing methods such as OOA processing of prepregs which is the topic of this thesis. The successful use of this production method depends on its ability to produce high quality parts at a low cost.

1.1 Porosity in Out of Autoclave Processing of Prepregs

Prepregs are a form of raw composite material in which the fibers (woven or uni-directional) are pre-impregnated with an uncured but catalyzed thermoset resin which will cure at elevated temperatures (Figure 1-1). Prepregs can also use thermoplastics as a matrix, but it is less common.

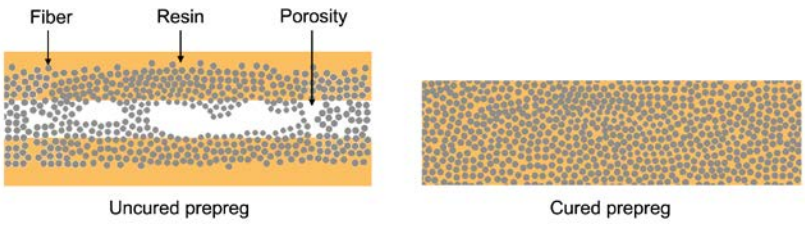

Figure 1-1 Schematic of prepreg microstructure before and after cure.

In prepreg processing the composite part is made by stacking the required number of prepreg layers on the mould in predetermined directions to obtain the desired mechanical properties. In the next step, the part is covered with a vacuum bag and processed under a defined temperature and pressure cycle. Compaction pressure and temperature are two important processing parameters which control the part consolidation, cure and final quality. Compaction pressure, the pressure difference between vacuum bag interior and exterior, creates the driving force for fiber bed compaction and resin impregnation in processing. Vacuum pressure helps with gas removal and porosity reduction throughout the process. The temperature cycle facilitates the flow of resin into the fibers and promotes the cure reaction. Initially, at room temperature, the prepreg resin is a high viscosity gel (e.g., 10^4 Pa.s) with short polymeric chains. As the cure cycle starts and temperature increases, the resin viscosity drops due to the increased mobility of the polymer

chains. Low viscosity enables the resin to flow and impregnate the fibers. Later in the process, the viscosity and degree of cure increase as the process advances and a fully cured solid laminate is obtained. In the case of AC processing, parts are cured in an autoclave under high compaction pressure (typically 6 atm). High compaction pressure improves part consolidation and reduces porosity by decreasing void size down to acceptable limits resulting in high quality parts. In OOA processing, parts are cured in an oven under atmospheric pressure. The reduced pressure generally leads to high porosity level (e.g., 5 - 10%) which does not meet the requirements of primary structural parts in the aerospace industry (1 – 2%) [3]. This problem has led to the development of a new generation of prepregs, called OOA prepregs, designed to enhance porosity reduction [4, 5]. Research studies have been performed aiming to improve the understanding of the interaction of process parameters and their effect on defects in OOA processing of prepregs [6, 7, 8, 9, 10, 11, 12, 13, 14]. However more work needs to be done to address the porosity issue in this process and extend its use for production of structural parts in the aerospace industry.

Chapter 2: Literature Review

2.1 Out of Autoclave Processing of Prepregs

2.1.1 Prepreg

Composite materials can be categorized into three groups based on their matrix: polymeric, metallic and ceramic matrix composites. The matrix is the continuous phase that surrounds the reinforcement phase in a composite material. Polymeric matrix composites (PMCs) have the widest range and largest quantity of applications among composites. There is a large variety of PMCs depending on the employed polymers and reinforcements. The polymer matrix can be thermoplastic or thermoset. Reinforcements come in different forms of fibers and particles. Technologically, fiber reinforced composites have the highest importance among PMCs as they offer high specific strength and modulus. Glass, carbon and aramid fibers are among the common types of fibers used in PMCs. Carbon fiber is widely used as high performance reinforcement in advanced applications [15]. Prepreg is the most common form of continuous fiber reinforced raw material used in manufacturing of high performance structural composites. It is a fiber form that is pre-impregnated with a known amount of partially cured thermoset resin or thermoplastic. The fibrous phase can be in the form of uni-directional or woven fabric (Figure 2-1). Two of the main advantages they offer are controlled resin content and good fiber alignment.

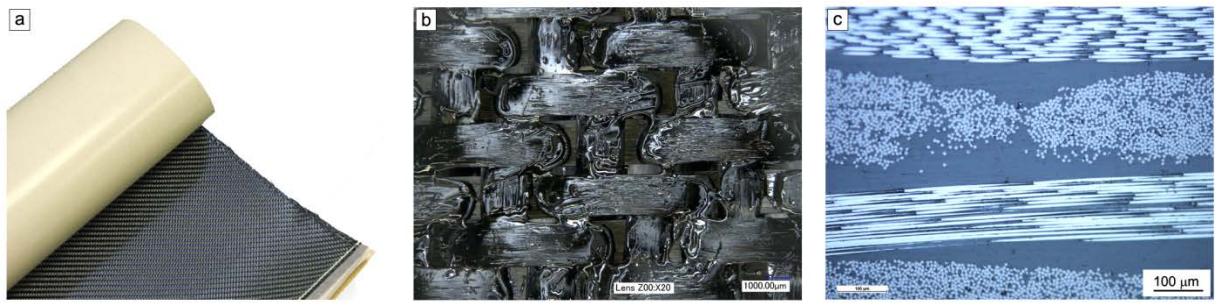

Figure 2-1 Prepreg a) roll, b) surface (woven fabric) and c) micrograph of a laminate cross-section made from a prepreg with 5HS woven carbon fiber embedded in epoxy matrix.

Prepreg manufacturing methods include: hot-melt impregnation, resin filming and solvent impregnation [3]. Prepregs have a limited out-time at room temperature, beyond which they cannot be used due to inferior properties, as the resin undergoes a slow cure reaction at room temperature. As a result they have to be shipped and stored in a freezer (≈ - 18 °C). Prepregs are expensive compared to many other forms of composite materials and are mainly used in the aerospace industry. The prepregs used in this study are MTM45-1/CF2426A and MTM45-1/GA045 (Advanced Composites Group (ACG), now Cytec Industrial Materials), with a toughened epoxy matrix and carbon fiber reinforcement in woven and uni-directional forms.

2.1.2 Prepreg Processing

Composites are processed with a wide range of manufacturing methods, which is a consequence of the numerous forms of raw materials. The processing methods for aerospace structural composites can be divided into liquid composite moulding composites (LCM) and prepreg processing methods. In these processes parts are manufactured under prescribed pressure and

temperature conditions. Liquid composite moulding generally involves resin infiltration of a dry preform in a one or two sided mold with the aid of pressure, vacuum or both. Depending on the resin cure temperature, the curing step is done at room temperature or at elevated temperature using specialized moulds or ovens. In either case it is critical to adjust the processing parameters to have the mould filled with resin before the cure advances and gelation occurs. There are many variations of the LCM process including resin transfer moulding (RTM), vacuum assisted resin transfer moulding (VARTM) and resin film infusion, all with their specific characteristics. RTM is the most widely used LCM manufacturing method in aerospace currently. Some of the main advantages of this method are dimensional stability, capability of complex part fabrication and good surface finish. Fiber displacement, dry spots and resin race tracking are some of the shortcomings of RTM [3].

In prepreg processing, pre-impregnated fabrics or uni-directional tapes are used for fabrication of high performance thermoset composite structures. As for LCM the main processing parameters in this method are pressure and temperature. Prepreg processing generally consists of three manufacturing steps: lay-up, vacuum bagging and cure (Figure 2-2). First, prepregs are cut into the required number of layers and sizes to form the right part thickness and shape. Prepreg layers are stacked on top of each other manually or using automated techniques. Intermediate debulking steps are performed to improve the conformation of the layers to the mold by application of vacuum at room temperature. Once the part has reached the required thickness it is vacuum bagged. Figure 2-2 c shows a typical vacuum bagging arrangement.

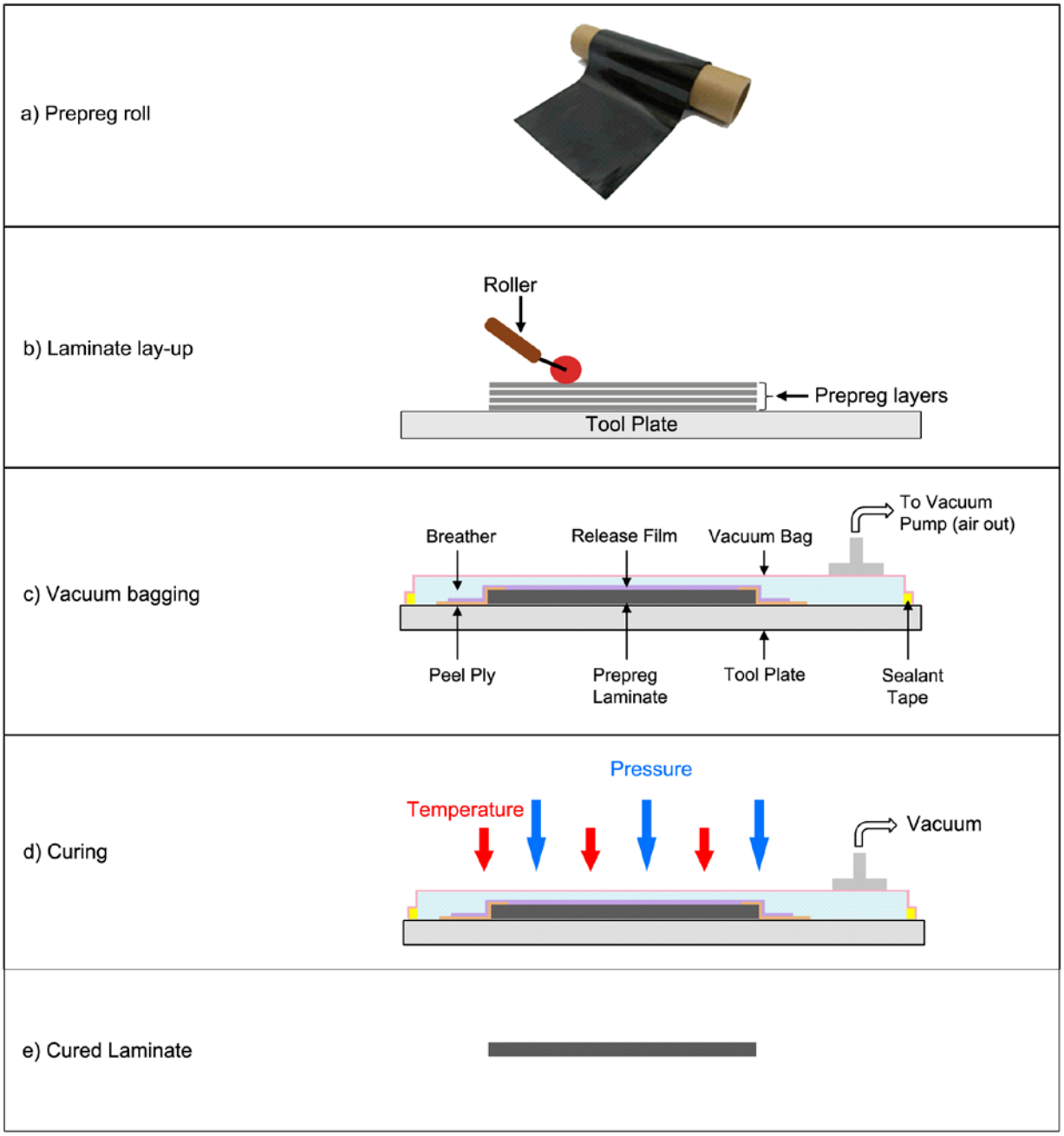

Figure 2-2 Schematic of Prepreg Processing a) Prepreg roll, b) Laminate Lay-up, c) Vacuum bagging, d) Curing, e) Cured laminate.

This bagging arrangement consists of a release agent coated mold, a laminate with glass tows or peel ply at the edges as breathing pathways, a Teflon layer to prevent resin bleeding, a breather

to distribute the vacuum, a vacuum bag sealed by tacky tape on top of all layers and a vacuum port that connects the bag to the vacuum pump. Details of the bagging can be customized according to the individual needs. The next step of the process is the cure stage, during which the vacuum bagged part is processed under a predetermined temperature and pressure cycle. Depending on the process, cure can be done in an autoclave under high compaction pressures (up to 6 atm) or in an oven under atmospheric pressure. In addition to the common temperature control methods such as autoclaves and ovens, there are a variety of other methods to cure a composite such as microwave, heated moulds, ultra-violet and infrared light [17, 18]. Figure 2-3 shows a typical cure cycle, defined by temperature and pressure cycles for processing a carbon fiber-epoxy prepreg in autoclave.

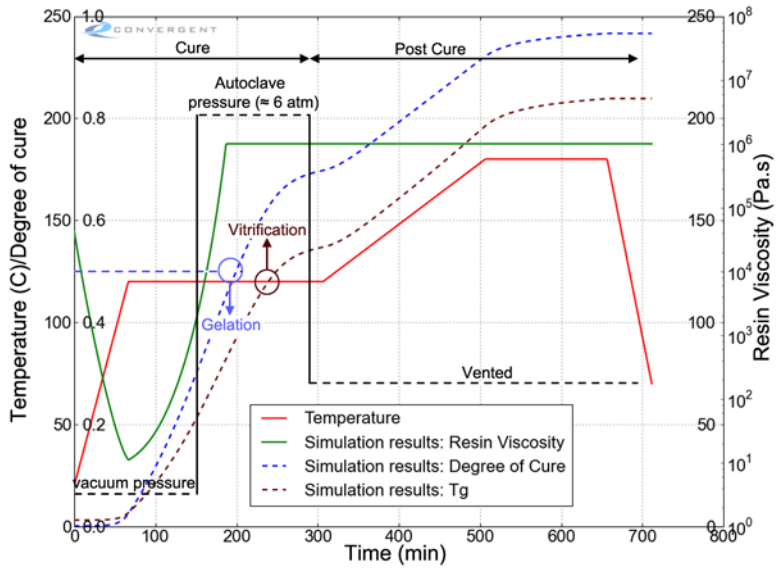

Figure 2-3 Typical cure cycle for a carbon fiber reinforced prepreg [19].

A typical cycle consists of one or two heat-up ramps followed by isothermal holds. The resin viscosity profile is superimposed on the cure cycle. The resin is semi-solid at room temperature,

but the viscosity decreases sharply during the heat up ramp. This portion of the cure cycle is intended to facilitate resin flow and volatile off-gassing in the low viscosity region. Later, during the isothermal hold, the resin polymerization portion of the process starts to take off. As polymerization and cross-linking progresses the resin viscosity increases. During the cross-linking process the low viscosity resin transforms into a three-dimensional solid network. This transition stage is called gelation. After gelation, the degree of cure (α) continues to increase as cross-linking advances and reaches full cure, providing high glass transition temperature (T_g) and mechanical properties. For some epoxy systems cure is followed by a post cure at elevated temperature, which increases the degree of cure, the glass transition temperature, and thus service temperature. Post-curing completes the polymerization reaction and further develops high temperature mechanical properties for some epoxies.

Pressure is the other processing parameter during the cure cycle. Laminates are cured under compaction pressure, which is defined by the pressure difference between the vacuum bag interior and the autoclave or oven environment. In autoclave cure, high compaction pressures (6 – 7 atm) are commonly used, while in an oven parts are cured under atmospheric compaction pressure. The compaction pressure improves ply compaction, resin infiltration and void suppression during the process.

2.1.2.1 Out-of Autoclave versus Autoclave Processing

Aerospace composite structures are extensively manufactured through prepreg lay-up and autoclave cure. In autoclave cure, high compaction pressures are attainable (e.g., 6 - 7 atm), which results in high fiber volume fractions, good compaction, and small amounts, of voids and

porosity [3, 20]. Despite the advantages offered by autoclaves, there is a strong desire in the aerospace industry to replace it with lower cost Out-of-Autoclave (OOA) processing methods, such as resin transfer molding (RTM), vacuum assisted resin transfer molding (VARTM) and vacuum bag only (VBO) processing of prepregs, which is the subject of current study [7, 21]. The advantages of OOA methods over autoclave processing are less initial capital investment, improved energy efficiency, cheaper tooling and elimination of part size limitations imposed by autoclave size [7, 22]. However, OOA methods can replace the autoclave only if parts produced by this method offer equivalent properties compared to their autoclave made counterparts. Voids and porosity are among the main problems in composite part manufacturing [3, 20]. In autoclave processing, high applied pressure suppresses voids and keeps volatiles dissolved in the resin, resulting into low void content (e.g., 1–2%) [3, 7]. However, in the VBO process, where the pressure is low (atmospheric pressure or less) the void content can be much higher (e.g., 5-10%) and it is challenging to produce void free parts with VBO processing methods [3, 7]. In order to address this issue, a new generation of prepregs was specifically designed for out of autoclave processing, named “out of autoclave prepregs” (OOA prepregs). Resin chemistry and fiber impregnation play a key role in OOA prepregs [23, 24]. These prepregs use addition-cured thermoset resins, which do not off-gas while curing [25, 26]. Another feature of these resins that decreases off-gassing and void formation is that they can be cured at lower temperatures compared to autoclave prepregs [25, 27]. These resins are also less tacky at room temperature, which reduces the probability of air entrapment during the lay-up [27]. Out of autoclave prepreg manufacturers employ different impregnation strategies, but they all impregnate the fiber preforms partially [23, 24]. Some prepregs are impregnated with resin on both sides while others are impregnated on one side or with a perforated pattern [23, 24]. The un-impregnated zones of

these prepregs are dry pathways through which entrapped gases can be evacuated from the prepreg, resulting in lower porosity [28, 29]. These pathways are called Engineered Vacuum Channels (EVACs) [23]. Another feature of OOA prepregs is their higher resin content. These prepregs are no-bleed, which ensures specific resin content for design purposes [23]. The development of OOA prepregs has moved the industry one step forward in the manufacture of void free parts through vacuum bag only processing, however a better understanding of void formation and evolution in this process is essential as high porosity is still a challenge in OOA processing of prepregs.

2.2 Porosity in Out of Autoclave Processing of Prepregs

2.2.1 Porosity

Voids and porosity are a concern in composite part processing [3, 20]. In this document, voids are defined as empty spaces within the composite material, that are not filled with resin or fiber, and porosity or void content is a measure of the volume fraction of voids. Porosity can be divided into surface and bulk porosity. As the name suggests surface porosity is a type of void located on the part surface and has aesthetic importance. Bulk porosity is located inside the bulk of the part and has a negative effect on mechanical properties of composites [30, 31, 32]. Matrix dominated mechanical properties such as inter-laminar shear strength, flexural and transverse strength are decreased as porosity increases [15, 32]. A 2% porosity increase causes an approximate 20% reduction in both flexural and inter-laminar shear strength [33]. The focus of

the current study is bulk porosity. In primary aerospace structures a certain amount of porosity (≈ 1 – 2%) is acceptable, below which strength and other property specifications are met [34].

The void content of a laminate is affected by many factors including: process conditions (temperature, vacuum, and pressure), type of prepreg (chemistry, fiber architecture), ply orientation, ply terminations, lay-up method, debulking, laminate size and shape, detailed geometry (curvature and radius), tooling (male or female) and bagging details [34].

Void formation phenomena in prepreg processing is complex and not yet fully understood [3, 34]. However, there are some basic principles that are fairly well understood [20, 35, 36]. Void formation can occur by mechanical entrapment of air (during lay-up, resin mixing, at ply terminations, etc), heterogeneously at resin-reinforcement interfaces or homogeneously within the resin [35]. Voids can also be formed during the process via off-gassing of volatiles and moisture, unintentional bag and tool leaks or incomplete wetting of the fiber bed by resin. Once a void is formed in the resin, its internal pressure equals to resin hydrostatic pressure plus the surface tension forces at equilibrium (eq. 2-1) [3, 20, 37]. However it should be noted that as soon as the resin viscosity increases and gelation occurs, the void morphology will be locked and no further porosity changes will occur [37].

$$P_g - P_r = \frac{\gamma_{LV}}{m_{LV}} \tag{2-1}$$

Where P_g: gas pressure, P_r: resin pressure, γ_{LV}: liquid resin-void surface tension, m_{LV}: ratio of void volume to its surface area.

Gas pressure is controlled by several parameters including gas type, amount and temperature. Resin pressure is a function of the compaction pressure, and flow and compaction phenomena (distribution of compaction pressure between fiber bed and resin). Void growth can occur via diffusion of moisture, air, or other volatiles into a void, temperature increase or coalescence of neighboring voids [35, 38]. If the diffusion gradient is reversed or the resin pressure is increased, the void shrinks or collapses [3, 7]. Kardos investigated void growth based on diffusion of water vapour in to a spherical air void surrounded by resin in the autoclave process [35]. The results of his study showed that the prepreg's initial relative humidity and the external pressure during the cure cycle (e.g., autoclave pressure) are two important parameters that control the final void diameter [35]. Gruenfelder and Nutt have investigated the effect of initial relative humidity on void content and showed that for VBO processed laminates, the void content increased substantially with initial relative humidity, while this was not the case in autoclave processing [7]. These results confirm the strong impact of autoclave pressure on dissolution of voids and the ability to produce void free parts. The high resin pressure attainable in AC processing is the main means of void reduction either by size reduction or gas dissolution. In VBO processes and in the absence of high resin pressures, an effective approach for void reduction is to reduce the pressure of the gas inside the voids. This can be done via evacuation of entrapped gases in the laminate through vacuum application [34]. While there is general knowledge of void formation and evolution, the influence and effectiveness of other factors such as sample size and geometry, vacuum level, etc which are dependent on the detailed process conditions, are not fully understood [7]. Systematic study of these factors will result in improved understanding of void formation and evolution phenomena, and thus optimization of process details to achieve low porosity parts.

2.2.2 Gas Transport in Out of Autoclave Processing of the Prepregs

In AC processing, the high compaction pressures generate high resin pressure and consequently reduced void size or dissolution of gaseous species in the resin. In OOA processing, the main means of void reduction is reducing the pressure of the gasses inside the voids. Gas removal is necessary but not sufficient for void reduction as some of the void spaces are rigid (surrounded with fiber or semi-solid resin) and once evacuated, they need to be compacted and/or filled with resin before the system gels. Gas evacuation can occur through diffusion or advection mechanisms.

2.2.2.1 Diffusion

Diffusion is the molecular movement of species in the bulk of the material, under concentration gradients. Fick's first law of diffusion is written as [40]

$$J = -D\frac{dC}{dx} \tag{2-2}$$

Where J (kg/m^{2}s): diffusion mass flux, D (m^2/s): diffusion coefficient, C (kg/m^3): concentration and x (m): distance.

Moisture is known as one of the primary sources of voids in OOA prepregs [3, 7, 41]. Void growth can happen through diffusion of moisture from the resin into a void [19, 20]. Researchers have investigated air and moisture diffusion in epoxy prepregs and have developed models that predict void growth and collapse via diffusion based on processing parameters such as pressure and temperature [7, 35, 42, 43]. Kardos model is the most commonly cited diffusion based void growth model [35]. Kardos model predicts the effect of resin moisture content on the void diameter [7, 35]. In this model it is assumed that a spherical void is located in an infinite

isotropic resin medium and its growth happens through water diffusion from the surrounding resin [7, 35]. Using this model the evolution of isolated resin voids through diffusion can be predicted.

$$d = 4\beta\sqrt{Dt} \tag{2-3}$$

$$\beta = \frac{C_{bulk} - C_{void}}{\rho_g} \tag{2-4}$$

Where d: void diameter (mm), β: growth driving force, D: diffusion coefficient of water in the resin (mm^2/hr), t: time (hr), C_{bulk}: concentration of water in the bulk resin (gr/mm^3), C_{void}: concentration of water at the surface of the void (gr/mm^3), ρ_g: gas density (gr/mm^3).

2.2.2.2 Advection

Advection is another means of gas transport, which refers to continuum or bulk flow of gas. Gas advection in porous medium is widely analyzed using Darcy's law [44], which states that the superficial gas velocity (*v)* is directly proportional to the gas permeability of the porous medium and the pressure gradient of gas phase in the direction of the flow. In one dimension, this can be expressed by

$$v = -\frac{K}{\mu}\frac{dP}{dx} \tag{2-5}$$

Where K (m^2): gas permeability, μ (Pa.s): gas dynamic viscosity, P (Pa): gas pressure, x (m): distance.

Darcy's law is applicable to laminar flow. The Reynolds number (Re) determines the boundary between turbulent and laminar flow regimes. The transition from laminar to turbulent flow

regime is determined by Reynolds number (Re) and occurs in the range of 1 to 10 [45]. In low pressure or low permeability medium there is a transition from laminar flow to Knudsen diffusion or free molecular flow. Gas advection in porous medium can be thought of as flow through many capillary tubes. In the case of large capillary tubes, the mean free path for gas molecules is much smaller than tube radius and thus continuum flow occurs. As the size of the capillaries gets smaller and close to the gas molecular mean free path, free molecule or Knudsen diffusion occurs [44]. Knudsen showed that at low pressures, the mass flux reaches a minimum and then increases as the pressure decreases. This increase is a result of free molecular flow or slip phenomenon in which the gas velocity is not zero at the wall [44]. This effect is also known as the Klinkenberg effect [44].

A prerequisite for advective or Darcy flow in a porous medium is the presence of a continuous network through which the bulk movement of gas can occur. A partially impregnated prepreg is a porous medium that has a complex microstructure which changes during the process. This porous network consists of both connected and isolated void spaces that are surrounded with resin and fibers. Darcy flow occurs through the interconnected network of voids as long as they are open and not filled with resin. The pressure inside the interconnected network of voids can be reduced via Darcy flow and vacuum application, whereas the pressure inside isolated voids can only change through gas diffusion mechanisms, under constant void volume conditions. The interconnected porosity network in prepreg laminates consists of their un-impregnated zones called Engineered Vacuum Channels (EVACs) [23, 28, 29]. The morphology of the EVACs change throughout the process, as they become infiltrated with heated low viscosity resin.

2.2.2.2.1 Permeability

Permeability quantifies the porous medium resistance to advective flow and depends on geometrical characteristics such as porosity, surface area and tortuosity [46]. Permeability is not measured directly, it is calculated based on an assumed flow model and measured flow related data (e.g., flow rate, pressure) [44]. For this reason, permeability measurements have meaning only in the context they are measured. This is why permeabilities measured for different flow geometries or different scales may give different values [44, 47]. Below, some of the available methods for measurement of air permeation in porous medium are reviewed.

Permeability is determined by application of pressure gradient across a porous medium and measurement of the resultant air flux. Air permeability in porous medium has been extensively studied in the fields of soil science, oil and gas extraction and filtration. Both steady and non-steady state methods are employed. The non-steady state or pressure decay method is commonly used for low permeability materials where steady-state flow condition can not be achieved in a reasonable time. The steady state method is commonly used in laboratory settings. In this test a steady state gas flow (Q) is produced by applying a constant pressure gradient across the sample. Permeability, K, is determined by solving the one dimensional Darcy flow equation for a compressible ideal gas at constant temperature [34, 46]

$$K = \frac{2\mu L Q_1}{A} \frac{P_1}{P_1^2 - P_0^2} \quad (2\text{-}6)$$

Where μ: gas viscosity, L: length of the sample, A: cross sectional area of the sample, P_1: the inlet pressure, P_0: outlet pressure.

The porous medium in prepregs is fibrous in nature. An important characteristic that distinguishes fibrous porous medium from granular medium is their relatively high porosity. Fibers form stable structures with high specific surface area and with relatively low resistance to flow [48]. However, in the case of prepregs the fibrous structure is partially impregnated with resin and during the cure cycle the porous structure changes as resin infiltrates into it which in turn affects the permeability of the laminate.

Prepreg gas permeability has been studied in the past [10, 11, 49, 50, 51]. Through-thickness permeability of prepregs was measured based on falling pressure technique by Tavares et al. [51]. In-plane and through thickness permeability at ambient and heated conditions was measured by Arafath et al. [34] with a steady-state experimental set-up based on work by Seferis et al. [50]. Studies have shown that gas permeability is anisotropic and generally significantly greater in in-plane compared to through-thickness at ambient conditions for prepregs that are created by applying a resin film to the surface of the dry fibres [11, 53, 54].

2.2.3 Void Characterization

Different methods are used for void characterization of composites including ultrasonic imaging [6, 55, 56, 57, 58], thermal imaging [59, 60], micro computed tomography (μCT) [61, 62, 63], microscopy [64, 65, 66], and the density method [16, 60]. The most suitable method is dependent on the component to be evaluated and on requirements of the study. Infrared thermography and ultrasonics are non-destructive methods which are commonly used in industry due to their speed and ease of use [67, 68]. The main drawbacks of these two methods are their low resolution (hundreds of microns) and the uncertainty associated with indirect measurements (e.g.,

quantification of defect location). Ultrasonic methods work based on ultrasonic sound wave attenuation. This method is usually used for planar samples in through-transmission or back scattering modes. Degradation of the feature contrast by shadowing of strong scattering features located above the area of interest [59, 67] and the requirement of a coupling medium between the transducer and composite part are some of the limitations of this method. Infrared thermography detects features of interest based on small changes in thermal diffusivity caused by inhomogeneities in composite materials [59]. In this method the composite is heat irradiated and thermal patterns are produced. Defects change the heat flow and the thermal pattern of a defective zone is very different than the undamaged portion of the composite. This creates the required contrast for flaw detection [67]. Sensitivity of IR thermography is generally restricted to defects near the surface [67].

Micro computed tomography (μCT) is a high resolution (tens of microns) non-destructive method which provides rich three-dimensional information about the internal microstructure of the laminate (Figure 2-4). The main limitations of this method are small sample size, high cost and long data acquisition and reconstruction times. In this method a series of X-ray attenuation measurements are generated with a μCT scanner and are used to create three dimensional computed reconstructed images of an object. This method has been used for defect characterization in fiber composites [61, 62, 63, 69]. To get an image with acceptable contrast, reinforcement and matrix should ideally be from different materials with high atomic numbers [64].

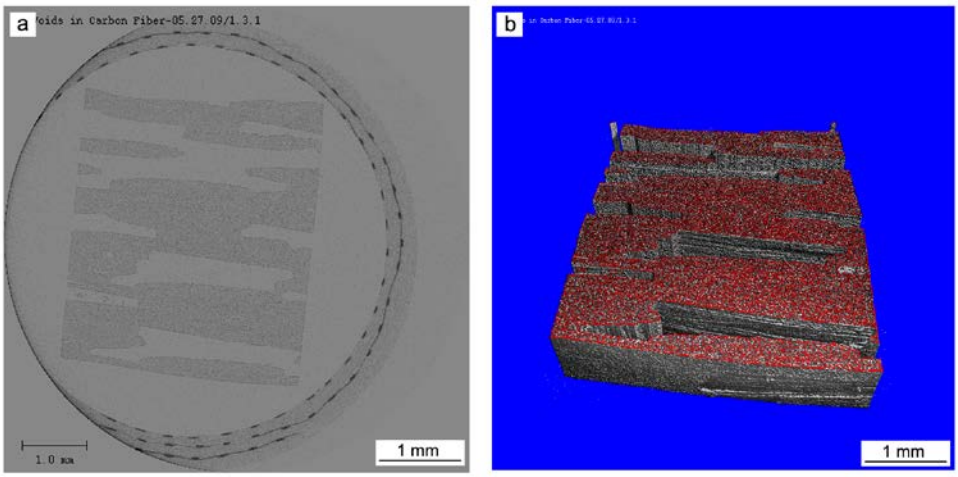

Figure 2-4 µCT of porous CFRP laminate, a) two-dimensional slice, b) three-dimensional microstructure.

Optical microscopy is a well-established and widely used method for microstructural investigation of materials. This method provides high resolution (≈ 0.2 µm) morphological information about void size, shape, distribution and content in a cross section. Optical microscopy is a destructive method and the results are from two-dimensional cross section of the sample as opposed to its bulk (Figure 2-5). An unbiased cross-section which is representative of voids in that sample is required. This method involves a lot of routine handwork and only partial automation is possible [16, 66, 64].

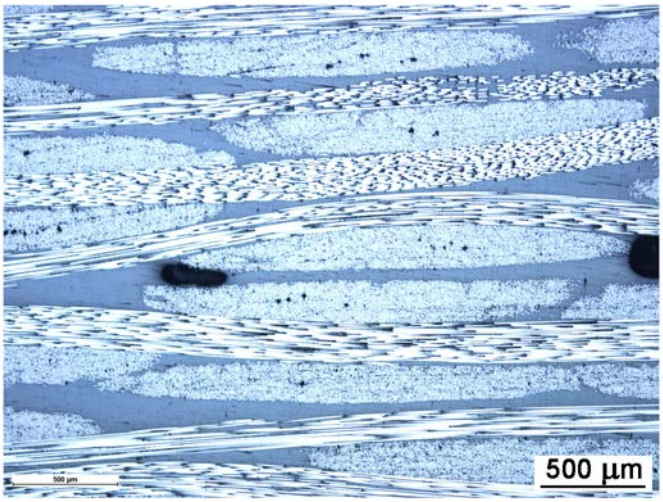

Figure 2-5 Optical microscopy image of CFRP laminate (voids are black).

The density method is the only standard method for porosity measurement in polymeric composites. In this method porosity is calculated based on the difference between the measured density of sample and its theoretical density. This method can only be used when the void content is required and morphological information is of no interest [23, 32, 37, 49]. This method is simple and fast and the measurement is based on the bulk of the material. However it is a destructive method and cannot be used as a reference method as it does not have numerical precision and bias statement [70].

The void characterization methods described in this section are well established and can be employed on fully cured rigid polymeric composites, but characterization of porosity in uncured or partially cured prepregs is challenging due to the soft (partially cured) nature of these laminates. In Chapter 4: of this thesis porosity of partially cured prepregs is investigated using optical microscopy and density methods.

Chapter 3: Thesis Objectives

Table 3-1 is an overview of the scientific literature about porosity in prepreg processing.

Table 3-1 Overview of the scientific literature on porosity in prepreg processing.

	Prepreg Type		Laminate Porosity Characterization		Fiber Tow Impregnation		Effect of Processing Parameters on Porosity		Gas Permeability Measurement (During Process)				Porosity vs. Permeability (During Process)
									In-Plane		Through-Thickness		
Principal Investigator	Auto clave	OOA	During Process	After Process	During Process	After Process	During Process	After Process	Continuous[1]	Interrupted	Continuous	Interrupted	
J. L. Kardos	[35]			[62]				[42, 62]					
B. Thorfinnson	[28, 29]							[28, 29]					
S. G. Advani		[49]			[49]	[49]				[49]			[49][2]
P. Hubert		[10, 71]		[71]	[61]	[61]		[71]			[10]		
S. Nutt		[7]		[7]	[6]	[72]		[72]					
J.-A.E. Manson		[51]									[51]		
Z. Zhang		[54]		[54]					[54]		[54]		
J. C. Seferis	[50, 73]								[50, 73]				
G. Fernlund		[21, 74]						[13]	[21, 74]		[21, 74]		

Green Cells represent fields where work has been presented in the literature. Red cells represent fields that are the subject of this thesis.

[1] In Appendix A it is shown that continuous and interrupted measurement of permeability gives different results due to effects on sample microstructure.

[2] This study investigates the relationship between resin impregnated area (not total porosity) and in-plane permeability [49].

This project started in 2009 and Table 3-1 shows that at that time the literature about porosity in OOA prepreg processing was limited. However, since 2009 more research focused on this topic has been undertaken and published which is reviewed throughout the thesis. These studies cover a wide range of topics, including the effect of various processing parameters on porosity and fiber tow resin impregnation in carbon epoxy laminates made from OOA prepregs [13, 49, 61, 71, 72], gas permeability measurements [10, 21, 49, 51, 74, 78] and porosity characterization methods for fully cured laminates [7, 71]. The focus of this project is on the areas that are shown in red in Table 3-1, which includes detailed investigation of porosity, permeability and their relationship. The main difference between this study and previous work is that it is done during processing of OOA prepregs with the actual vacuum bagging set-up, as opposed to most other studies in which only the final porosity is measured. By studying the evolution of voids and permeability during processing a better understanding of the fundamental mechanisms of gas and resin transport is developed, which serve as a basis for comprehensive physically based porosity models.

3.1.1 Objectives

Porosity is a concern in OOA processing of prepregs and the literature and understanding of fundamental mechanisms is limited in this field (Table 3-1). The goal of this thesis is to develop a fundamental understanding of porosity evolution during OOA processing of the MTM45-1/5HS prepreg. This material is representative of typical OOA carbon/epoxy prepreg system for primary aerospace structures and the findings from this system can be applied to other similar materials systems. To achieve this goal, the following objectives were defined:

1. Development of a robust method for porosity characterization of uncured and partially cured prepregs.
2. Determine the nature of void evolution in OOA processing of MTM45-1/5HS prepreg under different processing conditions.
3. Investigate the time scales for gas transport and vacuum debulk in OOA processing of prepregs on small lab scale samples and extrapolate results to large parts.
4. Develop a simple manufacturing aid that relates porosity to debulk time and other process parameters in support of better processing of these material systems.

To achieve these objectives a series of tests and analyses were performed which are summarized in Table 3-2.

Table 3-2 Summary of performed tests and analyses in the thesis.

Objective#	Test or Analysis		Chapter #
1	Characterization of porosity in partially -cured laminates using optical microscopy, density and thickness methods. Partially-cured laminates were made by stopping the process during the cure cycle.		4
2	Characterization of porosity and void distribution during 80 °C cure cycle using optical microscopy methods.		5
2	Investigation of the effect of different processing conditions on porosity during the process using optical microscopy methods.	Debulk time (hr): 0, 0.23, 4, 13.5	5
		Hold temperature (°C): 80, 120	5
		Relative humidity (%): 23, 75, 98	5
		Gas evacuation direction: In-Plane, Through-Thickness	5
		Vacuum release time: 0, 0.23, 1.23, 2.23, 4.23, 6.23, 8.23, 16.23, 22.23	6
2	Characterization of gas transport during 80 °C cure cycle using permeability tests in in-plane and through-thickness directions (in both continuous and interrupted gas flow measurement modes)		5
3	Determination of gas transport mechanisms in OOA prepreg processing by examining time scales for gas transport via Darcy flow and molecular diffusion and comparison with experimental gas permeability and porosity data. Gas transport time scales during the process are estimated based on one dimensional Darcy flow and Fickian diffusion under a constant pressure gradient for laminates of different thickness and lengths.		7
4	Development of a simple debulk map that determines the minimum required debulk time for a laminate with fixed geometry and permeability to achieve a target porosity level. This map is developed based on an existing one-dimensional model [34] for Darcy flow in a laminate with fixed porosity during debulk.		7

In the following chapters details of these tests and analyses are presented.

Chapter 4: Void and Porosity Characterization of Uncured and Partially-cured Prepregs

4.1 Introduction

There are well established methods for void characterization in fully cured polymeric composites, but characterization of porosity in uncured or partially cured composites is challenging. One of the main problems is the soft nature of the polymer matrix that may result in alteration of the void morphology during sample preparation by smearing of the matrix. There is scarce information about void characterization of uncured and partially cured prepregs in the literature. Void characterization has been used to better understand different phenomena in composites manufacturing. Centea et al. [61] studied the resin impregnation level in partially cured carbon epoxy prepregs using the micro computed tomography method (μCT). Thomas et al. [6] successfully used ultrasonic imaging in C-scan mode for detection of through-thickness resin flow through a composite laminate. Cender et al [76, 77] tracked resin film infusion in fabric prepregs using a CCD camera by placing the vacuum bag arrangement on an acrylic tool. Martin et al. [78, 79] used optical microscopy for characterization of uncured prepreg microstructure, but did not provide details of the sample preparation technique used. While these studies provide useful case specific methodologies, there are no established and validated techniques for evaluating porosity and void morphology of uncured or partially cured composites.

This chapter is focused on void characterization of partially cured carbon fiber epoxy prepregs. Porosity of partially cured prepregs is investigated using optical microscopy and density methods and the results are compared. Special sample preparation techniques were developed to enable the application of these methods to partially cured laminates. The possibility of porosity estimation based on thickness measurements as a robust, nondestructive method was also investigated. Additional studies are done on fully cured laminates to serve as a benchmark for partially cured laminates and to clarify potential uncertainties involved with porosity evaluation of partially cured prepregs.

4.2 Methods

4.2.1 Materials

MTM45-1/CF2426A prepreg manufactured by Advanced Composites Group (ACG), now Cytec Industrial Materials, was used in this study. MTM45-1 stands for the toughened epoxy matrix and CF2426A stands for HTS40 E13 6K carbon fiber reinforcement (Toho Tenax Europe GmbH company) with a five-harness satin weave pattern. The resin content of this prepreg is 36wt% and the fabric areal density 375 $\frac{gr}{cm^2}$. Two rolls of this partially resin impregnated prepreg were used in this study. The two rolls were different in terms of the resin impregnation level and therefore their initial ply thickness, initial porosity and gas permeability (Table 4-1). These two rolls of prepreg are named MTM45-1/5HS-Thin and MTM45-1/5HS-Thick, referring to their initial thickness. The results of this project suggest that the difference between prepreg rolls is consistent and intentional and not due to manufacturing inconsistencies.

Table 4-1 Specifications of the MTM 45-1 (ACG) prepregs used in this study

Name	Weave pattern	Reinforcement	Resin Content (wt%)	Areal Density (gr/m^2)	Ply thickness (mm)			
					After debulk[1]		After cure	
					average	STDEVA	average	STDEVA
MTM45-1/ 5HS "Thin"	5HS	HTS40 E13	36	375	0.46	0.015	0.395	0.004
MTM45-1/ 5HS "Thick"	5HS	HTS40 E13	36	375	0.53	0.016	0.395	0.004

[1] After 7 minutes of debulk for each four layers

4.2.2 Sample Preparation

The main goal of this study was to determine the porosity of "partially cured" laminates throughout the cure process. For this purpose a series of laminates were made by stopping the cure cycle at different times during the process (Figure 4-2 a) and evaluating the void morphology and porosity at that time in the process. Each laminate consisted of 8 prepreg layers of 127 mm × 127 mm and laminates were bagged according to the manufacturer's recommendations (Figure 2-2 c) [52]. A room temperature debulk was performed for 7 – 10 minutes for every 4 layers under full vacuum (absolute pressure < 4.0 kPa). The laminate was then placed on a release coated tool plate and peel ply strips were put on the edges to serve as breathing pathways as recommended by the prepreg manufacturer. The laminates were then covered with a non-perforated teflon release film and a breather layer, and the whole arrangement was vacuum bagged. The vacuum bagged laminates were placed in a Thermotron oven for the cure process (Figure 4-1). The cure cycle consisted of a 0.5 ($\frac{^\circ C}{min}$) heat up ramp to 80 °C, a 20 hour hold at 80 °C, followed by a two hour post cure at 180 °C. This cure cycle conforms to the manufacturer's recommended cure cycle (MRCC), except the heat up ramp which was selected to be lower than the recommended range (1 – 3 ($\frac{^\circ C}{min}$)). The lower ramp rate

was chosen to provide a larger time span for the void evolution study. Full vacuum (absolute pressure < 4.0 kPa) was applied during the entire cure process. The cure times for laminates made of MTM45-1/5HS-Thin were 0 (as-laid up), 0.23 (debulked), 1.23 and 22.23 hours. The cure times for MTM45-1/5HS-Thick laminates were 0 (as-laid up), 0.23 (debulked), 0.73, 1.23, 1.73, 2.23, 4.23, 6.23, 8.23 and 22.23 hours. The laminates were cooled down using a fan. Some rebounding occurred in as laid up and debulked samples (thickness data suggests it can contribute to porosity by maximum 4%). However, rebounding was negligible for partially cured laminates (Appendix I). In the case of rebound (as laid up and debulked), samples were taken for optical microscopy after reaching the rebound plateau.

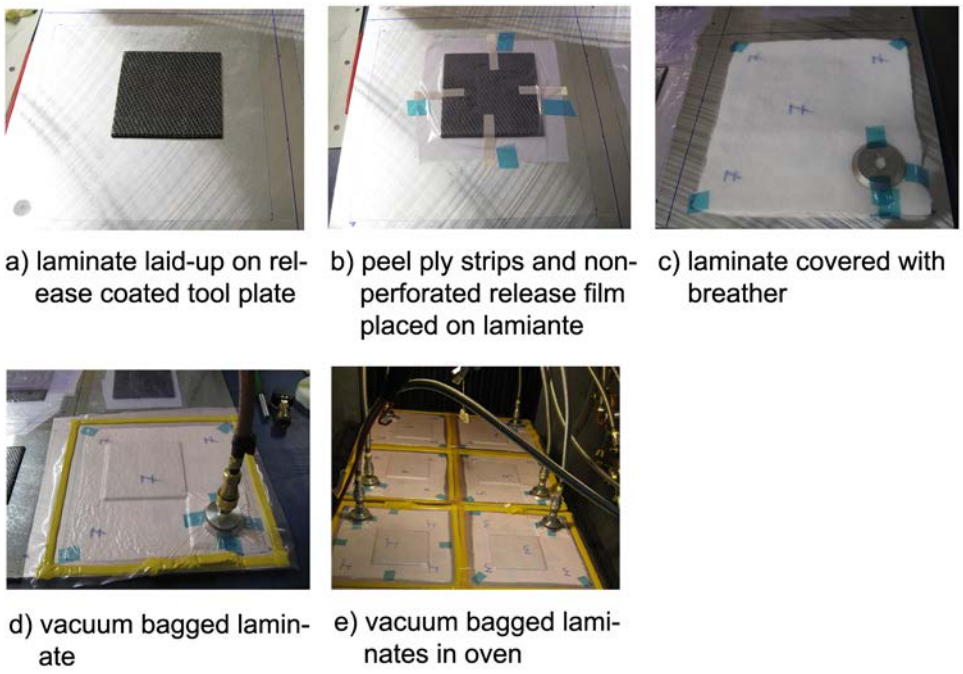

Figure 4-1 Vacuum bagging steps.

A series of “fully cured” samples were also made to serve as a bench mark for the study of partially cured laminates. These fully cured porous laminates were made by releasing the vacuum at different times during the process, but letting the samples continue to full cure through the complete temperature cycle (Figure 4-2 b). The fully cured laminates were made of MTM45-1/5HS-Thin prepreg and they had the same size and used the same bagging procedure and processing cycle as the partially cured laminates. The vacuum was released after 0 (as-laid up), 0.23 (debulked), 1.23, 2.23, 4.23, 6.23, 16.23 and 22.23 hours during the process.

Two to three replicate samples were made for both fully and partially cured laminates. The porosity of a “fully cured” laminate where vacuum was released at time “t” is different than a “partially cured” laminate that was removed from the oven at time “t”. For “fully cured” laminates, the compaction pressure is removed at time t, but the heating is continued to the end of the temperature cycle, which can potentially result in fiber bed rebound and creation of porosity after the vacuum is released, which is not seen in partially cured samples that at time t are removed from the oven.

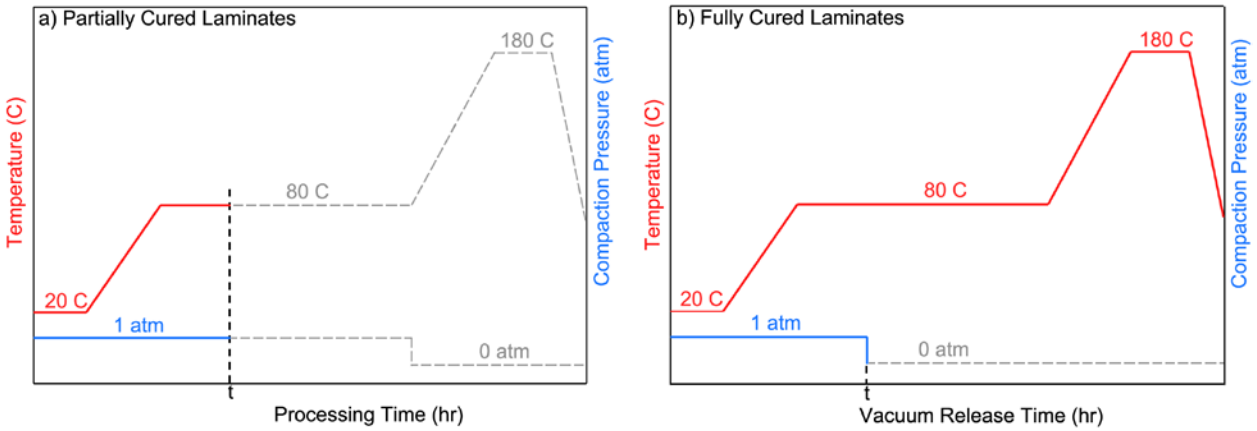

Figure 4-2 a) Processing cycle for "partially cured" laminate: In this test, both temperature and compaction pressure are stopped at time t and the sample is removed for further analysis. b) Processing cycle for "fully cured" laminate: In this test, compaction pressure is released at time t, while temperature cycle is continued to the end of the cycle. Then the sample is removed for further analysis.

4.2.3 Optical Microscopy

Optical microscopy and image analysis was used to determine porosity of partially and fully cured laminates. The first stage was surface preparation. Fully cured laminates were prepared based on standard procedures (ASTM E2015 - 04 "Standard guide for preparation of plastic and polymeric specimens for micro-structural examinations") [83]. Surface preparation of partially cured samples for optical microscopy needs special care, as the partially cured epoxy is still soft. The soft epoxy does not offer enough support during the surface preparation steps (cutting, grinding and polishing) which can potentially damage the surface and alter the surface morphology. In this study a new method was developed to create more support for partially cured samples during surface preparation (Figure 4-3).

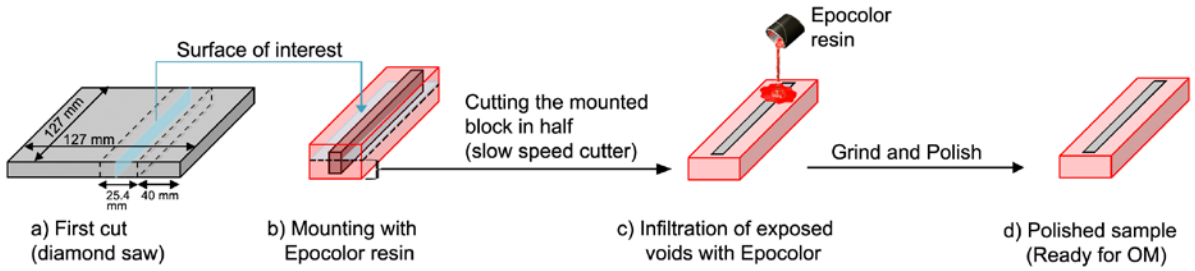

Figure 4-3 Preparation of partially cured samples for optical microscopy.

First, the location of the surface of interest (OM cross section) was determined. Then a 25.4 mm wide strip around that cross section was cut using a diamond saw (step a). The dried strip was mounted with a special low viscosity (0.55 Pa.s), room temperature curing resin (Epo color, Buehler). The mounted sample was cut into half with a slow speed cutter (step b). The cut cross section was then infiltrated with degassed Epo-color resin to fill the exposed voids (step c). After the Epo-color was fully cured, the surface was ground and polished using 320, 600 and 1200P (≈ 6 – 9 µm abrasives) grit papers and six and one micrometer polishing suspensions (step d). The aim of steps b and c is to provide enough support for the laminate during the cutting and surface preparation steps. A similar method has been used by Dillon et al. [84] to support fiber networks in uncured prepregs during polishing.

Once the surface is ready, 100X magnification mosaic images were taken automatically from the entire cross section in bright field mode for fully cured laminates and both bright-field and dark-field modes for partially cured laminates. A Nikon optical microscope (EPIPHOT 300) equipped with motorized stage and Clemex software were used for digital mosaic image acquisition from the laminate cross section (Figure 4-4).

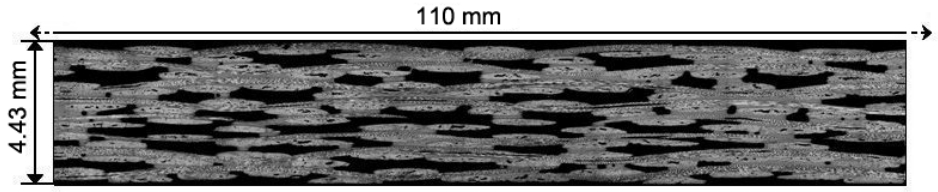

Figure 4-4 Part of an OM mosaic image (Vent time: 0 hour).

In partially cured laminates, voids are filled with Epo-color resin that has the same color as the epoxy matrix of the laminates in bright-field mode, which makes it hard to distinguish the filled voids from the matrix. However, the Epo-color mounting resin is dye enhanced and has a high contrast with the epoxy matrix in dark-field mode, so the voids can be distinguished from the epoxy matrix (Figure 4-5).

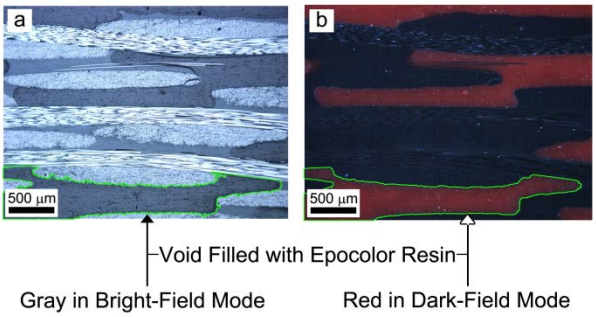

Figure 4-5 Use of Epo-color mounting resin for distinguishing the resin filled voids from the resin matrix by comparison of bright-field and dark-field images, a) Bright field, b) Dark field.

The area fraction of voids was used as a measure of porosity and the image – J software was used for image analysis and area measurements [85]. Voids were selected manually via comparison of bright field and dark field images (Figure 4-5). Image analysis was done on the whole laminate cross section (≈ 110 mm × 4 mm) to make sure that an accurate representation of the voids was captured. Two to three replicate samples were analyzed for each data point.

4.2.4 Density Measurements

The only standard test method for determination of porosity in polymeric composites is ASTM D2734 "Standard test method for void content of reinforced plastic" [70]. In this method porosity is calculated based on the difference between the measured density of the sample and its theoretical density.

$$\varphi\ (\%) = \frac{\rho_{\ (theoritical)} - \rho}{\rho_{\ (theoritical)}} \times 100 \qquad (4\text{-}1)$$

Where φ (%): porosity, $\rho_{\ (theoritical)}(\frac{gr}{cm^3})$: theoretical composite density, $\rho\ (\frac{gr}{cm^3})$: measured composite density. The theoretical density of fiber reinforced composites can be calculated using the following equation

$$\rho_{theoritical} = \frac{100 \times \rho_R \times \rho_F}{\%R \times \rho_F + \%F \times \rho_R} \qquad (4\text{-}2)$$

Where $\rho_R\ (\frac{gr}{cm^3})$: resin density, $\rho_F\ (\frac{gr}{cm^3})$: fiber density, $\%R$ (weight percent): resin in composite, $\%F$ (weight percent): fiber in composite.

Table 4-2 Required parameters for calculation of composite theoretical density

$\boldsymbol{\rho_R\ (\frac{gr}{cm^3})}$	$\boldsymbol{\rho_F\ (\frac{gr}{cm^3})}$	$\boldsymbol{\%R}$ **(wt%)**	$\boldsymbol{\%F}$ **(wt%)**	$\boldsymbol{\rho_{theoritical}\ (\frac{gr}{cm^3})}$
1.18 [**52**]	1.76 [86]	36 [52]	64 [52]	1.4953

The theoretical density of the prepreg used in this study (MTM45-1/5HS) is 1.49 $(\frac{gr}{cm^3})$ (Table 4-2). The sample density is determined based on test method A of D2734, "standard test method for density and specific gravity (relative density) of plastics by displacement" (ASTM D792) [87]. In this method the density is determined based on Archimedes law via measurement of the sample weight in air and water.

$$\rho = \frac{\rho_{water}}{1 - \frac{m_{water}}{m_{air}}} \quad (4\text{-}3)$$

Where ρ_{water} ($\frac{gr}{cm^3}$): density of distilled water at test temperature, m_{air} (gr): mass of sample in air, m_{water} (gr): mass of sample in water. The density of air free (boiled) distilled water at the test temperature (21° C) is 0.9979 ($\frac{gr}{cm^3}$) [87].

Five samples (30 mm × 30 mm × 4 mm) were used to generate each porosity data point. A Pinnacle series analytical balance from Denver instruments with a precision of 0.1 mgr was used. The surface of the sample has to be smooth and free of geometrical irregularities that tend to trap air bubbles. Some of the samples used in this study had surfaces with exposed porosity, which can be a source of error due to air bubble entrapment and water penetration. The surface of these samples was coated with an air drying polyurethane coat, M-Coat A (Vishay Company) [88]. A correction to account for the added layer of coat is required [89]

$$\rho = m_{ua}\left[\left(\frac{m_{ca} - m_{cw}}{\rho_w - \rho_a}\right) - \left(\frac{m_{ca} - m_{ua}}{\rho_c - \rho_a}\right)\right]^{-1} + \rho_a \quad (4\text{-}4)$$

Where ρ ($\frac{gr}{cm^3}$): measured composite density, m_{ca} (gr): mass of coated sample in air, m_{ua} (gr): mass of uncoated sample in air, m_{cw} (gr): mass of coated sample in water, ρ_w ($\frac{gr}{cm^3}$): water density, ρ_a ($\frac{gr}{cm^3}$): air density, ρ_c ($\frac{gr}{cm^3}$): coat density.

The density of dry air at 20 °C and atmospheric pressure is 1.2041 ($\frac{kg}{m^3}$) and the density of the coating material is 1.05 ($\frac{gr}{cm^3}$). All partially cured samples and fully cured samples with porous surfaces (vacuum release time = 0, 0.23, 1.23, 2.23, 4.23 hours) were coated.

4.2.5 Thickness Measurements

The thickness of the samples was measured with a Pro-Max digital caliper from the Fowler company (accuracy: 0.02 mm). The reported thickness of each laminate is the average of twelve measurements. Measurement points were located 25.4 mm away from the laminate edges on the 127 mm × 127 mm × 4 mm laminates.

4.3 Results and Discussion

Characterization of porosity during processing of prepregs is a challenging task and very limited work is available in the literature. In the following section, the possibility of using optical microscopy and density methods for characterization of porosity in partially cured laminates is evaluated. In the section after that prediction of porosity based on thickness measurements is investigated.

4.3.1 Optical Microscopy and Density Methods

The ultimate goal of this study is to develop a methodology to characterize porosity in partially cured samples using optical microscopy and density methods. The As a first step, porosity is studied for fully cured samples to serve as a benchmark for partially cured samples. A series of fully cured laminates were made for this study and all laminates were exposed to the same temperature cycle. The difference between them is the time when vacuum was released, and thereby the compaction pressure on the sample. The porosity of these laminates was measured via optical microscopy and density methods.

4.3.1.1 Fully Cured Samples

In the optical microscopy method porosity of a laminates is calculated based on the area fraction of voids in a mosaic image covering the entire cross section of the laminate. Figure 4-6 shows an optical microscopy mosaic image from the cross section of a sample that has been fully cured without vacuum (vacuum release time = 0 hour). A mosaic image from the entire cross section of the laminate enables investigation of porosity, porosity distribution and also provides a thorough representation of void morphology. This provides us with direct and detailed information about the type, shape and size of voids which is valuable information for understanding porosity in these material systems. For example two types of voids can be seen in Figure 4-6. The first type is located inside the fiber tows and the second is the large elongated voids between plies. It has been suggested that the first group play a key role in in-plane gas evacuation and porosity reduction in OOA prepregs [39]. These voids originate from the partial resin impregnation of the fiber tows, while the large elongated ones are the air pockets entrapped between the layers during the layup stage.

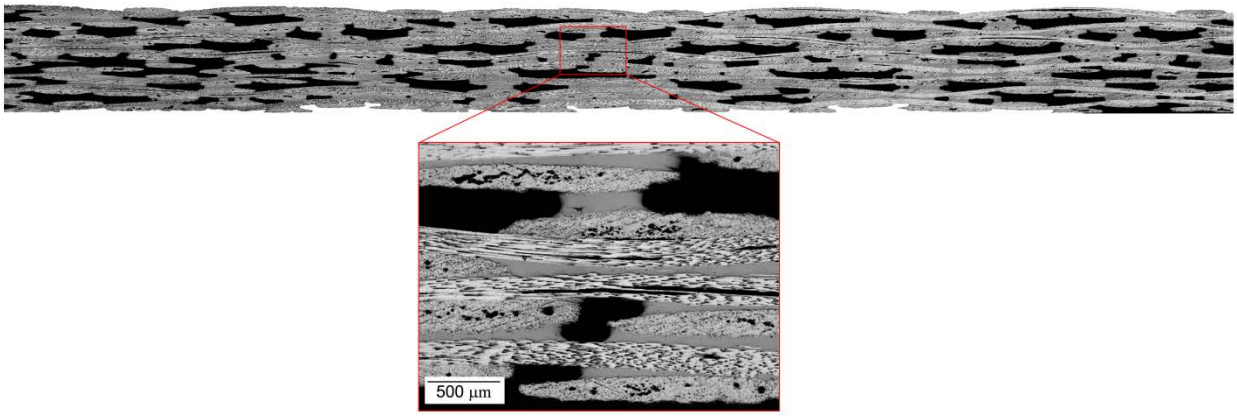

Figure 4-6 Part of a mosaic OM image of a laminate fully cured without vacuum (vacuum release time = zero hour).

The porosity of the fully cured laminates is also calculated using the density method [70]. This method has the advantage of investigating the porosity in the bulk of the material, compared to a two dimensional cross section used for optical microscopy. The density of each sample is calculated based on Archimedes law using weight measurements in air and water. Samples with exposed pores were coated to prevent water penetration into them. The weight of these samples was measured before and after coating in air and after coating in water (Table 4-3).

Table 4-3 Density of fully cured laminates and the required weight measurements for their calculation.

Sample vent time (hr)	mass in air (gr)				mass in water (gr)		ρ ($\frac{gr}{cm^3}$)	
	before coating		after coating					
	Average	STDEVA	Average	STDEVA	Average	STDEVA	Average	STDEVA
0	3.9487	0.1682	4.1290	0.1839	0.5392	0.0355	1.1528	0.0084
0.23	3.9911	0.0687	4.1771	0.0719	0.5163	0.0171	1.1432	0.0044
1.23	4.0164	0.0959	4.1541	0.1072	0.6294	0.0249	1.1811	0.0077
2.23	3.9951	0.0601	4.2044	0.0816	0.7496	0.0496	1.2248	0.0187
4.23	3.9511	0.1239	4.1077	0.1380	0.7898	0.0557	1.2443	0.0166
6.23	3.9711	0.1082	Not coated		1.2856	0.0362	1.4756	0.0017
16.23	3.9098	0.1298			1.2722	0.0443	1.4792	0.0021
22.23	3.8750	0.2653			1.2638	0.0880	1.4808	0.0015

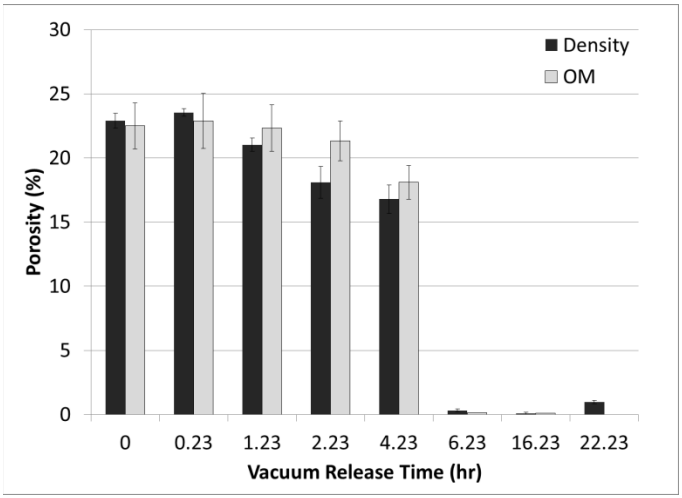

Figure 4-7 Comparison of measured porosity of fully cured laminates (MTM45-1/5HS-Thin) obtained from optical microscopy (OM) and density methods. Optical microscopy (OM) porosity at 22.23 hrs is 0.3% and not visible in the figure.

Figure 4-7 shows the porosity of fully cured laminates obtained from optical microscopy and density methods. The porosity values from these two methods are similar, with absolute deviations less than 3%. This level of deviation is not surprising as each of these methods have their limitations. In optical microscopy porosity is calculated based on information from a two dimensional cross-section and not the bulk of the material. The density method is the only standard for determination of porosity in polymeric composites, however as mentioned in ASTM D 2734, "This method does not yet contain a numerical precision and bias statement and it shall not be used as a referee method in case of dispute". Also, this method cannot be used on laminates with porosity less than 1% [70]. Ghiorse [16] did a comprehensive study on porosity measurement using these two methods in cured carbon epoxy prepregs. He reports a good relative agreement between results obtained from these methods but with an absolute deviation of up to 4% [16].

4.3.1.2 Partially Cured Samples

Optical microscopy and density methods are well established methods, traditionally used for determination of porosity in fully cured laminates [16, 65]. However, these methods cannot be applied to partially cured laminates in their original form. In this section the porosity of a number of partially cured laminates are studied using modified sample preparation techniques for optical microscopy and density methods. Four groups of laminates were prepared for this study: as laid-up, room temperature debulked, one hour partially cured and 22 hours fully cured laminates. Figure 4-8 shows section of a mosaic optical micrograph of an as laid up laminate (processing time = 0 hour) used for porosity measurement via the optical microscopy method. Table 4-4 contains the density and weight measurements in air and water for porosity calculation via the density method.

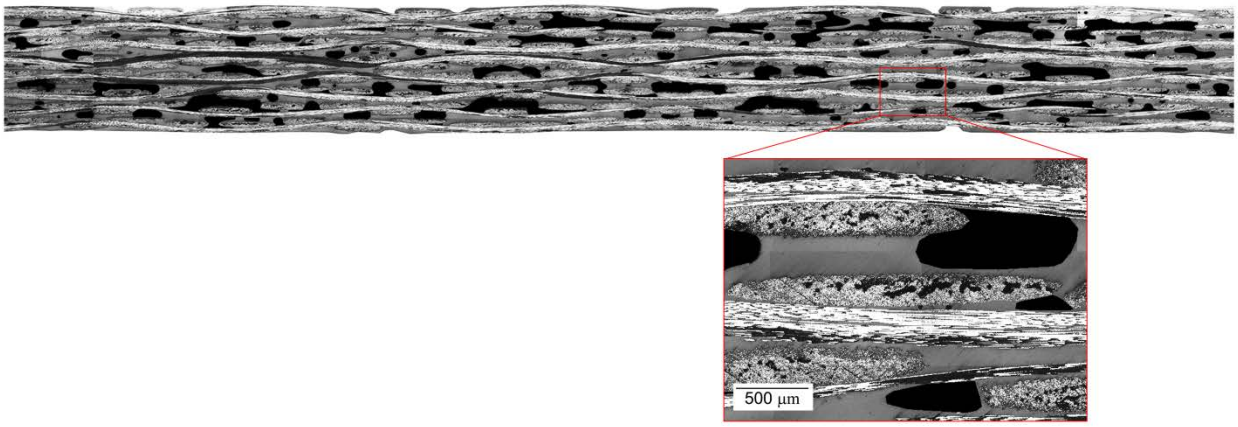

Figure 4-8 Part of a mosaic OM image of an as laid-up, uncured laminate (processing time = zero hour).

Table 4-4 Density of partially cured laminates and the required weight measurements for their calculation.

Sample vent time (hr)	mass in air (gr)				mass in water (gr)		ρ ($\frac{gr}{cm^3}$)	
	before coat		after coat					
	Average	STDEVA	Average	STDEVA	Average	STDEVA	Average	STDEVA
0	4.2999	0.0800	4.7093	0.0938	0.8755	0.0262	1.2458	0.0155
0.23	4.3015	0.1515	4.6486	0.1941	0.9512	0.0475	1.2747	0.0148
1.23	4.3489	0.1445	4.5632	0.2141	1.1303	0.0509	1.3436	0.0186
22.23	3.8750	0.2653	Not coated		1.2638	0.0880	1.4808	0.0015

To perform density test on partially cured samples, the samples have to be coated with a sealant to cover the exposed voids on the surface. The necessity of coating the surface of partially cured samples is illustrated by doing a density test on uncoated as laid-up samples. The uncoated samples have a higher measured density and lower apparent porosity ($\rho = 1.3228 \frac{gr}{cm^3}$, $\varphi = 10.63\%$) in comparison with coated as laid-up samples ($\rho = 1.2458 \frac{gr}{cm^3}$, $\varphi = 15.82\%$) due to penetration of water into their exposed pores. The measured porosity of partially cured samples are presented in Figure 4-9.

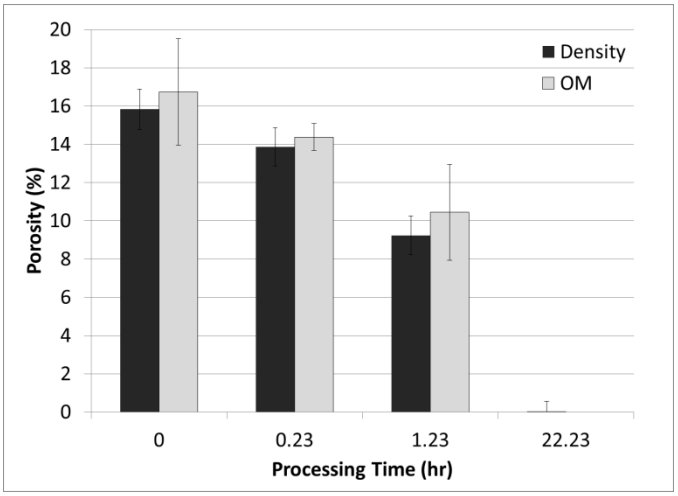

Figure 4-9 Porosity of partially cured samples obtained from OM and density methods (MTM45-1/5HS-Thin).

Porosity from optical microscopy and density methods are in close agreement with deviations less than 1% absolute. This means that using the sample preparation techniques developed in this study, these two methods can be used for determination of porosity in partially cured prepreg laminates. Optical microscopy can be used to gain more insight into the evolution of laminate microstructure including voids during the process. However, the drawback is that the sample preparation technique is time consuming and destructive. In the next section porosity estimation based on non-destructive thickness measurements is investigated.

4.3.2 Thickness as a Proxy for Porosity

The laminate thickness varies during the process. Factors such as porosity reduction, thermal and chemical shrinkage and resin bleed are potential sources of thickness reduction in prepreg processing. Net resin prepreg systems are designed to have insignificant resin bleed. Weight measurement in this study shows resin bleed to be in the range of 0.3 – 1 wt%. Thermal and chemical shrinkage is estimated to be about 4% at maximum [90, 91], and it can be assumed that porosity reduction is the major contributor to thickness reductions of more than 5% during the process. If porosity reduction is the only cause for laminate thinning, porosity (φ) can be estimated from the difference between instantaneous laminate thickness (t_i) and thickness of a fully cured zero porosity laminate (t_0)

$$\varphi = \frac{t_i - t_0}{t_i} \times 100 \qquad (4\text{-}5)$$

To investigate the validity and accuracy of porosity estimations by the "thickness method", porosity estimates using this method are compared with porosity values obtained from optical

microscopy and density methods (Figure 4-10). This comparison uses the available porosity data obtained from optical microscopy and density tests results for MTM45-1/5HS-Thin in section 4.3.1 (Figure 4-10 a, b). Another set of optical microscopy porosity data is taken from the work in section 5.3.1.3 on laminates made of MTM45-1/5HS-Thick prepreg (Figure 4-10 c). The porosity values estimated by the thickness method are calculated from the average thickness of the laminates measured by caliper (t_i) and the baseline thickness (t_0). The baseline thickness (t_0) is calculated based on the average cured ply thickness of fully cured zero porosity laminates processed under the same conditions as the laminate of interest (CPT_0). The average CPT_0 for laminates made from MTM45-1/5HS-Thin and Thick prepregs processed with an 80 °C cure cycle and measured with caliper is 0.41 mm. The difference between MTM45-1/5HS-Thin and Thick prepregs is in their initial impregnation level and porosity. Figure 4-10 shows porosity estimates from thickness measurements compared to porosity values obtained from optical microscopy and density methods.

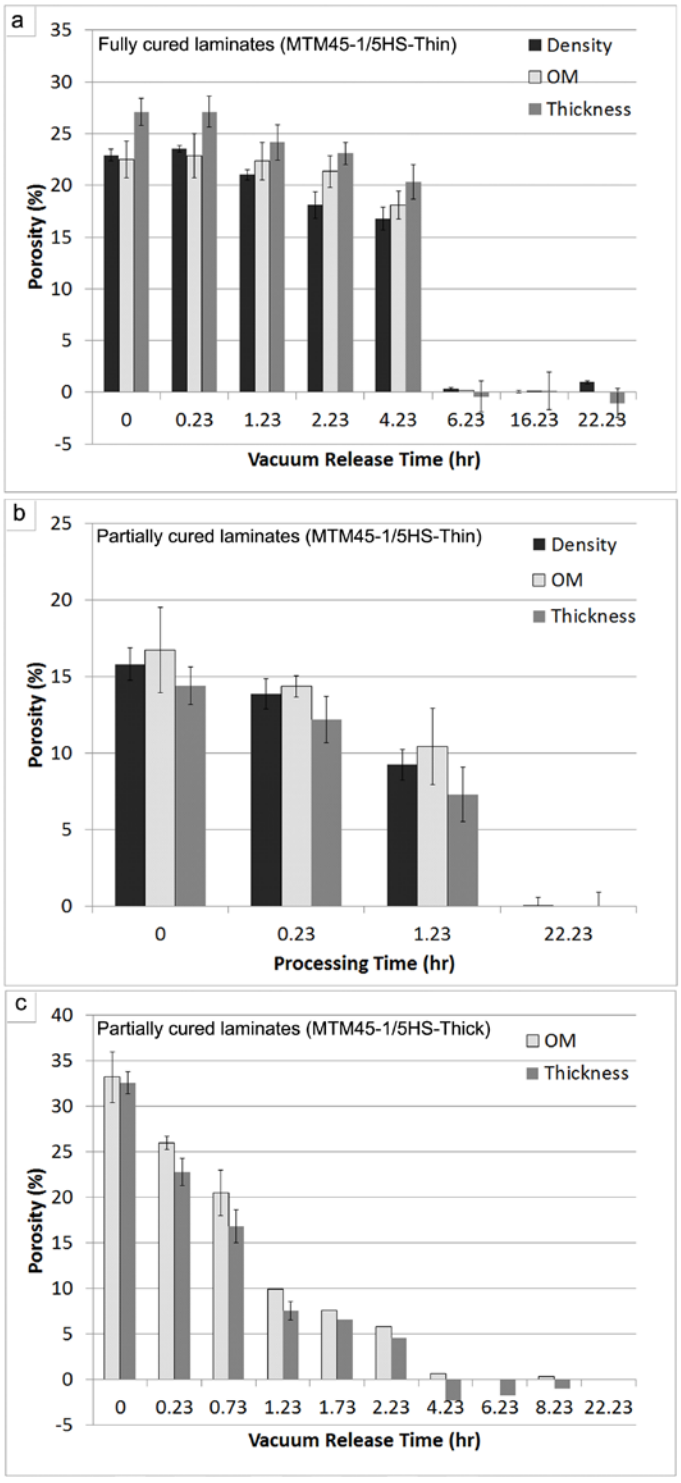

Figure 4-10 Porosity estimated from the thickness method compared with porosity from optical microscopy and density methods, a) fully cured laminates (MTM45-1/5HS-Thin), b) partially cured laminates (MTM45-1/5HS-Thin) and c) partially cured laminates (MTM45-1/5HS-Thick).

Thickness based porosity values shows the same trend as porosity measured by the other methods in all data sets (a, b and c). The absolute deviation from porosity values obtained from the other two methods is less than 5% for fully cured laminates and less than 2.5% for partially cured laminates. The thickness based porosity is higher than the other methods in fully cured laminates (Figure 4-10 a) but lower in partially cured laminates (Figure 4-10 b, c). A plausible explanation is that the thickness measurements of fully cured samples are higher than laminates' actual thickness as the samples used in this study had a rough bag surface (Figure 4-6) and the caliper sits on the rigid protrusions on the surface during measurements. Thickness measurements of partially cured samples may underestimate the actual thickness because these samples are soft and can elastically deform under moderate caliper pressure. This underestimation can result in a calculated negative porosity in the case of low porosity samples, which clearly does not have a physical meaning (Figure 4-10 a and c). Overall it can be concluded that the thickness method can measure porosity in each data set with less than 5% absolute deviation. The relationship between porosity estimated from the thickness and other methods is shown more clearly in Figure 4-11. As mentioned earlier, there is a difference between data sets belonging to fully cured and partially cured laminates.

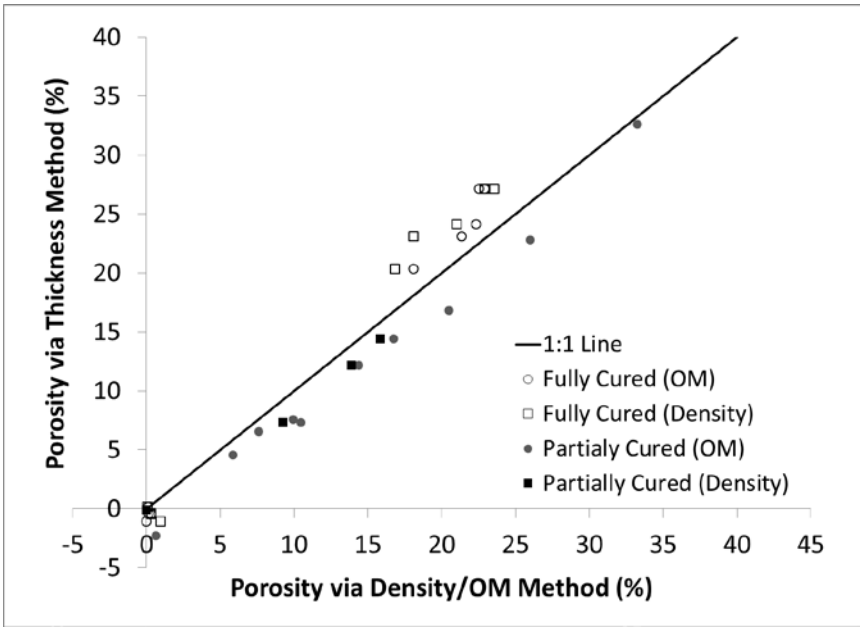

Figure 4-11 Correlation between porosity from thickness method versus optical microscopy and density methods. Thickness based porosity is above the line of equality for fully cured laminates and below it for partially cured laminates. A plausible explanation is that the thickness measurements of fully cured samples over estimates the actual thickness as the samples used in this study had a rough bag surface (Figure 4-6) and the caliper sits on the rigid protrusions on the surface during measurements. Thickness measurements of partially cured samples may underestimate the actual thickness because these samples are soft and can elastically deform under moderate caliper pressure.

Estimation of porosity based on laminate thickness is a quick, robust non-destructive method. However the results from this method are only good for rough estimations as they show up to 5% absolute deviation from the results by optical microscopy and density methods. This method is useful for porosity estimation in cases where high accuracy is not required, and when other methods are not feasible due to time and cost constrains. Each of the three methods investigated in this study have their own pros and cons and the most appropriate void characterization method

depends on the requirements and constraints of each study. Advantages and disadvantages of these methods are listed in Table 4-5.

Table 4-5 Advantages and disadvantages of three methods used for porosity determination in this study

Method	Advantage	Disadvantage
Optical Microscopy	Direct[1] method Image provides a rich source of information (void shape, size, distribution, tow geometry, …)	Labour intensive Destructive The results are from two-dimensional cross section of the sample as opposed to its bulk. An unbiased cross-section representative of the sample is required.
Density	Bulk of the sample is investigated Standard Method (ASTM D 2734)	Concerns with precision and robustness [70] Indirect method Destructive
Thickness	Fast Non-destructive	Lower accuracy Indirect method Results are affected by Resin bleed Surface profile/roughness Thickness measurement method/device Zero porosity baseline value (CPT_0)

[1] The characterization is done directly on the feature of interest.

4.4 Summary

A sample preparation technique was developed which enables optical microscopy for void and porosity characterization of soft, partially cured prepregs. In this method the soft prepreg is mounted and infiltrated with a low viscosity room temperature cure resin that provides the required support during the cutting and polishing stages. It is shown that by using this sample preparation technique, porosity of partially cured laminates can be determined by both optical microscopy and density methods. The results from these methods are in good agreement with deviations of less than 1% absolute for partially cured samples and less than 3% absolute for fully cured samples. Measured laminate thickness gave a good indication of porosity for these no-bleed prepreg samples. The correlation between porosity obtained from thickness measurements and from optical microscopy and density methods was evaluated. Porosity

calculated from laminate thickness deviates less than 5% absolute from porosity values obtained from optical microscopy and density methods

Chapter 5: Experimental Study of Void Evolution in Out-of-Autoclave Processing of MTM45-1/5HS Prepreg

5.1 Introduction

Void formation in autoclave processing has been the subject of several studies in the past [35, 3, 28, 41], and more recently for OOA processing [10, 12, 14, 75, 72, 71, 92]. Other important and relevant work in this field has been done in liquid composites molding (LCM) [77, 93, 94]. Porosity, or void content, is the volume fraction of voids in the material. To manage porosity in a part from a practical perspective we can think of it as a balance between void sources and void sinks, or void removal mechanisms. Void sources include air entrapped in the laminate during lay-up, prepregging or other processing steps (between layers, inside tows, etc), unintentional bag and tool leaks and volatiles released from the resin during processing [34]. Moisture is known as potential source of voids in composites processing and Kardos et al. [35] have done extensive research on void growth and void dissolution as a result of moisture diffusion in autoclave processing. They developed a model that predicts the void diameter as a function of processing parameters such as temperature, pressure and relative humidity. Grunenfelder et al. [7] compared the effect of relative humidity on porosity in autoclave and out of autoclave processes using a similar approach. Their results show that it is possible to produce void free parts even at high relative humidity in an autoclave, however the out of autoclave process is more sensitive to moisture and relative humidity levels higher than 75% can result in high porosity.

Due to the absence of high pressure in OOA processing, the main void sink, or void removal mechanism available to the process engineer, is vacuum evacuation of gases that are entrapped or generated inside the laminate [34]. Vacuum also provides the driving force for resin infiltration and fiber bed compaction for partially impregnated prepreg [9, 71]. Gas transport is promoted by using prepregs designed for OOA processing [25, 26], by improving laminate edge breathing [23] and by improving through-thickness gas transport via suitable consumables on top and bottom surfaces of the laminate [23, 25].

In OOA prepregs parameters such as fiber bed impregnation and resin chemistry are designed to improve their performance in terms of porosity. The un-impregnated zones of these prepregs are believed to provide dry continuous pathways through which entrapped gases can be evacuated from the prepreg, resulting in lower porosity. These pathways are often called Engineered Vacuum Channels (EVACs) [23]. EVACs are present in some autoclave prepregs too, but their importance is less than in OOA processing due to the effectiveness of the autoclave pressure to collapse and reduce the size of any entrapped or generated air [28]. Prepreg manufacturers have designed the OOA prepregs such that the EVACs can be used more effectively. The viscosity profile of OOA prepregs is designed to let the EVACs stay open for a longer time, providing the system with more time for gas removal [95]. The gas permeability of prepregs can be used to evaluate the performance of the EVACs in convective transport of entrapped air. Prepreg gas permeability has been studied in the past (see section 2.2.2.2.1) [10, 11, 50, 51]. Gas permeability in prepregs is anisotropic and at ambient conditions it is generally significantly greater in in-plane direction compared to through-thickness direction [11, 53, 54].

This chapter characterizes the evolution of voids, gas permeability and fiber tow compaction during OOA processing of small flat laminates. Several processing cycles are used: a long room temperature debulk, an 80˚C cure cycle, a 120˚C cure cycle with laminates conditioned at 23% (ambient) and 75% relative humidity conditions. The amount and distribution of voids as well as the tow geometry is studied throughout the cure cycles. The relationship between porosity evolution, gas permeability, resin infiltration and fiber tow compaction is investigated to establish the mechanisms for gas transport and void removal during cure.

5.2 Methods

5.2.1 Materials

The material used in this study is the out-of-autoclave carbon-epoxy prepreg MTM45-1/CF2426A produced by ACG (now Cytec). Two rolls of this partially resin impregnated prepreg were used in this thesis, MTM45-1/5HS-Thin and MTM45-1/5HS-Thick referring to their initial thickness (see section 4.2.1). The studies in this chapter are all done on MTM45-1/5HS-Thick prepreg. The resin viscosity during the different cure cycles was calculated using the Raven software (version 3) [19]. The software uses cure kinetics equations based on extensive calorimetric testing.

5.2.2 Sample Preparation and Partial Cycle Tests

Partial cycle tests were designed to study the evolution of voids during processing. 12.7 cm × 12.7 cm × 8 layer samples were made using a vacuum bag and oven cure according to the manufacturer's recommendations [52]. Laminates were laid up on a release coated aluminum

tool plate. A non-perforated FEP release film (A5000 high performance Violet) was placed on top of the laminate to prevent resin bleed in the thickness direction. Four strips of peel ply were placed between the laminate and the FEP film to improve the edge breathing. A breather layer covered the whole laminate and finally the entire assembly was sealed with a vacuum bag and tacky tape. Four different processing cycles were used in this study and each test was repeated three times.

Cycle 1: long debulk at room temperature. In this cycle laminates were laid-up, bagged and held under hard vacuum (absolute pressure < 4.0 kPa) at room temperature. The cycle was interrupted after 0, 0.23, 4 and 13.5 hours, and laminates were examined with optical microscopy.

Cycle 2: 80˚C cure cycle. This cycle included a seven minute room temperature debulk for every four plies in the laminate during lay-up, a 0.5 °C/min ramp to 80°C, a 20 hour hold at 80°C, followed by a 2.5 hour post cure at 180 °C [52]. A low temperature hold (80°C) and a slow heat up rate (0.5 °C/min) were chosen to minimize resin flow so that void evolution can be studied more easily. The laminates were under full vacuum (absolute pressure < 4.0 kPa) through the entire process. The cure cycle was stopped at times of interest and samples were taken out and cooled down and prepared for microscopy evaluation. Interruption times were 0 (as laid up), 0.23 (debulked), 0.73, 1.23, 1.73, 2.23, 4.23, 6.23, 8.23, 22.23 and 31 hours. All cure cycle details are according to the manufacturer recommended cure cycle (MRCC) [52], except the 0.5 ˚C/min heating ramp, which intentionally was chosen to be slower than the MRCC recommendation (1 - 3 ˚C/min) to provide longer time for void evolution during heat up.

Cycle 3: 120˚C cure cycle. This higher temperature cycle was chosen to study the effect of temperature on porosity evolution. The cycle has the same debulk time, vacuum level and ramp rate as cycle 2. It has a four hour hold at 120°C and the additional interruption times in this cycle were 2.23, 2.56, 3.23, 3.56, 4.23 and 7.56 hours. These times were selected to capture more information in the 80°C -120°C region during the heat-up ramp.

Cycle 4: Effect of humidity - Effect of 75% and 98% relative was studied.

75% Relative Humidity: Laminates were conditioned in a closed container at 75% relative humidity until equilibrium was reached (five days). The conditioning container contained $NaCl/H_2O$ salt solution and was prepared based on ASTM E104-02 “Standard Practice for Maintaining Constant Relative Humidity by Means of Aqueous Solutions”. Hsiao et al. [12] conducted experiments to determine the time required to reach equilibrium moisture content at 75% relative humidity for this material system. They showed that five days conditioning is sufficient for laminates to equilibrate. Conditioned laminates were cured according to cycle 3 and interruption times were 0, 0.23, 1.23, 2.23, 3.23, 4.23 and 7.56 hours.

98% Relative Humidity: Laminates were conditioned in a closed container at 98% relative humidity until equilibrium was reached (five days). The conditioning container contained K_2SO4/H_2O salt solution and was prepared based on ASTM E104-02. Conditioned laminates were fully cured according to cycle 3. Due to material and time constraints, no porosity evolution study was performed for 98% relative humidity.

5.2.3 Sample Preparation for Directional Breathing Tests

To evaluate the effect of the gas transport direction on porosity, samples with different sealing configurations were made from MTM45-1/5HS-Thick prepreg (Figure 5-1). 5HS laminates were made of 8 layers of 12.7 cm × 12.7 cm prepreg, cured ply thickness (CPT ≈ 0.39 mm). The laminates were prepared based on the sealing configurations shown in Figure 5-1. After edge or surface sealing, a room temperature debulk (laminate held under full vacuum under a vacuum bag at room temperature) was performed for 0.23 to 0.5 hours.

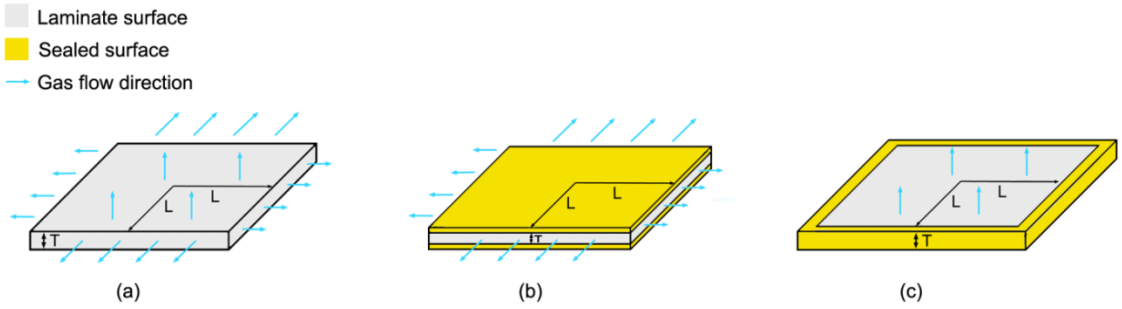

Figure 5-1 Sealing configurations: a) surface and edge breathing, b) edge breathing only, c) surface breathing only.

Configuration (a) is the manufacturer's recommended bagging procedure in which the laminate is free to breathe from all sides except the surface that is in contact with mold. In configuration (b) the laminate is sealed at top and bottom surfaces and is only able to breathe in the in-plane direction. In configuration (c) the laminate is sealed at all edges and breathing is limited to the through-thickness direction. After sealing the laminates with standard sealant tape, bagging materials were placed sequentially according to the manufacturer's recommendations (Figure 5-2) [52]. Edge breathing dams were used at the edges of the laminates with configurations (a) and

(b). All laminates were covered with non-perforated release film and a larger breather layer on top of that. Strips of peel ply were placed around the edges of the laminates to allow air paths under the release film into the breather (to provide an air path between the breather and the top surface of the laminate). A vacuum bag covered the whole arrangement and was sealed with sealant tape to the Aluminum tool. Figure 5-2 shows the laminate preparation steps. Once the samples were prepared they were cured in a Thermotron oven (Holland, Michigan, USA) with 80 °C cure cycle. Details of the 80 °C cure cycle are presented in section 5.2.2. In edge breathing tests, samples were taken out after 0 (as laid up), 0.23 (debulk), 1.23, 2.23, 4.23 and 22.23 hours. In surface breathing test samples were taken out after 0 (as laid up), 0.23 (debulk), 1.23, 2.23, 6.23, 8.23 and 22.23 hours. The times were chosen based on the in-plane and through-thickness permeability graphs (Figure 5-15) to enable evaluation of the relationship between porosity and permeability. Three repeats were done for samples with “edge and surface breathing” and all the fully cured samples (22.23 hr). One repeat was done for partially-cured samples in “edge breathing only” and “surface breathing only” tests.

Edge Breathing

a) tool plate preparation

b) sealing layer underneath tacky tape

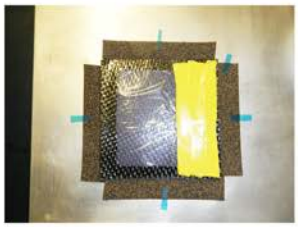

c) sealing of the laminate top surface with tacky tape

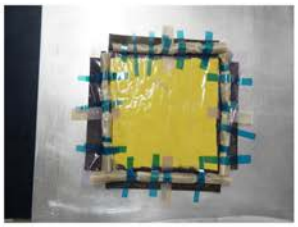

d) edge breathing dams at laminate edges

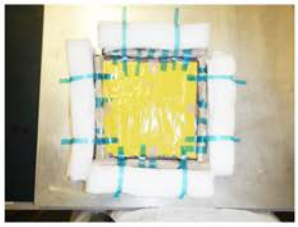

e) breather placed adjacent to edge breathing dams

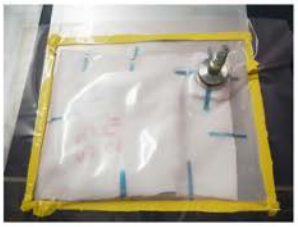

f) vacuum bagged assembly

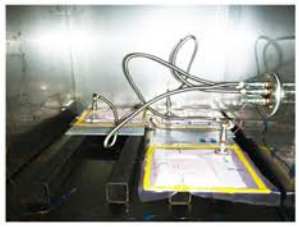

g) cure in oven

Surface Breathing

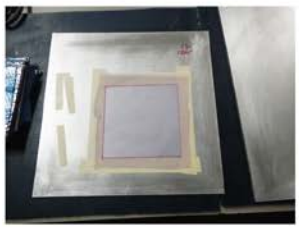

a) tool plate preparation

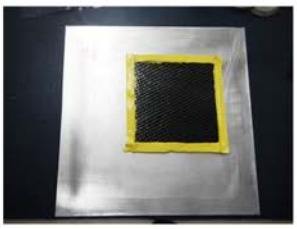

b) edge sealed laminate

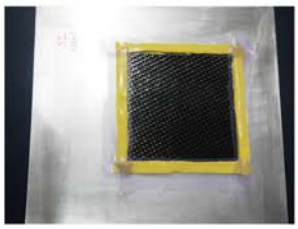

c) tacky tape covered with non-stick release film

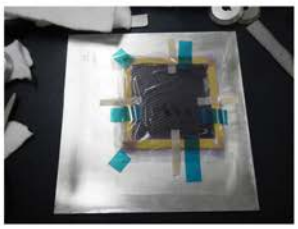

d) peel ply strips and non-perforated release film

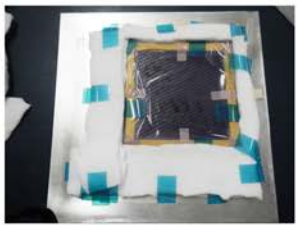

e) peel ply strips connecting laminate surface to breather

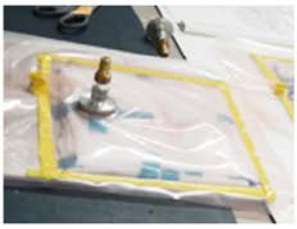

f) vacuum bagged assembly

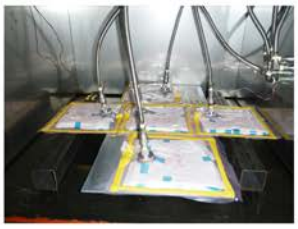

g) cure in oven

Figure 5-2 Laminate preparation steps in edge breathing and surface breathing tests.

5.2.4 Void Characterization

It is necessary to measure and characterize voids during the process to gain a thorough understanding of void evolution and underlying mechanisms. In this study several methods including µCT, density and optical microscopy were evaluated but optical microscopy (OM) was chosen as the primary characterization method due to the level of detail required from the images. Optical microscopy was used to characterize porosity and tow geometry in partially and fully cured laminates. A Nikon stereo microscope (SMZ745T) in reflection and transmission light modes was used to investigate the surface morphology of uncured prepreg. X-ray micro computed tomography (µCT35-Scanco Medical) was employed for studying the three dimensional micro structure of the laminate before processing. An X-ray voltage of 70 kV and intensity of 154 µA were used to achieve a 3µm/pixel resolution. A 7.62 cm × 6.35 cm 8 layer laminate of MTM45-1/5HS-Thin laminate was laid up at room temperature and a 5 mm × 28 mm section of this laminate was cut and scanned. The scanned data was processed and reconstructed using the µCT35 scanner software creating two dimensional slices and three-dimensional information about the porous structure of the laminate.

Optical microscopy and image analysis were the main tools used to characterize porosity and tow geometry of semi-cured and cured laminates. The first step was surface preparation of the samples. Fully cured laminates were prepared according to conventional procedures [83]. The preparation of semi-cured samples for optical microscopy requires special attention, as the partially cured matrix is still soft (see section 4.2.3). The samples were therefore mounted with a special low viscosity, room temperature curing resin (Epo-color Buehler) that filled the pores and vacant spaces of the laminate. The cured mounting resin supported the soft composite material

during the subsequent grinding and polishing steps and reduced surface damage [83,84]. Surface preparation and image acquisition steps are described in section 4.2.3. Two to three replicate samples were analyzed for each data point. To characterize voids and the geometrical features of fiber tows, the mosaic images were analyzed using the Image – J software [85]. The area fraction of voids is used as a measure of porosity. The voids are categorized into three groups: inter-laminar, fiber tow and resin voids. Details of different void types and their origins, are presented in section 5.3.1.1. The area fraction of each type of voids is measured individually and their sum is reported as void content or porosity.

$$\varphi_T = \varphi_I + \varphi_F + \varphi_R$$

Where: φ_T (%): Total porosity, φ_I (%): Inter-laminar porosity, φ_F (%): Fiber tow porosity, φ_R (%): Resin void porosity.

In partially cured laminates, direct area measurement of all voids located inside fiber tows is impractical because many of the smaller voids are located between the individual fibres and are of the size of the individual fibres or smaller. In previous work on this prepreg system, only the area fraction of larger size fiber tow voids were reported, which gives an underestimate of the total fibre tow porosity in the laminate [39, 96]. In the current work, the total fiber tow porosity of partially cured laminates is calculated based on measurements of the total area and subtracting the inter-laminar and resin void areas and the area of the final cured porosity free laminate. The location and coordinates of different voids were also measured and used to study their distribution within the laminate. The geometry of individual elliptically shaped tows were studied and characterized by measuring their minor and major axes.

5.2.5 Gas Permeability

Gas permeability is a measure of the ability of a material to transport gases under a pressure gradient, and void evolution of a laminate is related to the gas permeability. Permeability tests were performed to investigate the relationship between void evolution and gas transport during the process. The prepreg used in this study is reinforced with a woven fabric (five harness weave) and has anisotropic gas transport properties. The in-plane and through thickness permeabilities were measured at 0, 0.23, 0.73, 1.23, 1.73, 2.23, 3.23, 4.23, 5.23, 6.23, 8.23, 17.23 and 22.23 hours during the cure cycle to directly correspond with the samples used for optical microscopy. For each data point three repeats were performed. Samples were laid up, sealed on all sides except vacuum and vent sides, and vacuum bagged. The dimensions of the in-plane test samples were 5.08 cm × 10.15 cm × 8 layers and the through thickness samples 8.25 cm × 8.25cm × 8 layers. Gas flow occurs in the L = 5.08 cm direction in the in-plane test and in the thickness direction in the through thickness test (Figure 5-3). The set-up was placed in an oven and the sample was cured with the 80˚C cure cycle described in section 5.2.2. Further details of the permeability test set-up are presented in reference [74] and Appendix B .

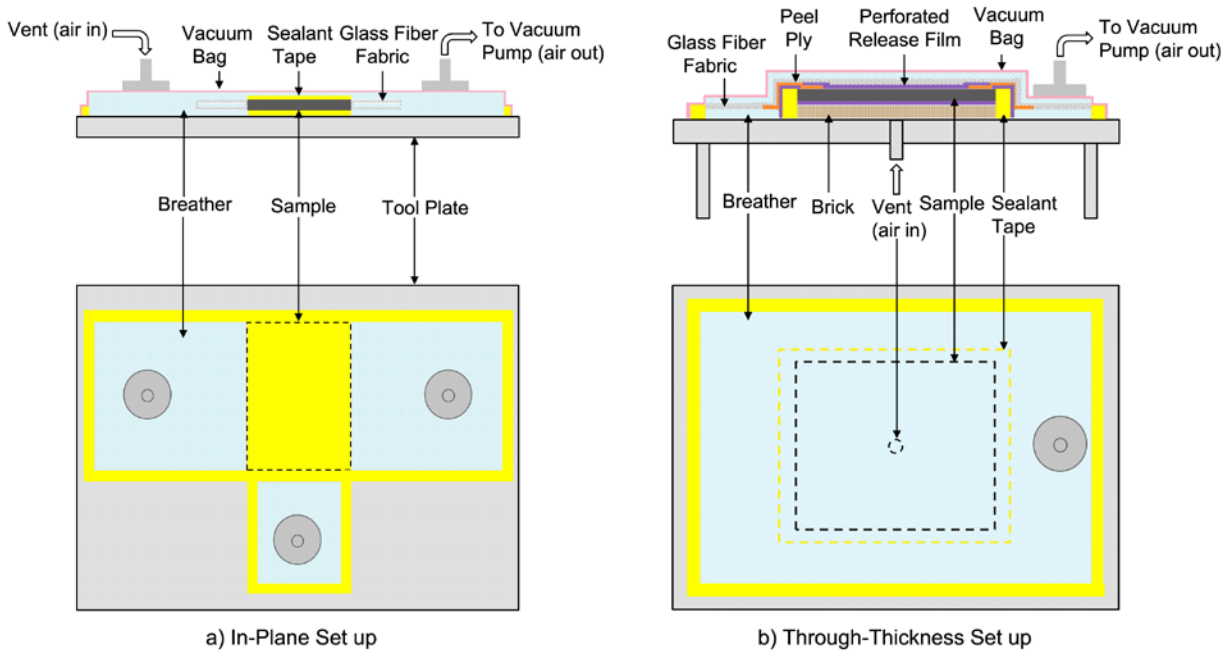

Figure 5-3 Permeability test set-up, a) in-plane b) through-thickness.

Under steady-state flow conditions, gas permeability can be calculated by measuring the gas flow rate on the vent (ambient pressure) side, the cross sectional area, the length of sample, and atmospheric and vacuum pressures. Assuming that the flow obeys Darcy's law and the gas (air) obeys the ideal gas law [34]

$$Q_a = \frac{AK}{2\mu L}\left(P_a - \frac{P_v^2}{P_a}\right) \tag{5-1}$$

Q_a is the volumetric gas flow rate measured at the vent side (m^3/s), A is the cross sectional area perpendicular to the transport direction (m^2), K is the gas permeability (m^2), μ is the dynamic viscosity of the gas (Pa.s), L is the length of the sample (in the transport direction) (m), P_a is the atmospheric pressure (vent side) and P_v is the vacuum pressure (Pa).

To determine the permeability at the specified times the sample was vented temporarily on one side as the other side was kept under full vacuum. A few minutes after the sample was vented, the airflow through the sample reached steady state and the air flow was measured with high precision mass flow sensors. The gas permeability K was subsequently calculated using equation (5-1). The dynamic viscosity of gas has a temperature dependency, which is considered in the calculations [45]. The dynamic viscosity of air at standard ambient temperature and pressure conditions is 1.82×10^{-5} Pa.s.

Through-thickness permeability of the FEP release film and the porous brick used in through thickness permeability measurement of the laminates were also measured to ensure they will not affect the gas flow, as they are placed in parallel with the laminate in through-thickness test set-up. The test set-up and measurement method is the same as the through thickness permeability test of laminates (Figure 5-3). In each test , the edges of the sample (brick or release film) was sealed with tacky tape and then the rest of the bagging materials were placed on it and bagged as shown in Figure 5-4. In the brick test, the brick was covered with non-perforated release film as opposed to perforated film which was used for laminate permeability test. The width and length of brick and release film was 78 mm and their thickness is listed in Table 5-1. In the brick test flow rate measurements was done with rotameter (37288 omega scientific rotameter, glass ball) as they were higher than digital mass flow sensor capacity (maximum flow rate = 1 L/min).

Table 5-1 Thickness of brick and release film samples used in through-thickness permeability test

	Brick	**Release Film**
Thickness (mm)	6.2	0.025

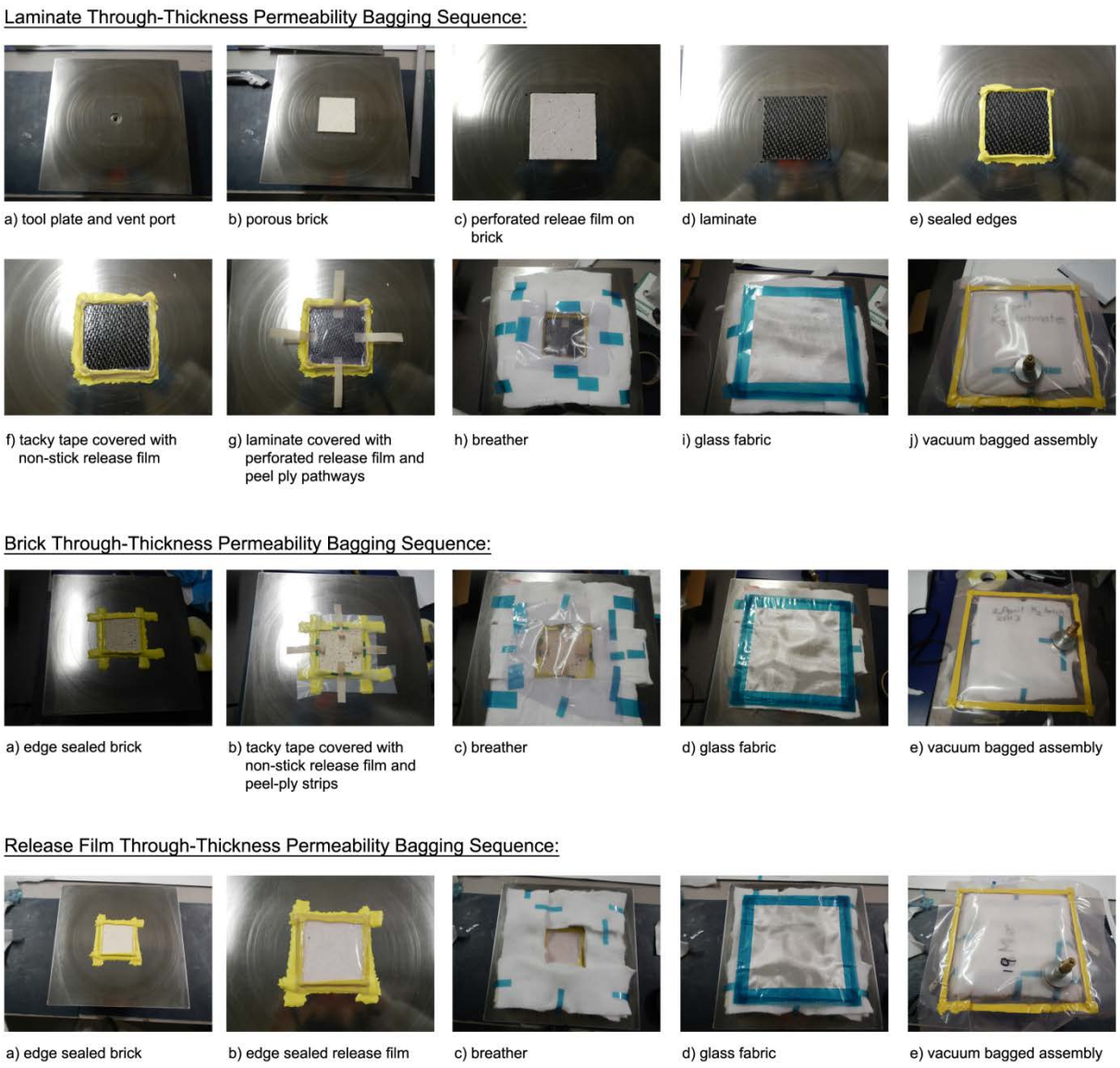

Figure 5-4 Through-thickness permeability test bagging sequence for laminate, brick and release film permeability measurements (top view).

5.2.6 Flow Measurement

This test was done to measure the gas flow rate during the long room temperature debulk test. An eight layer laminate of 124 mm × 124 mm × 4.7 mm was laid-up and bagged using the same procedure described in sample preparation section 5.2.2. Then the laminate was debulked under

full vacuum (absolute pressure < 4.0 kPa) at room temperature for a period of 10 hours. The flow rate of the gas out of the laminate during debulk was measured by the same mass flow sensor used in permeability studies (section 5.2.5). The mass flow sensor was placed in line with the vacuum line, between the laminate and the vacuum pump.

5.2.7 Thermogravimetric Analysis (TGA)

Thermogravimetric study was performed to evaluate the amount of off-gassing in three different temperature cycles (Table 5-2) and two humidity levels (ambient and 75% relative humidity). Test was done according to ASTM D3530/D 3530M, "Standard test method for volatiles content of composite material prepreg". The Discovery TGA (TA Instruments) was used for weight measurements.

Table 5-2 Temperature-time cycles used in TGA test

Cycle	Heat up ramp (°C/min)	Hold	
		Temperature (°C)	Time (hr)
80 °C cycle	0.5	80	4
120 °C cycle	0.5	120	4
200 °C ramp	0.5	200	0

Five samples were made from MTM45-1/5HS-Thick prepreg for TGA measurements. All samples had four layers and a diameter of about 7 mm. The initial weight of the samples was in the range of 75 mgr to 95 mgr. All tests were carried out in Nitrogen atmosphere with a flow rate of 25 mL/min. One repeat was done for each test.

Humidity conditioning at 75% relative humidity was done by placing the samples in a close conditioning container contained $NaCl/H_2O$ salt solution for five days (ASTM E104-02) (see

section 5.2.2.). For ambient humidity conditioning samples were placed in an open container at ambient conditions for five days (Figure 5-5). The relative humidity and temperature of the ambient condition and $NaCl/H_2O$ salt solution was measured for five days using a Fisher scientific hygrometer (Table 5-3). The exposure time of the samples during their transition from conditioning chamber to the TGA, was minimized.

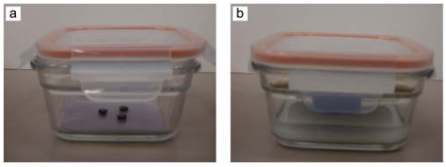

Figure 5-5 Humidity conditioning containers, a) ambient condition, b) $NaCl/H_2O$ salt solution (RH = 75%).

Table 5-3 Temperature and relative humidity of conditioning containers.

Conditioning container	**T (°C)**		**RH (%)**	
	Average	STDEVA	Average	STDEVA
Ambient	21.5	0	31.5	2.7
$NaCl/H_2O$ salt solution	21.2	0.4	69.9	1.2

5.3 Results and Discussion

5.3.1 Void Evolution Studies

5.3.1.1 Void Morphology before Processing

Figure 5-6 shows the surface morphology of the uncured prepreg. The distribution of resin film on the dry fiber tows is non-uniform and patchy; the protruding regions of the fabric are covered with resin film while the depressed regions are dry. We can visualize how when prepreg layers are placed up on top of each other, gaps will form between them as a result of the patchy resin application on the surfaces as well as the undulation of the fiber tows in the woven system. In Figure 5-6 b one layer of prepreg is imaged under a transmitted light condition to show the open spaces – pin holes - at the intersections of warp and weft tows. These pin holes are potential pathways for through-thickness gas transport at room temperature [10]. More information about the surface morphology of the prepreg can be found in Appendix C. A typical microstructure of a laminate after lay-up is shown in Figure 5-6 d. The epoxy matrix is light gray; the carbon fiber tows are white and voids are black. The voids have a complex morphology with a wide range of shapes and sizes and are categorized into three groups based on their location. Inter-laminar voids are large and elongated and their initial shape is dictated by the fiber bed architecture and resin application, and are the result of entrapped air between the layers during lay-up. Due to the non-uniform distribution of resin film on the prepreg surface (Figure 5-6 a), inter-laminar voids are surrounded with both resin film and dry fibres. Resin voids are entirely embedded in the resin and are generated during resin mixing, prepreging or potentially by resin off gassing during the cure process. Fiber tow voids are located inside the un-impregnated regions of fiber tows and are

the result of partial resin impregnation and lack of fibre tow compaction (Figure 5-6 d). Figure 5-6d shows regions with high and low fiber volume fractions within a tow for this undebulked and uncompacted laminate. Micro computed tomography (μCT) was performed to get a three-dimensional understanding of the porous structure of the prepreg (Figure 5-6 c). In this figure resin and fiber are red and voids green. Inter-laminar and resin voids are isolated from each-other, while fiber tow voids appear to have a continuous structure extending across the laminate. These images provide a fairly clear picture of the nature of porosity in un-processed, as laid up laminates. In the next sections, the evolution of voids under different processing conditions is investigated.

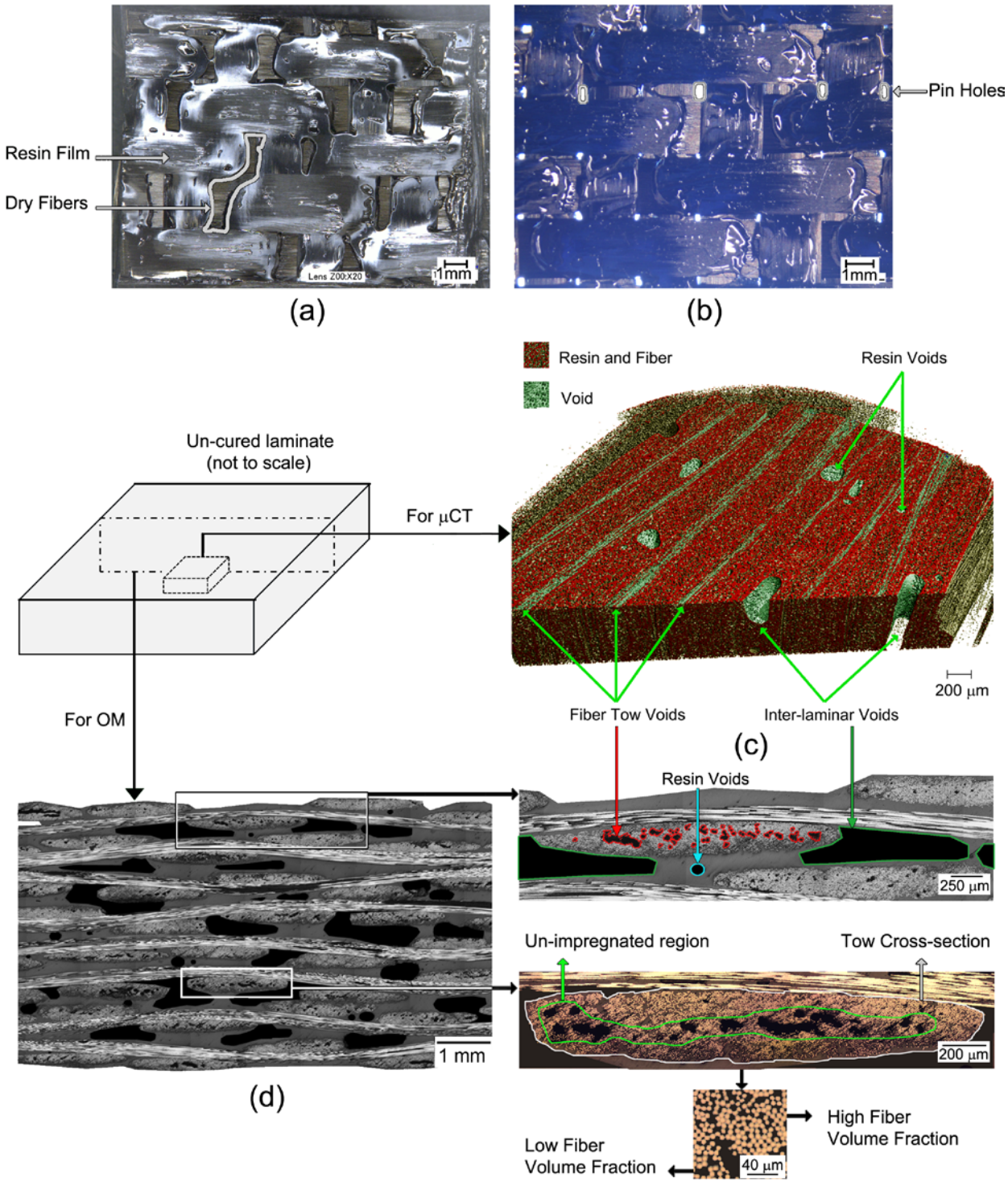

Figure 5-6 Initial state of an undebulked and uncured laminate. Stereo microscopy images of a) laminate and b) prepreg surface, c) Three-dimensional µCT image of laminate, d) Optical microscopy image of a laminate cross section.

5.3.1.2 Porosity Evolution during a Long Room Temperature Debulk

A room temperature debulk is one of the main processing steps in OOA processing in order to remove entrapped air and achieve low porosity. Some OOA prepreg manufacturers suggest debulking times as long as 16 hours or more for large complex parts [97]. In this study a room temperature debulk is performed for 13.5 hours and the microstructure and porosity of the laminate is evaluated at four different times during this period (Figure 5-7 a).

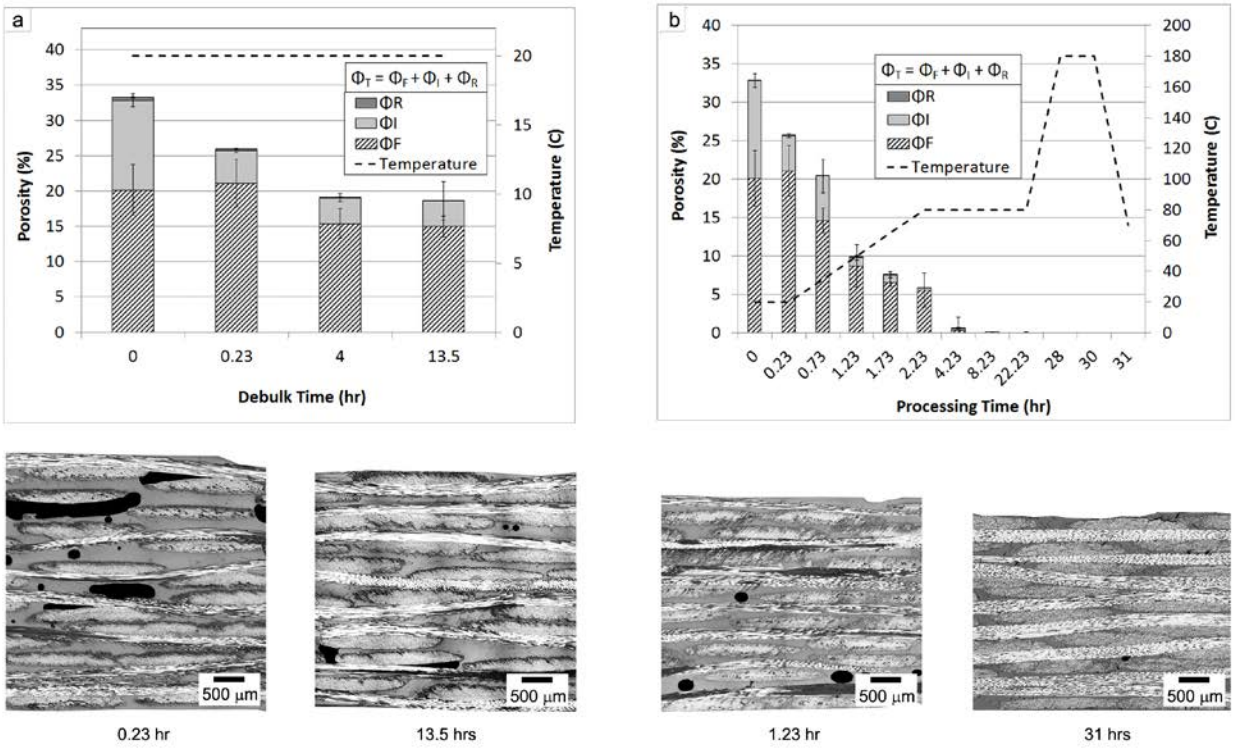

Figure 5-7 Void Evolution during a) Long room temperature debulk and b) Heated 80°C cure cycle. Note that the data for 0 and 0.23 hours are the same for the two cycles (Error bars denote +/- one standard deviation). φ_T: Total porosity; φ_R: Resin porosity; φ_I: Inter-laminar porosity; φ_F: Fiber tow porosity.

The initial total porosity (Φ_T) of the as laid up laminate is 33%. Once room temperature debulk starts, porosity decreases up to four hours, after which it stays constant at 19%. Fiber tow porosity (Φ_F) is the largest contributor to the total porosity and shows a decrease from 20% to 15% between 0.23 and four hours but is approximately constant after four hours. Fibre tow porosity is reduced via two mechanisms: tow compaction and resin infiltration. The resin viscosity of MTM45-1 is high at room temperature (~ 10^4 Pa.s), resulting in minimal resin infiltration into the fibre tows at room temperature. This suggests that fibre tow compaction is the main mechanism by which the fibre tow porosity is reduced during the room temperature debulk (Figure 5-7 a). The relationship between fiber tow porosity, fiber tow compaction and resin infiltration is studied in more detail in section 5.3.3. Inter-laminar porosity (Φ_I) is the second largest contributor to the total porosity. It decreases from 12.5% to 4.5% during 0.23 hours of debulk and reaches a 3.5% plateau value after four hours. After lay-up, prepreg layers are loosely in contact with each other and there is a fair amount of entrapped air between them. Inter-laminar voids are adjacent to fiber tows and are in contact with interconnected network of dry fiber tows (Figure 5-6 a). Thus vacuum application can relatively quickly remove much of the entrapped air and make prepreg layers better conform to each other, reducing inter-laminar porosity. Because of the stiffness of the inter-woven fibre tows and the patchy resin application on the prepreg surface some of the inter-laminar voids will remain after a room temperature debulk and will not be filled in with resin or fibres until the resin viscosity is lowered during heat up. Note that even if most air molecules are removed after debulk, there will still be an inter-laminar void until resin and/or fibres flows into the void. The amount of resin porosity (Φ_R) is small (less than 0.2%) and approximately constant during the debulk process. Resin voids can

only be evacuated through gas diffusion which is a slow process at room temperature (see section 7.3.2).

5.3.1.3 Porosity Evolution during Heat-Up and Cure

The next processing step after a room temperature debulk is heat up and cure. The first cure cycle studied consists of a 0.23 hour debulk at room temperature, a 0.5˚C/min ramp to 80˚C, a 20 hour hold at 80˚C, a 1 hour hold at 180C and cool down to room temperature. Figure 5-7 b shows the evolution of porosity and void morphology during this cure cycle. The laid up sample (0 hr) has about 33% total porosity, consisting of fiber tow voids in the partially impregnated fiber tows (20%), large inter-laminar voids (12.5%) and a small amount of resin voids (< 0.2%). After a 14-minute (0.23 hr) room temperature debulk under vacuum, the total void content decreases to about 26%, mainly due to a reduction in the inter-laminar voids. As the temperature is increased the total porosity (Φ_T) decreases, with a fairly rapid decrease in the first two hours during the temperature ramp, and becomes about 6% after 2 hours into the heat-up. At four hours, the total porosity is less than 0.4 %. Inter-laminar voids and fiber tow voids reach their minimum values (< 0.3%) after two and four hours, respectively. Reduction of inter-laminar voids can be due to Darcy evacuation through the interconnected network of fiber tow voids. Inter-laminar voids are located adjacent to fiber tows and can connect to their dry core through the un-impregnated zones between them or coalescence with them as the resin viscosity drops [98]. Resin porosity is very small throughout the process (< 0.2%) and decreases as the temperature increases. This decrease can be due to diffusion evacuation of resin voids as diffusion becomes faster at higher temperatures. It can also be due to coalescence of resin voids with low pressure fiber tow voids [98]. With the current cure cycle, the void morphology is fixed

long before gelation (18.5 hours). The continuous decrease of inter-laminar, fibre tow, and resin voids with time, suggests the absence of significant off-gassing.

5.3.1.4 Void Distribution during Heat up and Cure

The spatial distribution of voids in-plane and through thickness was evaluated based on optical micrographs. During the long room temperature debulk the distribution of voids was uniform throughout the laminate. In the 80˚C cure cycle voids are uniformly distributed up to two hours. After two hours a gradient starts to form both in-plane and through-thickness (Figure 5-8). The void distribution through the thickness is illustrated by comparing the porosity in the half of the laminate adjacent to bag versus the half adjacent to the mould. Figure 5-8 shows how the ratio of the voids on the mold side to the bag side evolves during the cure cycle. At the beginning of the process this ratio is approximately one, which means that the void distribution is uniform. At two hours the void content on the mold side is twice that on the bag side and about 4.5 times that on the bag side at the end of the cure cycle. A similar but less pronounced behaviour is seen in the in-plane direction. Figure 5-8 shows that the void distribution in-plane is uniform up to two hours into the cycle. At two hours the porosity in the end sections is less than that in the middle section of the laminate. The data shows that porosity gradients are formed towards the vacuum boundaries. Studies by other students in our group have shown that larger gradients are expected in thicker parts. Hsiao et al. [12] have also reported the presence of an in-plane void gradient with respect to the vacuum source. A potential linkage between porosity gradients and gas permeability of the laminate is discussed in section 5.3.2.2.

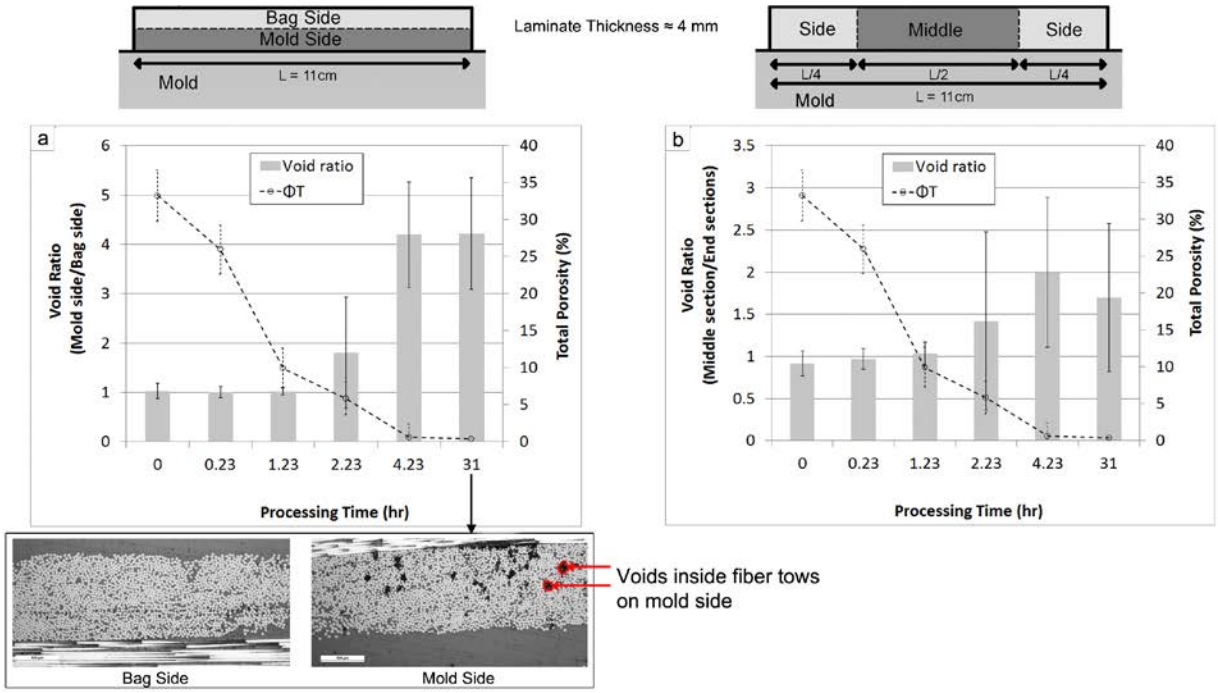

Figure 5-8 Evolution of porosity distribution during 80 ˚C cure cycle, a) Through-Thickness, b) In-Plane (Error bars denote +/- one standard deviation).

5.3.1.5 Effect of Temperature and Humidity on Porosity Evolution

To understand the effect of temperature and humidity on porosity evolution, two more cycles were studied. The first study compares the porosity evolution during an 80˚C cure cycle with a 120˚C cycle. The second study compares the porosity evolution in two series of laminates conditioned at ambient (23%) and 75% relative humidity during a 120˚C cure cycle. Figure 5-9 a to c shows the evolution of different types of porosity during 80˚C and 120˚C cure cycles.

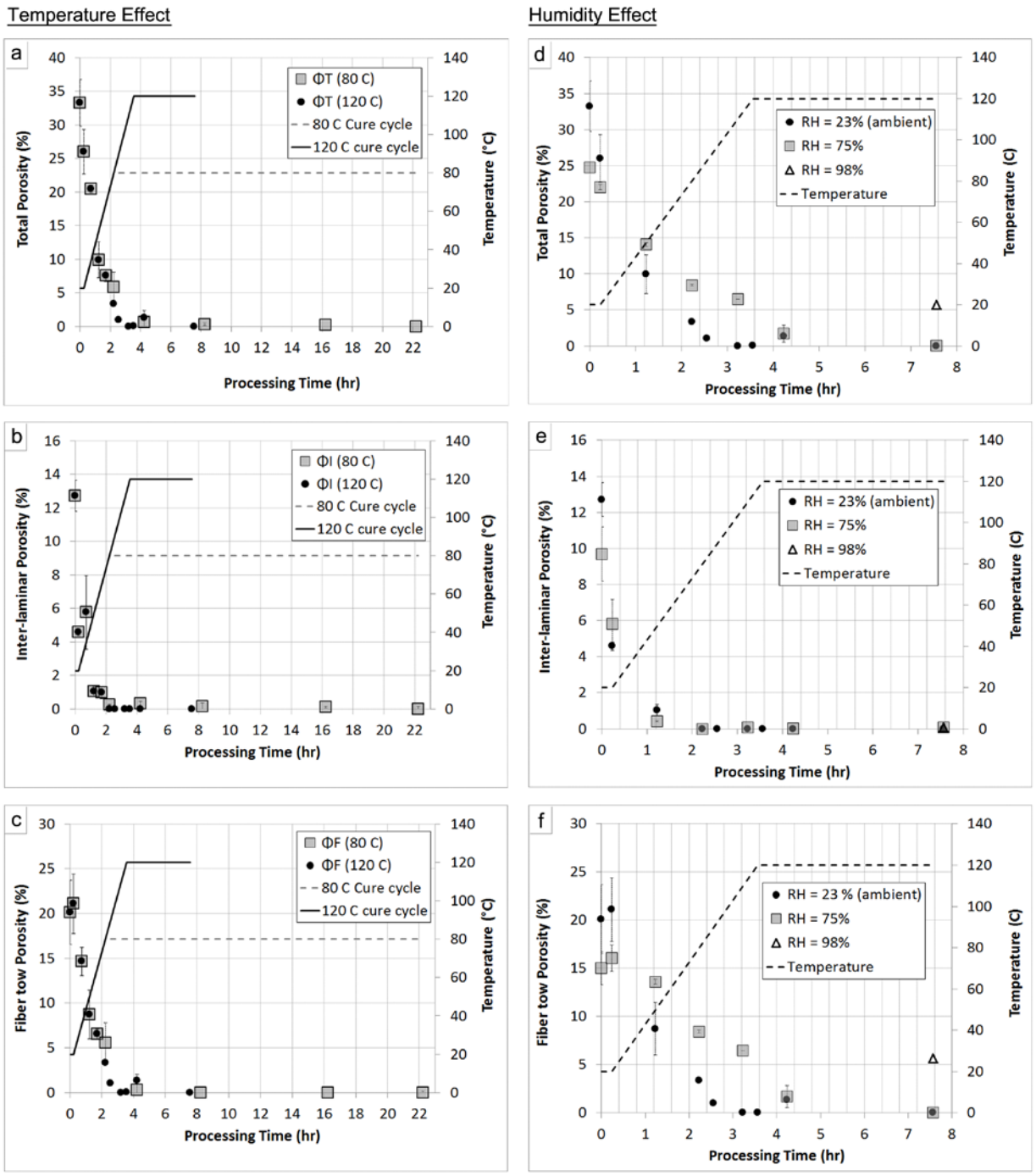

Figure 5-9 a to c) Effect of cure cycle hold temperature (120 ˚C vs. 80 ˚C) on the evolution of different types of porosity. d to f) Effect of relative humidity on the evolution of different types of porosity in a 120 ˚C cycle (Error bars denote +/- one standard deviation).

Figure 5-9 (a to c) shows that the porosity evolution in 80˚C and 120˚C cycles is very similar. There is no evidence of appreciable off-gassing in the 120˚C cycle compared to the 80˚C cycle, confirming that OOA prepregs are intentionally made with low volatile content resin systems to prevent off-gassing and porosity [99]. Another source of off-gassing is moisture in the prepreg, controlled by the relative humidity of the air during handling and lay-up. It has been reported that increasing moisture content results in higher porosity levels in OOA prepregs [7, 13]. Grunenfelder et al. [7] reported 75% relative humidity as the threshold at which porosity levels are higher than the acceptable limit by common aerospace standards. In this study the evolution of voids in a series of laminates conditioned at 23% (ambient) and 75% relative humidity were studied (Figure 5-9 d to f).

A difference in the initial porosity of as-laid up and debulked samples at the two humidity levels was observed. The difference is believed to be related to the differences between applied forces and tack levels during manual lay-up or potential material variability along the roll. During heating the total porosity of the 75% humidity conditioned laminates is higher than that for the ambient conditioned (23%) laminates and they reach zero porosity later in the cure cycle than their ambient conditioned counterparts. The main difference between the two laminates is the amount of fiber tow voids during heat up and early in the hold. By increasing the humidity level from ambient to 98%, the final porosity or porosity of a fully cured laminate is also increased to 5.7%. The majority of porosity resides in the fiber tows (Figure 5-10 b). Samples conditioned at 98% RH do not have well-controlled moisture content due to potential effects of water condensation. For this reason, no void evolution study is done for this humidity level. However,

porosity data for fully cured laminate are included to illustrate the adverse effect of large amounts of moisture.

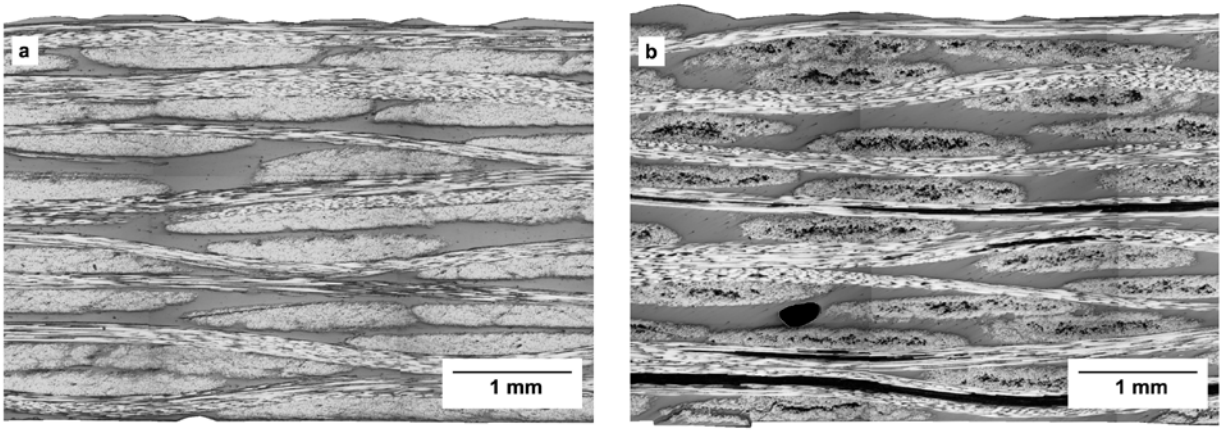

Figure 5-10 Effect of humidity on porosity of fully cured samples. a) RH = 75% (zero porosity), b) RH = 98% (5.7% porosity).

Kardos studied growth of spherical resin voids via diffusion of resin moisture into them [35]. This study shows that increasing the moisture content increases the content of fiber tow voids but it does not affect the resin voids significantly. Kardos assumed that the resin voids were surrounded by an infinite amount of pressurized resin (as in a fully impregnated prepreg) whereas in the current case the fibre tow voids provide a connected porous network with low gas and water vapour pressure, likely creating a greater driving force for moisture diffusion into the fibre tow voids rather than into the isolated resin voids. Note that in this study the porosity level reaches zero before the resin gels (at about 4.5 hours) and we obtain a cured laminate with very low porosity despite conditioning at 75% relative humidity. For humid laminates with larger and more complex geometries it can be challenging to evacuate entrapped air and moisture before the system gels or the gas transport mechanism cease to be effective. It becomes essential to

understand the timescale of relevant transport mechanisms in order to manufacture more challenging laminates with low porosity.

5.3.1.5.1 Off-Gassing during the Cure Cycle

Off-gassing or out-gassing during the cure cycle is one of the potential sources of porosity. It is believed that OOA prepregs are designed to have minimum volatile content to reduce porosity [26]. The moisture content of the prepreg is known as another source of off-gassing, which is controlled by the relative humidity of the prepreg during storage and lay-up. Researchers have shown that increasing moisture content, results in higher porosity levels in OOA prepregs [7, 13]. The current study shows that increasing the relative humidity of the laminates from ambient humidity to 75% and 98% results in an increase in porosity. Thermo gravimetric (TGA) analysis is performed to evaluate prepreg off-gassing during the cure cycles used in this study. The TGA study is done for samples conditioned at 31% (ambient) and 75% relative humidity and three different cycles (Figure 5-11).

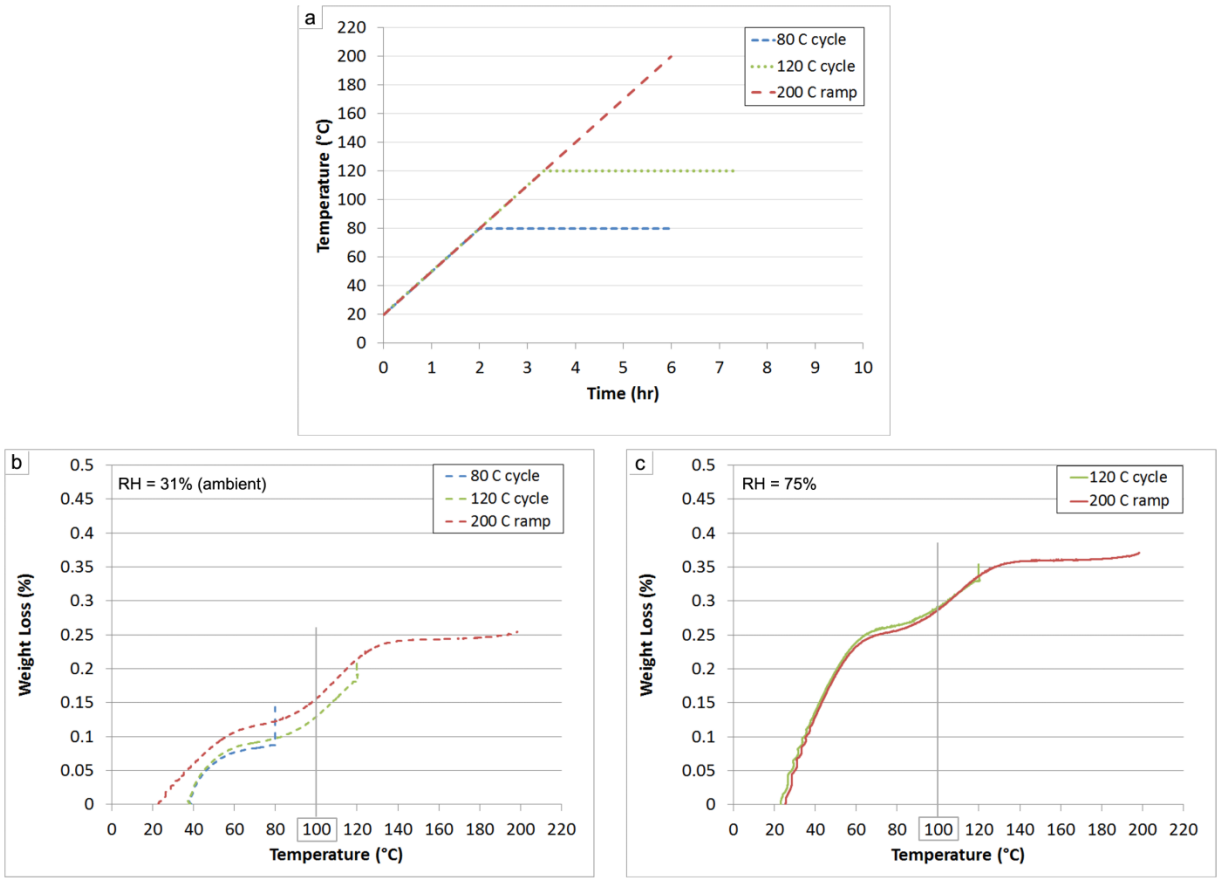

Figure 5-11 a) Temperature-time cycles; Weight loss during different cycles, b) at RH = 31% (ambient) and c) at RH = 75%.

Figure 5-11 a shows the mass loss of 31% (ambient) and 75% humidity conditioned samples during different cycles. The mass loss increases as the temperature is increased and reaches a plateau in the temperature range of 140 °C to 200 °C. Samples conditioned at 75% humidity show higher mass loss compared to their 31% (ambient) conditioned counterparts (0.36% vs. 0.25% at their maximum plateau). The type of the off-gas is not directly measured in this study, however the amount of off-gas suggests that moisture is the main constituent. The initial moisture content of the prepreg used in this study at room temperature is in the range of 0.15%

and 0.32% for ambient and 75% relative humidity conditioned samples [35,12]. The amount of mass loss during the cycles used in this study is slightly higher than the initial moisture content of these samples (0.25% and 0.36% respectively). This difference is expected as the initial moisture content of the laminates is measured at room temperature, while in the current study the temperature goes up to 200 °C. This increased temperature provides the required energy for removing the water molecules that are harder to remove [100]. The non-linearity of these graphs at around 60 °C suggests a shift from the removal of free to bound water, followed by boiling at 100 °C [100].

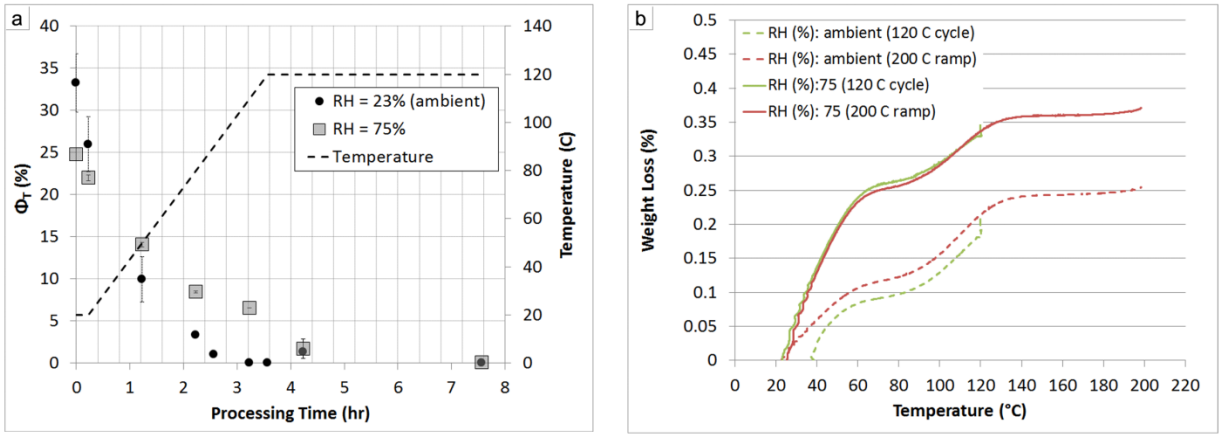

Figure 5-12 a) Effect of relative humidity (23% vs. 75%) on porosity evolution in a 120˚ C cycle, b) effect of relative humidity (31% vs. 75%) on the weight loss in 120˚C cycle and 200 ˚C ramp.

The effect of relative humidity on the porosity evolution in a 120 °C cycle is shown in Figure 5-12 a. During heating the porosity of the 75% humidity conditioned laminates is higher than the ambient conditioned (23%) laminates. The higher amount of off-gas from the 75% relative humidity conditioned samples during the cure cycle is likely the cause of the higher porosity

(Figure 5-12 b). Note that the TGA test is performed under ambient pressure and laminates processed under a vacuum bag, undergo a different pressure condition.

5.3.1.6 Effect of Gas Evacuation Direction on Porosity Evolution

In this section the effect of gas evacuation direction or breathing direction on void evolution during the cure cycle is studied. Figure 5-13 shows porosity evolution in laminates with different sealing configurations. In group (a), samples are able to breath from both the edge and surface, while in group (b) and (c) breathing is limited to either edges or surface. The results show that regardless of the sealing configuration a porosity free laminate is achieved at the end of the cure cycle and that all types of porosity follow a decreasing trend. After room temperature debulk the inter-laminar voids decrease to 4%, 7% and 9% in configurations (a), (b) and (c) respectively. The lowest porosity value in configuration (a) (edge and surface breathing) is likely due to availability of both in-plane and through-thickness gas evacuation in this sealing configuration. Inter-laminar voids decrease to values smaller than 1% in an hour. Fiber tow voids start at about 20% in as-laid up laminates and remain almost constant during the short room temperature debulk (0.23 hr). Once the heated cycle starts, porosity follows a decreasing trend and reach values around 1% after 4 hours. The differences in evolution of fiber tow porosity for different sealing configurations seem to be correlated to the variations in the tow minor dimensions for corresponding condition (Figure 5-13 d). Note that at two hours, the porosity of the laminate with configuration (c) (surface breathing) is about 4% lower than the laminate with configuration (a) (edge and surface breathing). This behavior cannot be explained and this data point is considered to be an outlier. More repeats of this test is needed to ensure the validity of this data

point. Resin voids have small values, lower than 0.2 %, throughout the entire cycle in all sealing configurations.

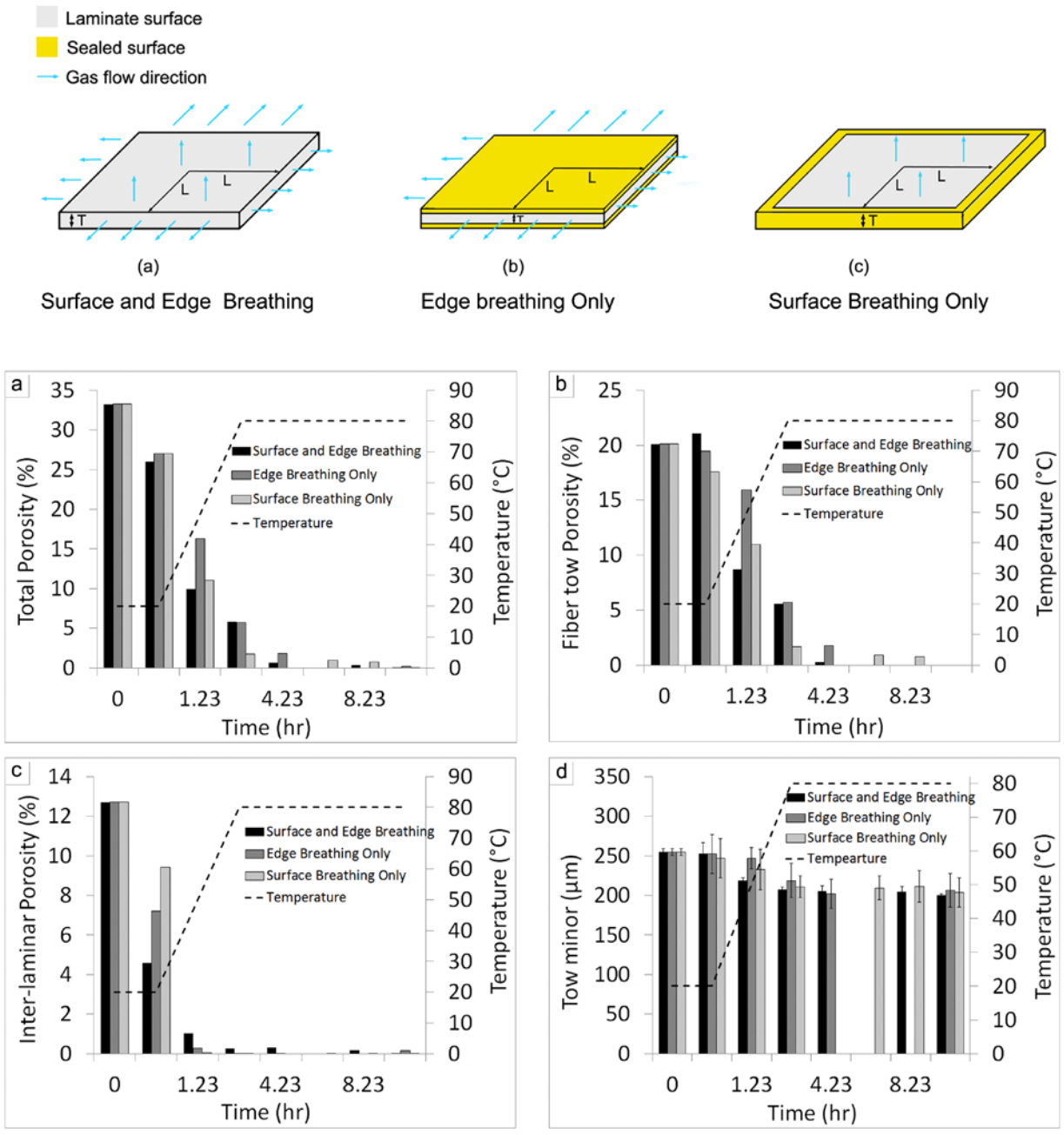

Figure 5-13 Effect of breathing direction on void evolution during an 80 °C cure cycle. a) total porosity, b) fiber tow porosity, c) inter-laminar porosity, d) tow minor dimension.

5.3.2 Gas Flow Rate and Permeability Studies

5.3.2.1 Gas Flow during Long Room Temperature Debulk

The flow of gas out of the laminate during a long room temperature debulk was measured with a gas flow sensor (Figure 5-14), despite the very small gas flow compared to the sensivity of available flow sensors. The data is therefore only qualitative and can not be used for quantitative analysis. After about two hours the gas flow reaches a plateau (≈ 0.0093 L/min), which suggests that gas evacuation has occurred mainly during the first two hours and the plateau flow after that is an artifcat caused by a small leak or bias in the gas flow sensor. In section 5.3.1.2 it is shown that during a 13.5 hour room temperature debulk porosity does not change by increasing the debulk time from 4 to 13.5 hours. These observations suggest that in this study both gas removal and porosity reduction occurs in the early hours of the debulking process (< 4 hours).

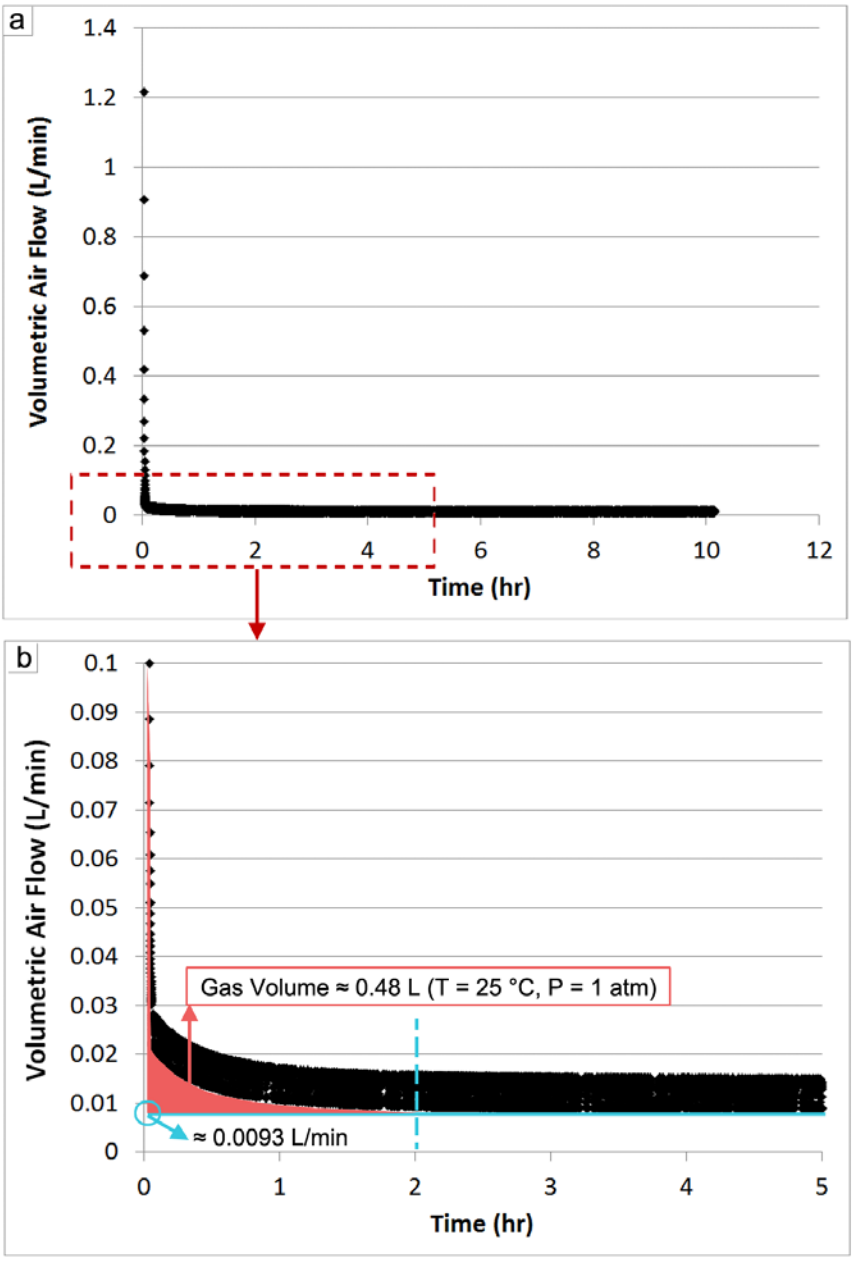

Figure 5-14 a) Flow rate measured during a 10 hour room temperature debulk. b) magnification of early hours of debulk (The flow rate plateau (0.0093 L/min) is indicated on the magnified graph). The red color shows the area under the graph. The black color shows the fluctuating data points due to the noisy signal in this low flow regime.

The volume of the gas removed during the debulk test is estimated by measuring the area under the flow diagram to be about 0.48×10^{-3} m^3 at ambient conditions ($\approx 5.76 \times 10^{-1}$ gr) (Figure 5-14 b). This measured amount is almost one order of magnitude more than the amount of gas expected in the laminate (details in Appendix G). This discrepancy may be due to air entrapped in vacuum hoses, consumable, etc.

5.3.2.2 Gas Permeability during Heat-Up and Cure

Permeability is a measure of the ability of a porous material to transport gases via Darcy flow and is a function of porosity, surface area and tortuosity [46]. During the cure cycle the porous structure of the laminate changes which affects the permeability of the laminate. Figure 5-15 shows the measured gas permeability in-plane and through-thickness through-out an 80˚C cure cycle. Also shown is the relative amount of volumetric gas flow, Q, in-plane and through thickness, accounting for permeability, distance to the vacuum port and available cross-sectional area of the flow.

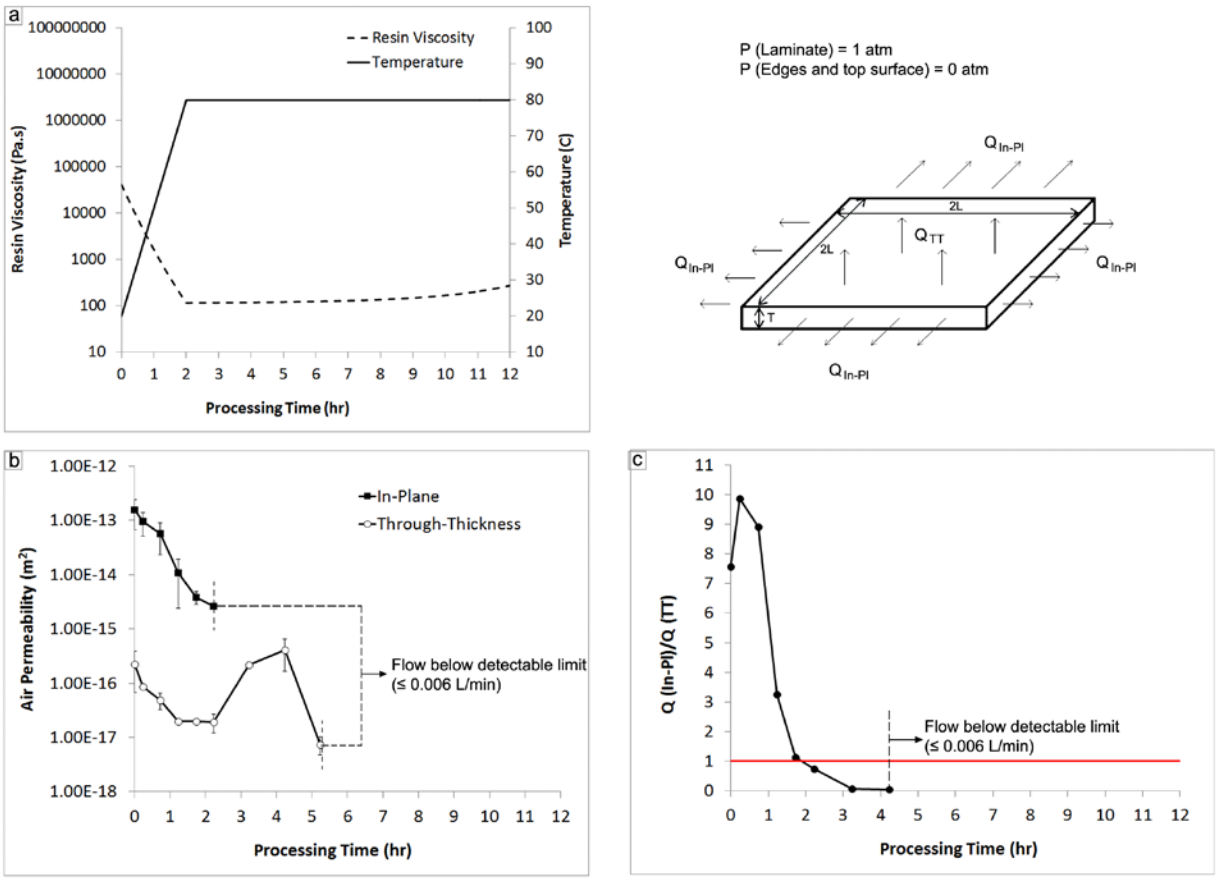

Figure 5-15 a) MTM45-1 resin viscosity, b) In-plane and through thickness gas permeability and c) Calculated gas flow ratio throughout an 80˚C cure cycle. Flow and permeability values below detectable limit (Q ≈ 0.006 L/min, K (In-Plane) ≈ 10^{-15} m^2, K (Through-Thickness) ≈ 10^{-17} m^2) are assumed to be effectively zero. (Error bars denote +/- one standard deviation).

The in-plane permeability is maximum (≈ 1.5 × 10^{-13} m^2) at the beginning of the process, which is within the range of the in-plane permeability values reported in literature for other prepreg systems (10^{-12} – 10^{-15} m^2) and close to the theoretical in-plane permeability (Appendix E) [11, 49, 53]. The in-plane permeability decreases during the heat up and becomes effectively zero after two hours. The minimum measurable in-plane and through thickness permeability are about 10^{-15} m^2 and 10^{-17} m^2 based on the minimum measurable flow rate in the test set-up (≈ 10^{-7} m^3/s =

0.006 L/min). Flow and permeability values under this limit are assumed to be effectively zero and are shown with dashed line in Figure 5-15. For more information about the detection limit of the mass flow sensors used in this study refer to Appendix F. The through thickness permeability is significantly smaller than in-plane and has three distinct stages. In the first stage (0 - 2.23 hours), it decreases during the initial compaction of the laminate and becomes very small in one hour. The second stage (2.23 - 4.23 hour) starts at the end of the temperature ramp, when the resin viscosity becomes minimum (≈ 100 Pa.s), and the through thickness permeability starts to increase rapidly. The permeability reaches its maximum ($\approx 2 \times 10^{-16}$ m^2) early in the hold (4.23 hours), after which it decreases and becomes zero again (5.23 hours). The permeability tests are performed by creating a temporary one atmosphere pressure gradient across the laminate. The prepreg morphology with pin holes at warp/weft intersections (Figure 5-6 b) and the observation that the through-thickness permeability is maximum at minimum viscosity, suggests that low viscosity resin is pushed aside by the air to create gas transport pathways through thickness. To confirm this, a permeability test was performed under a continuous one atmosphere pressure gradient across the thickness (see Appendix A, Figure A-3). It is shown that under this condition, large pinholes are formed at warp/weft intersections (Figure 5-16). A similar behaviour for through-thickness permeability of prepregs and their relation to resin viscosity during processing has been reported by Tavares et al. and Louis et al. [11, 51].

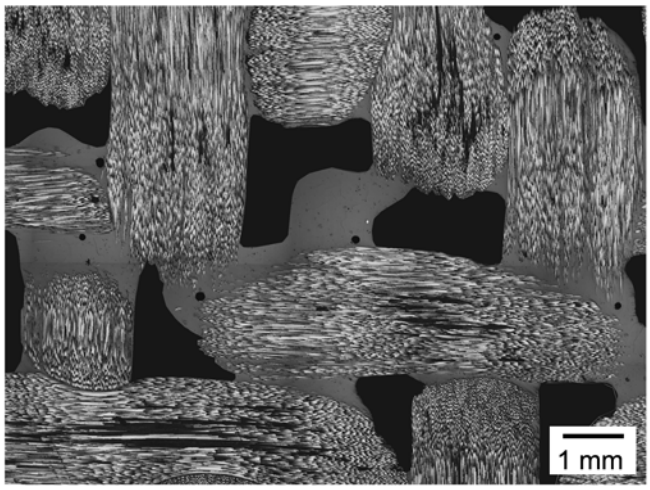

Figure 5-16 Pin holes formed at warp/weft intersections when prepreg is subject to permeability testing when resin viscosity is low.

The relationship between in-plane permeability and fiber tow porosity is shown in Figure 5-17. When porosity is high permeability is high and when the porosity is less than 6%, the permeability becomes effectively zero. This suggests that below 6% porosity the pores are no longer interconnected and gas transport via Darcy flow is no longer possible. It has to be noted that a 6% threshold refers to the average porosity. The standard deviation at this porosity level is about 2%. Because of the variability of fiber tow porosity along the length of a fiber tow, the interconnectivity of the gas path out of the laminate will stop before the average porosity is zero. Figure 5-17 also shows the relationship between through-thickness permeability and fiber tow porosity. The figures clearly show that through-thickness permeability is not controlled by fiber tow porosity but by other air transport paths. In a complex porous medium, the fluid is not flowing in the entire pore space and an “effective porosity” can be defined as volume fraction of the porosity in which flow occurs [101]. Microstructural observations (Figure 5-6 c) showed that inter-laminar and resin voids are isolated from each other while fiber tow voids are more or less

continuous in the plane of the laminate. This implies that fiber tow voids, i.e. the non-impregnated dry core of the fiber tows, provide the required interconnected pathway for in-plane gas transport. The proximity of the inter-laminar voids to the dry fibre tows (Figure 5-6 a) allows them to be evacuated via the fibre tows. Figure 5-7 b shows that the inter-laminar voids disappear before the fibre tow voids, supporting that the entrapped gas is evacuated via the fibre tows.

Vacuum applied at the perimeter of the laminate can reach different points of the laminate and remove air through these dry regions of tows as long as they are open and interconnected [39, 96]. It is therefore critical to keep these vacuum channels open until sufficient amount of gas has been removed from the laminate. Viscosity is of one the main factors that control the infiltration rate of fiber tows with resin [9]. When the resin viscosity drops the fiber tow voids close off. By postponing the drop in viscosity, fiber tow voids may stay open for a longer time, which can be achieved by decreasing the ramp rate or adding an intermediate dwell at a lower temperature [95].

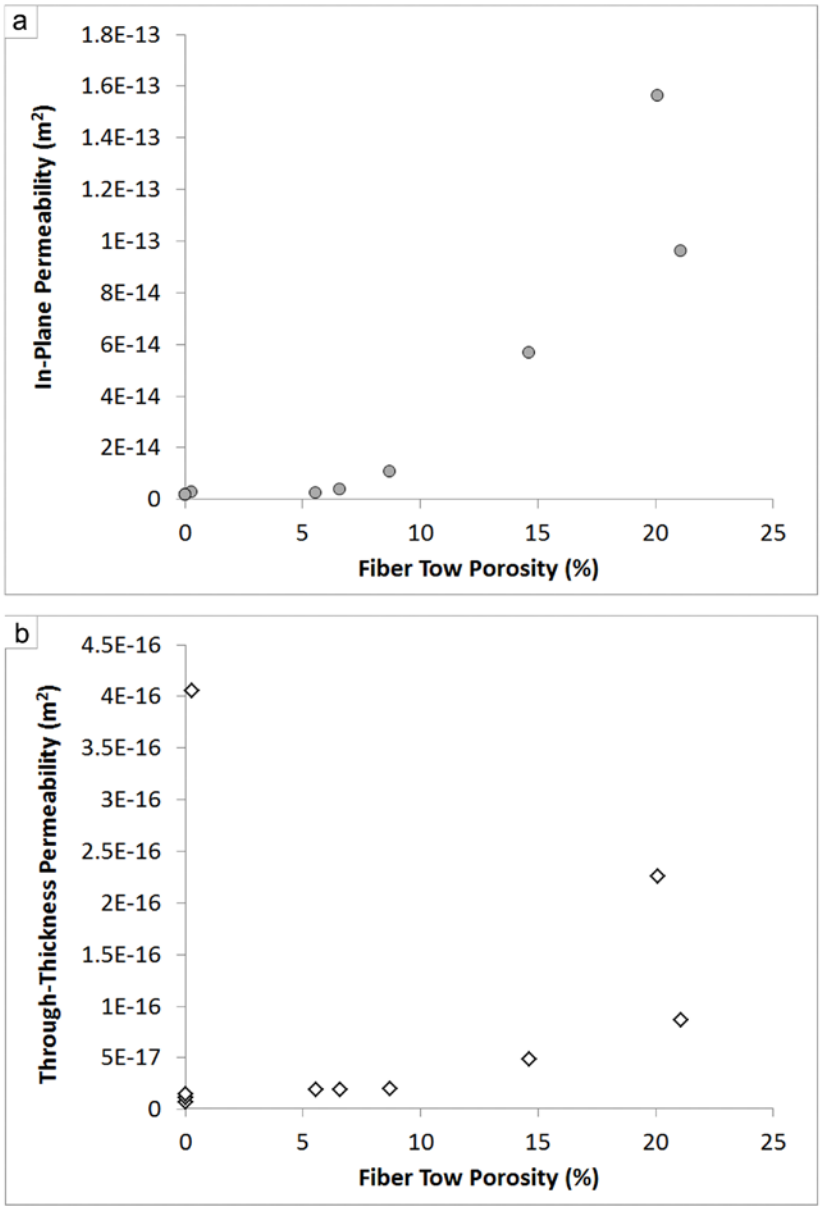

Figure 5-17 Relationship between fiber tow porosity and a) in-plane permeability, b) through-thickness permeability.

The void distribution study showed that the void distribution is uniform throughout the laminate in the early stages of the cure cycle, but that after two hours a gradient start to form in both thickness and in-plane directions (Figure 5-8). This is also the time when the in-plane

permeability becomes zero and the through thickness permeability starts to increase (Figure 5-15). This suggests that when the in-plane pathways have been closed off because of resin infiltration of the fibre tows, the preferential pathway out for any remaining gas is through thickness, facilitated by the low resin viscosity. Ridgard et al [95] have also reported the existence of "some degree of through thickness movement of entrapped air" with the same prepreg and processing method.

The time required for removing a specified mass fraction of gas in a porous laminate with a constant permeability during a room temperature debulking can be estimated by the following equation developed by Arafath et al. [34]:

$$t \approx \varphi_0 \left(\frac{\mu}{P_0}\frac{L^2}{K}\right)\left[-\frac{1}{0.9} ln\left(\frac{m}{m_0}\right)\right]^{\frac{1}{0.6}} \quad (5\text{-}2)$$

Where: t: time, φ_0: initial volume fraction of porosity, μ: gas viscosity, L: distance to vacuum port, P_0: initial gas pressure, K: prepreg permeability, m: mass of gas in laminate, m_0: initial mass of gas in laminate.

This equation can be used for one dimensional Darcy flow of gas in a porous medium at constant temperature and permeability. Using the measured in-plane permeability after a room temperature debulk (~ 9.61×10^{-14} m^2) gives us a conservative estimate of gas remaining in the laminate after a certain debulk time. If it is assumed that any gas remaining in the laminate after debulk will equilibrate with liquid resin at one atmosphere of pressure, the mass ratio m/m_0 will equal the final porosity ratio in the cured laminate. For example, if the initial porosity is 35% and the desired final porosity is < 1%, m/m_0 in eq. (5-2) should be less than 1/35 ≈ 3%. Using this

approach, about two minutes of debulk is required to achieve a porosity of 0.3%, which is the observed value for the cured laminates in this study (see section 5.3.1.3). Given that the debulk time in the cure cycles used are about 14 minutes or more, it can be assumed that the prepreg is fully evacuated during the debulk stage and there is full vacuum in the interconnected pore space. Debulk time requirements are discussed in detail in Chapter 7.

5.3.2.2.1 Through Thickness Permeability of Bagging Materials (Brick and Release Film)

The through-thickness permeability of brick and non-perforated release film during the 80 °C cure cycle is measured to ensure their permeability is not limiting the transport of gas in the measurement system (Figure 5-18).

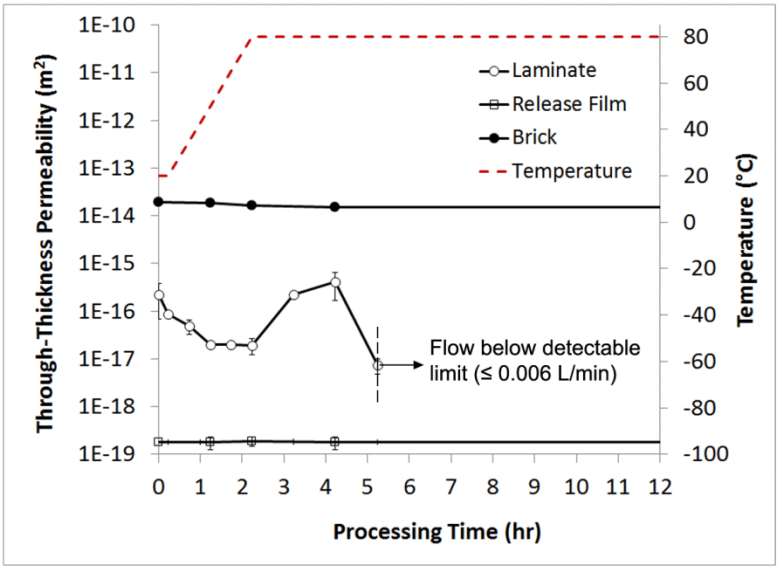

Figure 5-18 Through thickness permeability of laminate, brick and release film during 80 °C cure cycle.

Figure 5-18 shows that permeability of brick and release film is almost constant during the cure cycle. Permeability of brick is about 1.7×10^{-14} m^2 and is always significantly (~ 2 orders of magnitude) higher than laminate permeability. Thus it can be deduced that brick permeability is not limiting the gas transport in through-thickness laminate permeability tests. On the other hand, permeability of release film is about 1.8×10^{-19} m^2 and much lower than laminate permeability. The lower permeability of the release film will not limit the gas transport in the set-up used for measurement of laminate through thickness permeability (Figure 5-3). In the laminate through-thickness permeability measurement set-up, the edges of the release film are free and not sealed with tacky tape, unlike the release film test set up. Also, the peel ply strips - extending from laminate top surface towards breather cloth – act as a gas transport pathways between laminate and breather [52]. The good performance of the combination of release film and peel ply strips for gas transport is also confirmed in brick test, as high flow rates (maximum flow rate = 3 L/min) was measured in this test.

5.3.3 Fiber Bed Compaction and Resin Infiltration

Fiber bed compaction and resin infiltration are two important factors that affect void morphology during the process. If the gas pressure in the porous medium is lowered due to gas evacuation there will be a net pressure on the fibre tow acting to compact it. Low gas pressure inside the porous medium will also cause a pressure gradient across the resin front promoting resin infiltration into the pore space. The time scales for resin infiltration of the pore space are large at room temperature due to the high viscosity of the resin (~ 10^4 Pa.s). When heat is applied the resin will readily infiltrate the pore space, provided that entrapped air has been removed and the pore space is under low pressure.

Evolution of fiber tow voids is evaluated using fibre tow compaction data from this study and a resin infiltration model developed for the same prepreg system by Centea et al. [9]. This model predicts the degree of resin impregnation (β) in a single cylindrical rigid fiber tow in OOA prepregs (eqs. 5-3 and 5-4).

$$\beta = 1 - \sqrt{\frac{A_f}{A_{tow}}} = 1 - \frac{R_f}{R_{tow}} \tag{5-3}$$

$$\frac{d\beta}{dt} = \frac{K}{\mu R_{tow}^2 (1-V_f)} \left(\frac{P_\infty - P_f}{(1-\beta)\ln\left(\frac{1}{1-\beta}\right)}\right) \tag{5-4}$$

Where A_f (m^2): cross sectional area of un-impregnated section of circular tow, A_{tow} (m^2): total cross sectional area of circular tow, R_f (m): circular radius of resin flow front, R_{tow} (m): outer radius of circular tow, t (s): time, K (m^2): transverse tow permeability, μ (Pa.s): resin viscosity, V_f (-): fiber volume fraction, P_∞ (Pa): resin pressure at R_{tow}, P_f (Pa): resin pressure at R_f.

Predictions from this tow infiltration model are compared to measured values of fiber tow porosity (dry section of the tow). The input parameters used are same as the ones used in original reference [9] and are listed in Table 5-4. The parameter β is one when the tow is fully impregnated with resin.

Table 5-4 Tow impregnation model parameters [9]

Parameter	
R_{tow} (m)	1.27×10^{-4}
K (m^2)	10^{-15}
μ (Pa.s)	Same viscosity model and input parameters as reference [9] is used.
V_f	0.74
P_∞ (atm)	1
P_f (atm)	-0.176 [9]

Fiber bed compaction is characterized by measuring the evolution of the fiber tow geometry during the process. Fiber tows have a nearly elliptical cross section and their geometry can be represented by the minor and major axis of an ellipse. Measurements show that the major axis of the fibre tows, which are located in the plane of the prepreg, is almost constant (2.145 ± 0.024 mm), whereas the tow minor axis serves as a good measure of fibre tow compaction. The parameter ε_T, transverse tow compaction, is used to represent the compaction of tow, ε_T is zero when tow is not compacted:

$$\varepsilon_T = \frac{a_0 - a_i}{a_0} \tag{5-5}$$

Where a_i: tow minor axis at time i, a_0: tow minor axis for an un-compacted tow

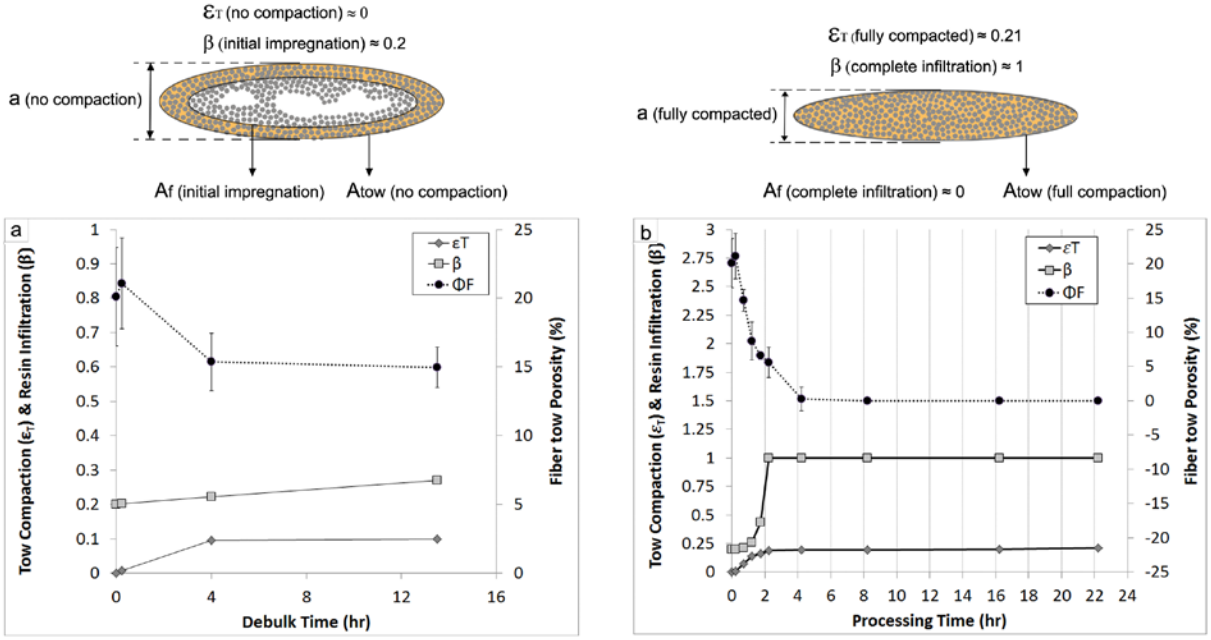

Figure 5-19 Evolution of fiber tow porosity (Φ_F), tow compaction (ε_T) and resin infiltration (β) during a) long debulk and b) 80˚C cure cycle. Error bars denote +/- one standard deviation.

Figure 5-19 and Figure 5-20 show the evolution of the fibre tow porosity (Φ_F), resin infiltration (β) and tow compaction (ε_T) for the cycles discussed in section 5.3.1. In the long debulk cycle there is a drop in Φ_F in the (0.23 – 4 hour) time interval. This drop can be described by compaction of the fiber tows (ε_T), as the infiltration degree (β graph) is not changing significantly at this time interval due to the high viscosity of the resin at room temperature ($\approx 10^4$ Pa.s). During the 80 ˚C cure cycle Φ_F continuously decreases and reaches a very small value at four hours. Fibre tow measurements and calculations of resin infiltration show that both factors have a role in Φ_F evolution. In the first hour, the rate of infiltration is slow and fiber bed compaction is largely responsible for the Φ_F reduction. At two hours, when the resin viscosity gets closer to its minimum and fibre tow compaction has almost stopped, and resin infiltration is the main cause of reduction of fibre tow porosity.

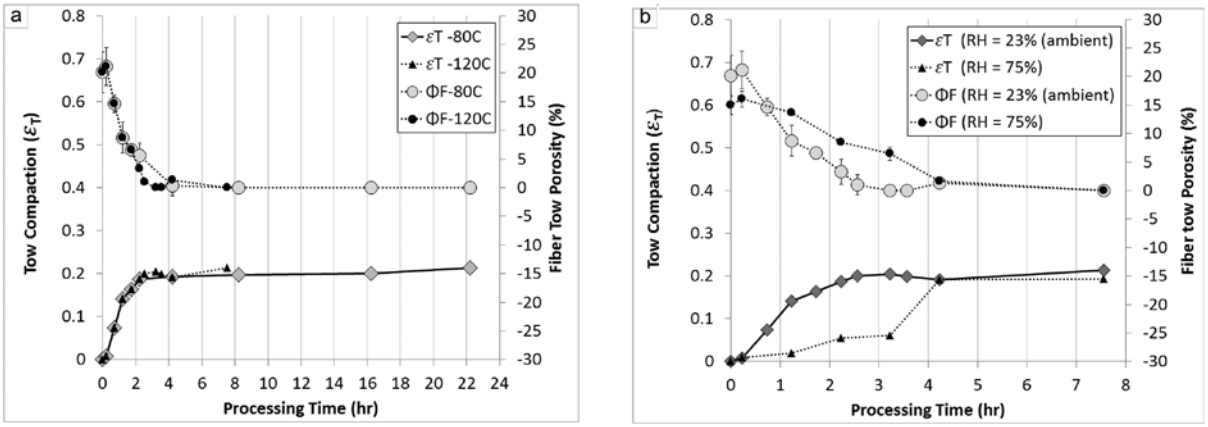

Figure 5-20 Comparison of fiber tow porosity (Φ_F) and tow compaction (ε_T), evolution at different temperature cure cycles and relative humidity levels. Error bars denote +/- one standard deviation.

Figure 5-20 shows the effect of cure cycle temperature and relative humidity on the evolution of Φ_F and ε_T. Fiber tow infiltration (β) is not presented in Figure 5-20 as it is identical to

Figure 5-19 b in all cases. The infiltration model does not include effect of humidity and consequently β calculated from this model is not affected by a change in humidity. However, note that moisture absorption affects resin properties such as viscosity and gel time. Grunenfelder et al. [7] showed that in the MTM44-1 (ACG) epoxy resin, gel time decreases from about 2.5 days at 50% relative humidity down to about 2 days at 90% relative humidity. Figure 5-20 shows that both Φ_F and ε_T in the 80 ˚C cycle are very close to their counterparts in the 120 ˚C cure cycle. Thus the hold temperature does not significantly affect the evolution of fiber tow voids or fibre tow compaction. Figure 5-20 b shows the effect of humidity level on fiber tow porosity and compaction. Figure 5-9 e shows that the fiber tow porosity is higher for laminates with higher humidity. The same trend is found in measurements of tow compaction (ε_T). This suggests that higher humidity increases the gas pressure inside the fiber tows and slows down tow compaction and void removal.

The laminates in this study were small and flat, and not surprisingly, the end result was always porosity free laminates. However, the observed void evolution patterns give good insight into the governing transport mechanisms and how the observed results are expected to scale with laminate size and process conditions. Chapter 7: will address the topic of size scaling in detail.

5.4 Summary

The main findings in this chapter are:

- In partially impregnated prepregs voids can be divided into three distinct groups: inter-laminar, fiber tow and resin voids, all with different origins and evolution pattern during processing.

- For the OOA prepreg studied, room temperature debulk decreased porosity from 33% down to about 20% in four hours and further debulking did not reduce the porosity of the uncured prepreg.
- In an 80˚C cure cycle, the initial porosity was 33% but decreased to less than 0.3 % after four hours, well ahead of resin gellation time for the cure cycle used.
- Increasing the hold temperature from 80˚C to 120˚C did not affect the porosity evolution for this prepreg system.
- Increasing the relative humidity of the laminates from 23% (ambient) to 75% resulted in an increase in porosity during the cycle but the final porosity was zero in both cases. However, increasing the relative humidity to 98% increased final porosity to about 6%.
- Increasing the relative humidity from 31% (ambient) to 75%, increases the amount of off-gassing throughout the cycle.
- It is possible to obtain void free laminates regardless of gas evacuation direction (in-plane versus through-thickness) in small flat laminates of 127 mm × 127 mm × 4 mm.
- The gas evacuation direction does not significantly affect void evolution during the process (in small flat laminates of 127 mm × 127 mm × 4 mm).
- Laminates are permeable both in-plane and through-thickness. The maximum in-plane permeability is approximately three orders of magnitude higher than the maximum through thickness permeability and permeability in both directions vary during the process. The majority of gas transport occurs in-plane during debulk. However, later in the process, when in-plane permeability is zero due to resin infiltration of the dry fibre tows, the main gas transport path is through-thickness.

- There is a direct relationship between fiber tow voids, i.e. the non-impregnated core of the fibre tows, and in-plane gas permeability. Partially impregnated tows act as vacuum channels and facilitate gas removal in this prepreg system. The vacuum channels are open and effective until they are closed off by low viscosity resin flow at a total porosity level of about 6%.
- A void gradient starts to form with higher porosity on the mold side and in central regions of laminate after two hours of processing, illustrating the effect of through-thickness gas transport on void removal.
- Laminate permeability, fiber bed compaction and resin infiltration all play an important role in porosity evolution in this prepreg system. It is shown that in high viscosity regions as during the room temperature debulk, the evolution of fiber tow voids are mainly controlled by fiber bed compaction. However during the cure cycle, both fiber bed compaction and resin infiltration affect evolution of fiber tow voids.
- The above statements are valid for small flat laminates (127 mm × 127 mm × 4 mm) used in the current study and the results may be different for large complex parts as the time scale for gas evacuation in the in-plane direction is very different from through-thickness direction due to permeability anisotropy (Chapter 7:).

Chapter 6: Effect of Vacuum Release Time on Final Porosity during Heated Cycle

6.1 Introduction

Vacuum evacuation of entrapped air is the main means of porosity reduction in OOA processing of prepregs. This chapter investigates the effect of vacuum release time on porosity. This is important for understanding the effect of bag and tool leaks during processing.

6.2 Methods

6.2.1 Materials

MTM45-1/CF2426A prepreg manufactured by ACG (now Cytec) was used in this study. MTM45-1 stands for the toughened epoxy matrix and CF2426A for the five harness (5HS) woven carbon fiber fabric with 6K tows. The resin content of this prepreg is 36wt% and the fabric areal density 375 $\frac{gr}{cm^2}$. The prepreg roll used in this study was MTM45-1/5HS-Thin referring to prepreg initial thickness (see section 4.2.1).

6.2.2 Sample Preparation

The main goal of this study was to study the effect of vacuum time on porosity throughout the heated portion of the process. For this purpose a series of laminates were made by releasing the vacuum at different times during the process (Figure 6-1). Each laminate consisted of 8 prepreg layers of 127 mm × 127 mm. Laminates were debulked and vacuum bagged according to the manufacturer's recommendations (see section 4.2.2) [52]. The vacuum bagged laminates were

placed in an Autoclave (American Autoclave C. model number: AAC4866-R10-NB231) for the cure process. The samples can be cured in an oven, however because a suitable size oven was not available at the time of this study, samples were cured in an un-pressurized autoclave with one atmosphere bag pressure (same condition as an oven). The cure cycle consisted of a 0.5 $(\frac{^{\circ}C}{min})$ heat up ramp to 80 °C, a 20 hour hold at 80 °C, followed by a two hour post cure at 180 °C. Full vacuum (absolute pressure < 4.0 kPa) was applied during a portion of the cure process. Laminates were made by releasing the vacuum at different times during the process, but letting the samples continue to full cure through the complete temperature cycle (Figure 6-1). The vacuum was released after 0 (as-laid up), 0.23 (debulked), 1.23, 2.23, 4.23, 6.23, 16.23 and 22.23 hours during the process. Three replicate samples were made for each vacuum release time.

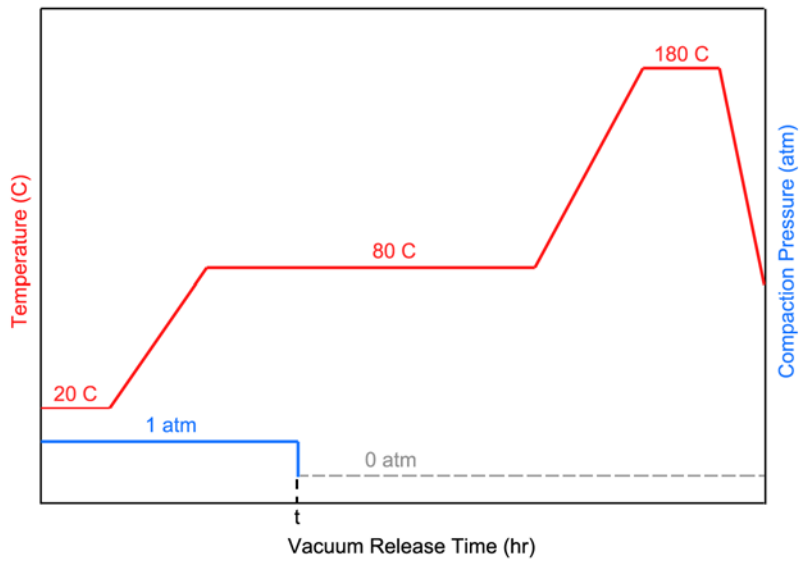

Figure 6-1 Processing cycle; Vacuum is released at time t, while the temperature cycle is continued to the end of the cycle.

6.2.3 Void Characterization

Void characterization was done via optical microscopy imaging and area fraction measurements. (for comparison of optical microscopy versus camera measured porosity refer to Appendix H). The typical steps in optical microscopy method are sample surface preparation, image acquisition and image analysis. Surface preparation and image acquisition was done using the procedures described in section 4.2.3. The “Image J” software was used for image analysis [85]. Porosity is defined as area fraction of voids in a cross section. Three groups of voids are identified: inter-laminar, fiber tow and resin voids. In order to measure the area of voids, the first step is to identify the pixels corresponding to voids. In this study the black pixels are considered to be voids. The illumination setting was chosen such that voids were black, thus by selecting zero threshold, a black and white binary image was created (Figure 6-2 b). At this stage the noise should be removed from the binary image. Noise was mainly created as a result of imperfect sample preparation which produced black features with the same color as voids (e.g., stains, scratches). Black areas smaller than 130 μm^2 (equivalent to a 13 µm circular void), were considered to be noise and were removed automatically. The critical 130 μm^2 area was chosen based on experience. In most of the cases, black areas smaller than this were due to noise, including stains, scratches and fibre breakage. In some cases noise was removed manually. After noise removal the image is ready for final measurements (Figure 6-2 c). The area, major and minor axis of voids were measured using the “analyze particle” and “fit ellipse” commands of the “Image J” software. Using “fit ellipse” command, the void is approximated as an ellipse and the aspect ratio is defined as the ratio of ellipse major axis to minor axis. The area fraction for each type of voids was calculated individually and added together to give the total void volume fraction or porosity of the sample. Applying this procedure for inter-laminar and resin voids is

relatively straight forward, whereas quantification of fiber tow voids needs more explanation. First, it was assumed that area of parallel and perpendicular fiber tows and their corresponding voids are equal (based on measurements). This allows us to quantify the fiber tow voids based on perpendicular fiber tows, which makes the procedure more feasible and robust. Second, a total of twenty tows were randomly selected and their average void area was generalized to the whole cross section. This generalization was done based on the total number of fiber tows, which contain voids, in the cross-section. The coordinates of the voids were used to study the distribution of the voids. The geometrical features of the tows (area, major and minor axis) were also studied using the “fit ellipse” command in the Image J software.

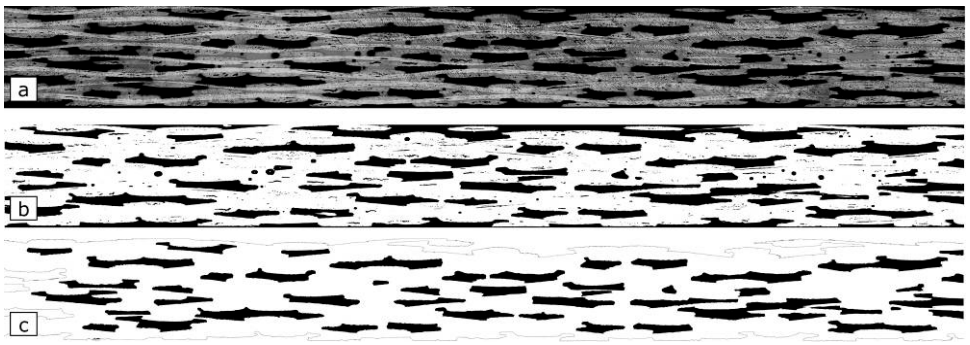

Figure 6-2 Image analysis steps for inter-laminar voids, a) original image, b) binary image, c) binary image after noise removal (ready for measurement).

6.2.4 In-Plane Permeability Measurement and Resin Infiltration

In-Plane permeability measurement was done to study gas transport in laminates with different porosity levels. This was done using the in-plane permeability measurement test set-up described in section 5.2.5. Permeability measurement was performed for samples vented after 2, 4 and 8 hours. In the cases where the digital mass flow sensor was maxed out (maximum flow rate = 1

L/min), the flow rate was measured using the large glass ball rotameter (37288, Omega engineering Co.) (maximum flow rate = 14 L/min).

Resin infiltration tests were done to investigate the connectivity of voids in a highly porous sample with high permeability (vacuum release time = 4 hours). This was achieved by infiltration of the porous sample with a low viscosity color enhanced resin (Epo-color, Buehler Co.) under a one atmosphere pressure gradient (Figure 6-3). Once the infiltrated resin was cured, samples were cut along the flow direction and the cross-section and were examined using the same optical microscope (Nikon EPIPHOT 300) and imaging method mentioned in void characterization section. Imaging was done in both bright-field and dark-field modes as the Epo-color resin has a high contrast with the epoxy matrix in the dark-field mode, thus the infiltrated resin can be distinguished from the epoxy matrix easily.

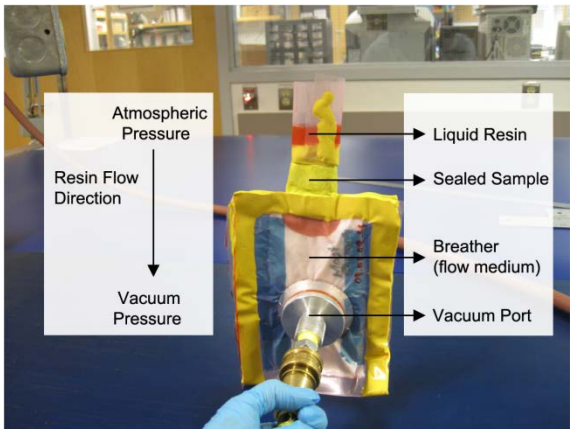

Figure 6-3 Set up used for resin infiltration test.

6.3 Results and Discussion

6.3.1 Effect of Vacuum Release Time on Porosity

Releasing the vacuum in early stages of the process results in highly porous and thick samples (Figure 6-4). Inter-laminar voids are the main contributor to the total void content of these samples. These large inter-laminar voids are likely created as a result of an elastic rebound of the fiber bed because of the release of vacuum pressure. After six hours, the porosity reaches a minimum plateau value and porosity is not affected if vacuum is applied beyond six hours into the cure cycle. The results from this test can be used to optimize the vacuum application time for a cure cycle and also to predict the porosity in the case of a bag leak or sudden loss of vacuum during the process.

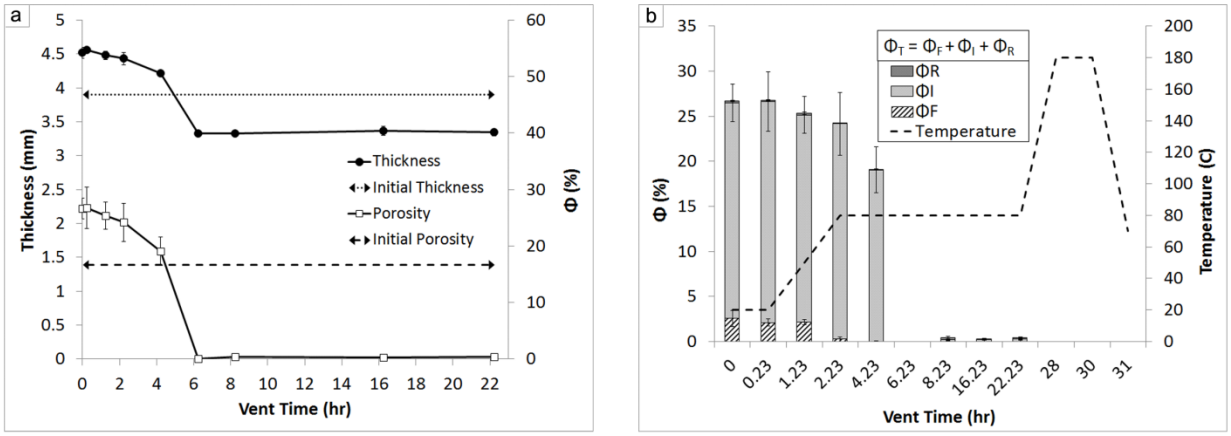

Figure 6-4 a) Thickness and porosity vs. vent time, b) Porosity Type vs. vent time. Porosity is less than 0.3% at 6.23 hours and not visible on the graph.

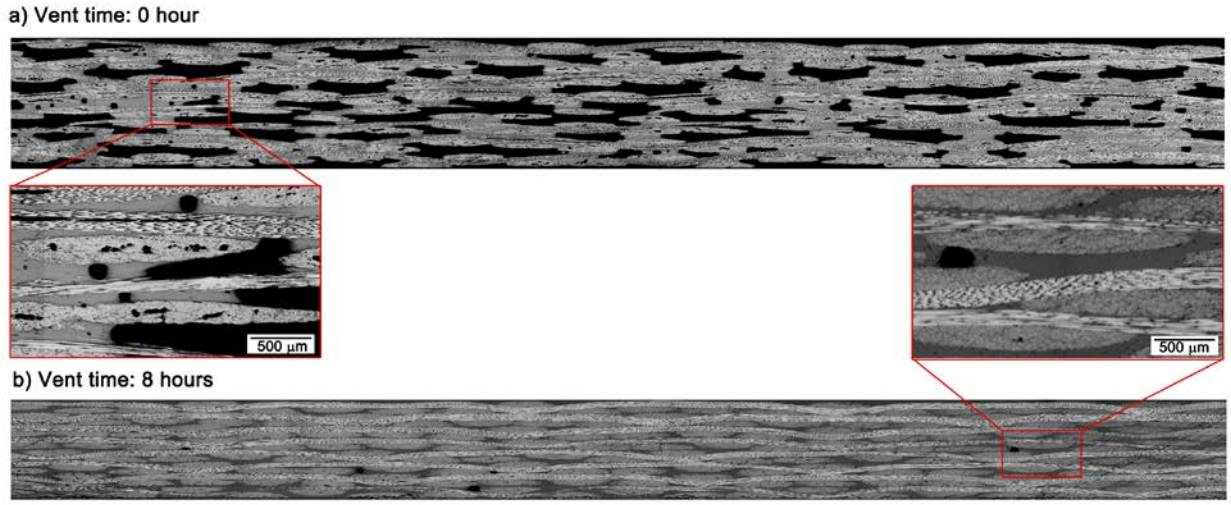

Figure 6-5 Optical microscopy image a) vent time: 0 hour, b) vent time: 8 hours.

6.3.2 Effect of Vacuum Release Time on Void and Tow Geometry

The aspect ratio (major axis divided by minor axis) is used to characterize the shape of the voids. A value of one indicates a circle and a higher value indicates an elongated shape in the in-plane direction. Figure 6-6 a shows the change of aspect ratios for the different types of voids during the process. All types of voids become rounder with time. The change in aspect ratio for fibre tow and resin voids is small whereas there is a large reduction in the aspect ratio of inter-laminar voids up to eight hours, after which the aspect ratio reaches a plateau value. A driving force for making voids rounder with time is minimization of the surface energy of the voids. Due to their location and origin, the aspect ratio of resin voids is lower than for the other types of voids and is almost constant during the process.

The fiber bed compacts under vacuum during the cure cycle. Fiber bed compaction can be quantified by evaluating the geometry of fiber tows. The aspect ratio of the fiber tows increases

as they become compressed and more elongated during the process (Figure 6-6 b). The minor axis decreases continuously throughout the process, but the major axis stays almost constant over time. During the process the geometry of the tows changes due to the extraction of gas out of them and impregnation with resin. The relationship between fiber tow compaction and fiber tow porosity during the process is studied in section 5.3.3.

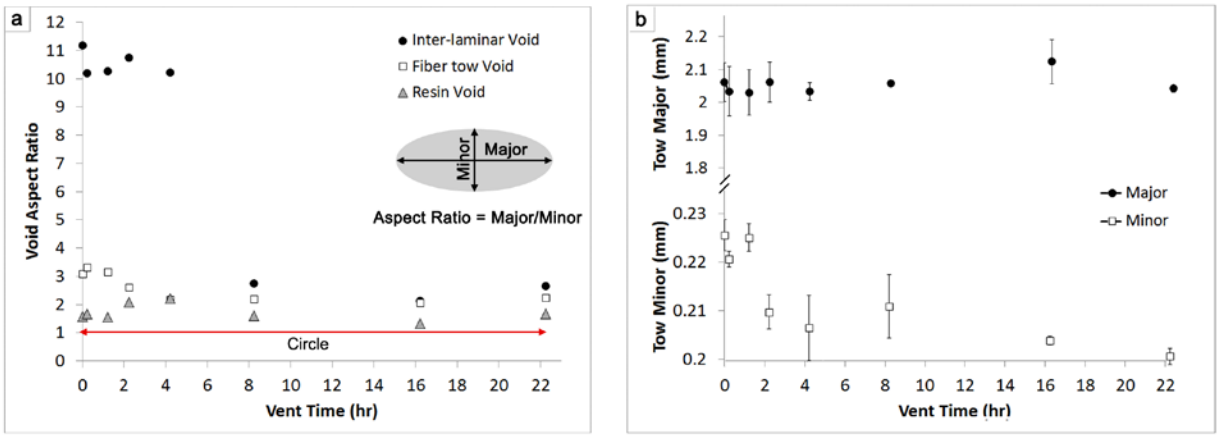

Figure 6-6 Void and tow geometry, a) void aspect ratio, b) tow minor and major.

6.3.3 Effect of Vacuum Release Time on Permeability

In-Plane permeability measurements are performed to investigate gas transport of laminates with different porosity levels (Table 6-1).

Table 6-1 Permeability measurements of the laminates vented after 2.23, 4.23 and 22.23 hours

Vent Time (hr)	Φ (%)	In-Plane Permeability (m^2)	Velocity (m/s)	Reynolds Number
2.23	24.21	2×10^{-11}	2.1633	0.64
4.23	19.07	2×10^{-11}	2.1690	0.65
22.23	0.39	0[1]	0[1]	-

[1] At this level of permeability, the gas flow rate is below detectable limit (< 6 mL/min)

Results show that the permeability of high porosity samples (19% - 24%) is 2×10^{-11} m^2 and the permeability of low porosity sample (0.39%) is effectively zero. The high permeability of high porosity samples is due to the presence of an inter-connected network of large inter-laminar voids in these samples which is visualized by infiltration of resin into this continuous network (Figure 6-7). The absence of a porous network in the low porosity sample (0.39%) results in zero permeability.

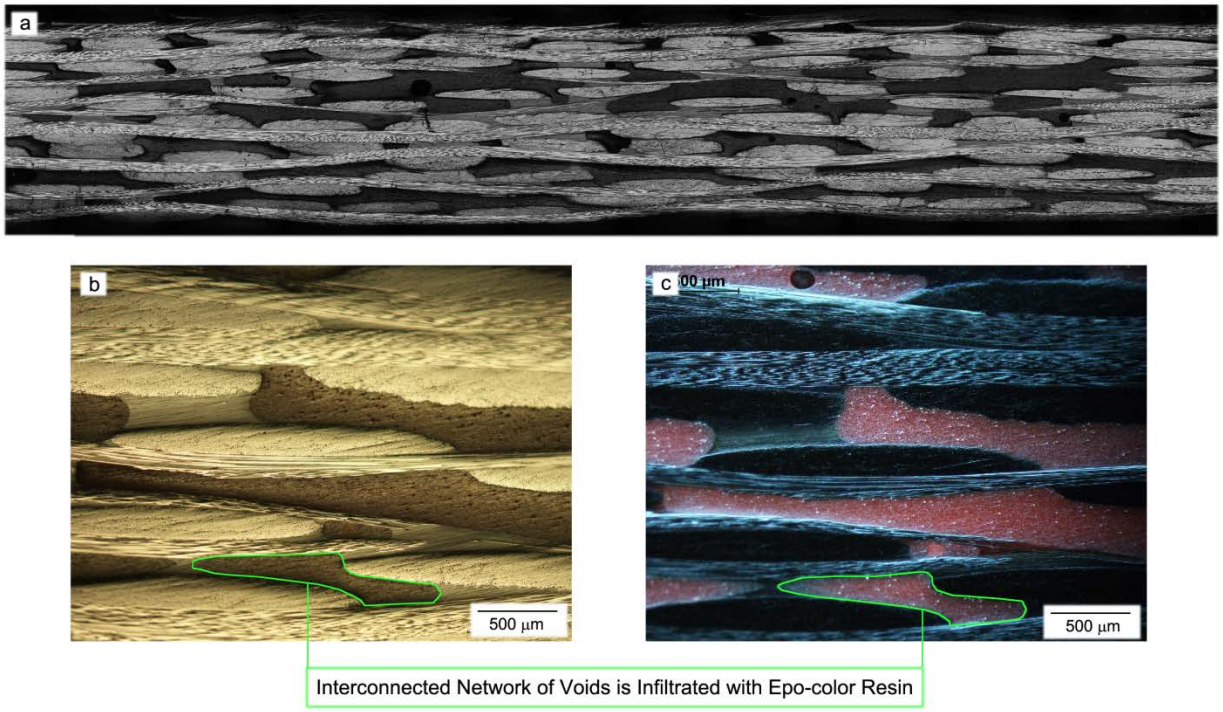

Figure 6-7 a) Resin infiltrated network of interconnected inter-laminar voids (vent time: 4 hours). High magnification images b) bright field image, c) dark-field image.

The Reynolds number (Re) is generally used to determine the boundary between turbulent and laminar flow regimes. The Reynolds number associated with the flow condition in the high porosity samples in this test was investigated due to their high permeability value (2×10^{-11} m^2)

and potential presence of turbulent flow. The permeability related Reynolds number is defined as follows [44]

$$Re = \frac{\rho v \sqrt{K}}{\mu} \quad (6\text{-}1)$$

Where ρ (kg/m^3): gas density, v (m/s): gas velocity, K (m^2): gas permeability and μ (Pa.s): gas viscosity.

The transition from laminar to turbulent flow regime occurs in the Reynolds number range of 1 to 10 [44]. The Reynolds number for the current flow conditions is about 0.65 (Table 6-1), indicating that the flow is close to the laminar-turbulent transition regime. The air viscosity at ambient condition is 1.82×10^{-5} Pa.s and its density is 1.2 kg/m^3. The air flow velocity is estimated for a one atmosphere pressure gradient over the short 0.051 meter flow distance in this test (section 7.3.2).

6.4 Summary

The main findings of this chapter are:

- Porosity decreases as the vacuum time increases.
- Releasing the vacuum in the early stages of the process (< 6 hours) results in high porosity samples (20% - 28%). An inter-connected network of inter-laminar voids makes up the majority of the porosity in these samples.
- Releasing the vacuum after 6 hours into the cure cycle does not affect the void content.

Chapter 7: Time Scales for Gas Transport and Vacuum Debulk in Out of Autoclave Processing of Prepregs

7.1 Introduction

The evolution of porosity in OOA processing of prepregs is a complex phenomenon which involves interaction of mechanisms such as gas transport, resin transport, cure, heat transfer, and fiber bed compaction. A better understanding of void formation, void evolution, void removal, and the process parameters that drive these phenomena is required to better mitigate porosity in large complex parts. Most OOA prepregs are partially impregnated to allow for gas transport and air removal. Initial porosity values are often around 25-35% due to partial impregnation of the fibres but the requirements on cured laminates are often less than 2% porosity, which requires that most of the entrapped air needs to be removed or dissolved during the process.

Figure 7-1 shows a schematic of gas transport and porosity in these material systems based on laboratory studies of porosity evolution (section 5.3.1.2 and 5.3.1.3). The as laid-up laminate has a porosity around 30% because of the partial impregnation of the prepreg plies and the air gaps formed between plies during lay-up. Before heating up and curing the laminate, the laminate is typically subject to a room temperature vacuum debulk for a few hours with the purpose of removing entrapped air from the laminate. During this vacuum debulk, significant amounts of air is removed from the laminate but the porosity (volume fraction void space in the laminate) only drops slightly, mainly due to fibre bed compaction as the air pressure inside dry fibre tows and within gaps in the laminate is lowered. At the end of the room temperature debulk there is still a lot of void space inside the laminate but the air pressure is now very low so when the laminate is

heated up, the resin viscosity drops and the resin readily flows into the evacuated void space and a laminate with low final porosity is achieved. Given the great importance of gas removal to achieve low porosity levels, the aim of this chapter is to better understand the gas transport processes and in particular the time scales associate with gas transport in order to be able to predict the required debulk time to achieve a specified porosity level.

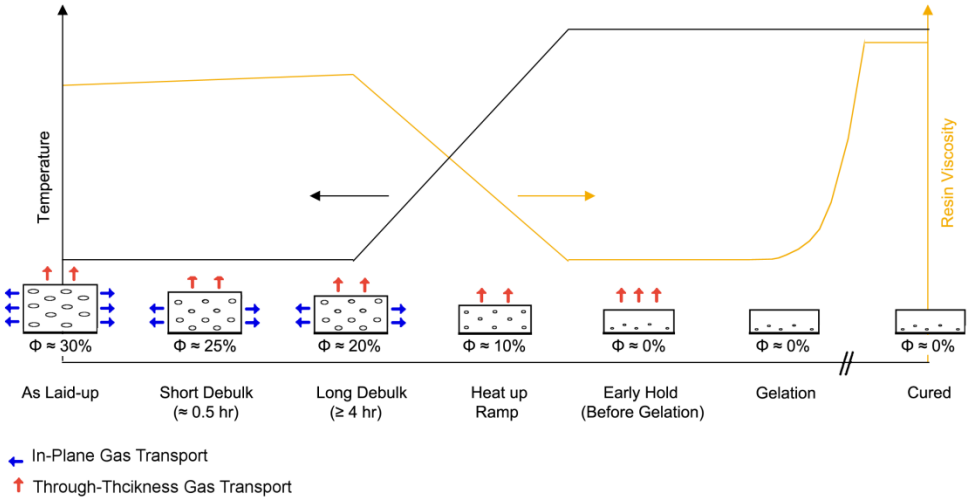

Figure 7-1 Schematic of gas removal and porosity (φ) evolution in processing of OOA prepregs (section 5.3.1).

In OOA prepregs, gas transport can occur through diffusion or momentum transport. Momentum transport is typically described by Darcy flow through porous medium [45] and is evaluated through Darcy's law and permeability measurements [51]. The anisotropic nature of prepreg gas permeability, in-plane and through thickness, has been studied via both pressure decay [10, 49, 51] and steady state flow [11, 34, 39, 54, 74, 102] measurement techniques. Several researchers have studied air and moisture diffusion in epoxy prepregs and have developed models that predict void growth and collapse via diffusion based on processing parameters such as pressure

and temperature [42, 7, 35, 43]. Diffusion coefficients for species of importance in epoxy prepregs, such as moisture and nitrogen, are reported to be in the range of 10^{-13} to 10^{-9} m^2/s under atmospheric pressure and for typical temperature ranges seen in prepreg processing [42, 35]. In gas transport studies related to prepreg processing to date, either diffusion or Darcy flow have been studied. However, an improved understanding of the relative efficiency of these two transport mechanisms during OOA processing is required to develop better guidelines for process design and ultimately quantitative models that can predict porosity under industrial process conditions. This study is limited to the role of gas transport on porosity reduction. Effect of factors like resin impregnation, compaction and void migration on porosity removal in OOA prepregs has been presented in the recent literature [71, 98, 103].

7.2 Methods

7.2.1 Materials

Two different forms of the OOA carbon/epoxy prepreg material MTM45-1, a five-harness satin (5HS) weave and a unidirectional (UD) tape, were used in this study (Table 7-1). Two different rolls of the five-harness satin fabrics were used and as the degree of resin impregnation and therefore initial thickness and porosity was quite different, the two rolls are referred to as “Thin” and “Thick”, respectively.

Table 7-1 Specifications of the MTM 45-1 (ACG) prepreg forms used in this study

Name	Weave pattern	Reinforcement	Resin Content (wt%)	Areal Density (gr/m^2)	Ply thickness (mm)		Initial porosity (φ_0) (%)
					After debulk[1]	After cure	
MTM45-1/ 5HS "Thin"	5HS	HTS40 E13	36	375	0.46	0.395	16.7
MTM45-1/ 5HS "Thick"	5HS	HTS40 E13	36	375	0.53	0.395	33
MTM45-1/ UD	UD	GA045	32	149	0.18	0.15	20[2]

5HS = Five harness satin weave; UD = Uni-directional; All reinforcements were in 6k tows.
[1] After 7 minutes of debulk for each four layers
[2] Estimated based on thickness measurements

7.2.2 Laminate Preparation

Effect of the gas transport direction on porosity was evaluated by making samples with different sealing configurations from three types of prepreg (Table 7-1). Flat square 5HS laminates were made of 8 layers of 127 mm × 127 mm prepreg (cured ply thickness (CPT) ≈ 0.39 mm), and uni-directional laminates were made of 18 layers of 127 mm × 127 mm prepreg (CPT ≈ 0.15 mm, $[0]_{18}$), to compensate for the smaller ply thickness. The final thickness of 5HS and UD laminates was about 3.2 mm and 2.8 mm respectively. A thick 90 layer uni-directional laminate, $[0]_{90}$, was also made for thickness comparison purposes (127 mm × 127 mm × 13.5 mm). A room temperature debulk (laminate held under full vacuum under a vacuum bag at room temperature) was performed for half an hour. After that, the laminates were prepared using three different sealing configurations: surface and edge breathing, edge breathing only and surface breathing only. Details of sample preparation and cure cycle (80 °C cure) are described in section 5.2.3 (Figure 5-1). Once cured, laminates were post cured at 180 °C for 2 hours (heat up at 0.3 °C/min and cool down at 2 °C/min).

7.2.3 Characterization of Voids and Porosity

The void content or porosity of the laminates was quantified by measuring the void area fraction of sectioned laminates using optical microscopy. All laminates were cut and their whole cross section was prepared for optical microscopy using standard grinding and polishing steps described in ASTM E2105 [83]. A mosaic image was taken from the entire cross section at 100X magnification using a Nikon optical microscope (EPIPHOT 300) and the Clemex software (vision PE 6.0). The Image J software [85] was used for measurement of the area fraction of voids from the mosaic images. Two to three replicate laminates were analyzed for each data point of MTM45-1/5HS-Thin and Thick laminates and one for MTM45-1/UD laminates.

7.2.4 Permeability Measurements

Permeability tests were performed to evaluate the air permeability of the MTM45-1/5HS-“Thin” prepreg during room temperature vacuum debulk and during heat-up and cure. Permeability measurements were performed both in-plane and through thickness as described in section 5.2.5. The measured permeability values for MTM45-1/5HS-“Thick” are taken from the study in section 5.3.2.2, using the identical test set-up and the UD permeability is estimated based on measurements on another partially impregnated UD prepreg [34].

7.3 Results and Discussion

7.3.1 Effect of Breathing Direction on Final Porosity

The porosity of cured laminates with different sealing configuration was determined via optical microscopy. Measured porosity and optical micrographs for these samples are shown in Figure 7-2 and Figure 7-3. The initial porosity of these samples is in the range of 15 to 30% depending on the prepreg type (Table 7-1). Despite high initial porosity, Figure 7-2 shows that the final porosity can be reduced down to less than 2% regardless of the sealing configuration used during debulk and cure. Laminates made of 5HS-Thick prepreg, with highest permeability, have the lowest porosity under all breathing conditions. The other two prepreg systems, 5HS-Thin and UD, have higher porosity when sealed at the edges (c), compared to samples that can breathe from the edges (b) or on all sides (a). Optical micrographs of edge sealed samples are shown in Figure 7-3 b and d. Both these samples have higher porosity on the mould side than the bag side, where vacuum is applied. This observation of a porosity gradient towards a vacuum source, has been reported previously in section 5.3.2.2.

To study the effect of thickness, a thick laminate was made from MTM45-1/UD prepreg. The length and width of this laminate is equal to other UD laminates (≈ 127 mm × 127 mm), but its thickness is five times higher (13.5 mm versus 2.8 mm). This laminate was cured with all sides breathing, configuration (a), and had less than 0.01% porosity after cure. This is similar to its thinner counterpart when breathing was allowed in all directions, configuration (a), Figure 7-2. However, porosity of thick laminate is lower than its thinner counterpart ($\varphi \approx 0.45\%$) when it is able to only breath in the, low permeability, through –thickness direction (configuration (c)).

These results show that both in-plane and through thickness gas transport are important in these prepreg systems as void reduction can be achieved via gas evacuation in both directions.

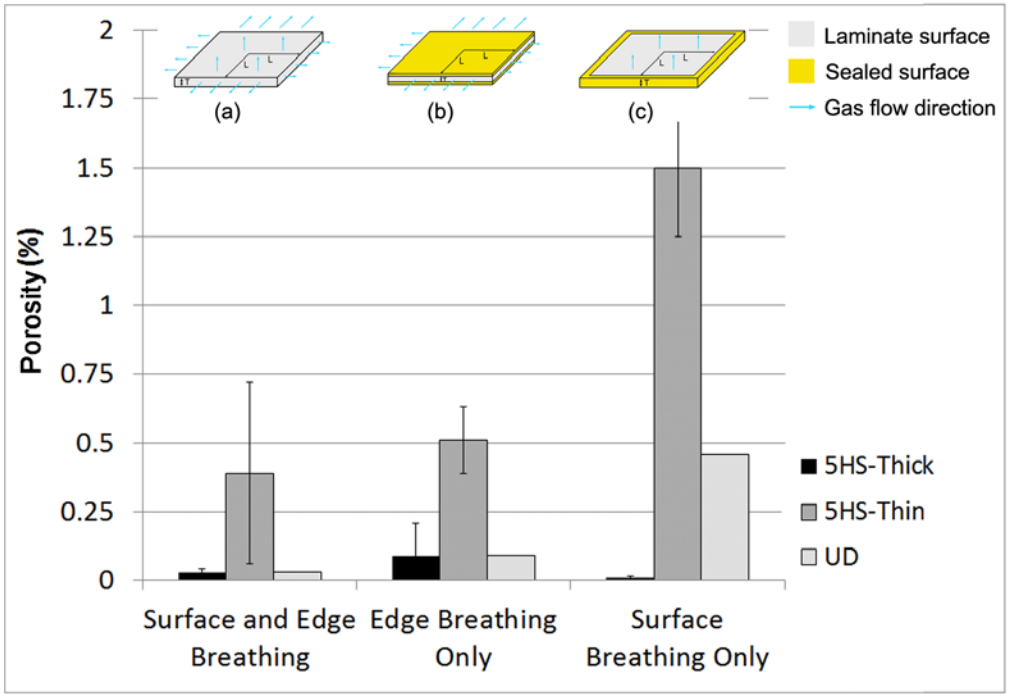

Figure 7-2 Effect of sealing configuration and breathing direction on porosity (φ) (Error bars denote +/- one standard deviation).

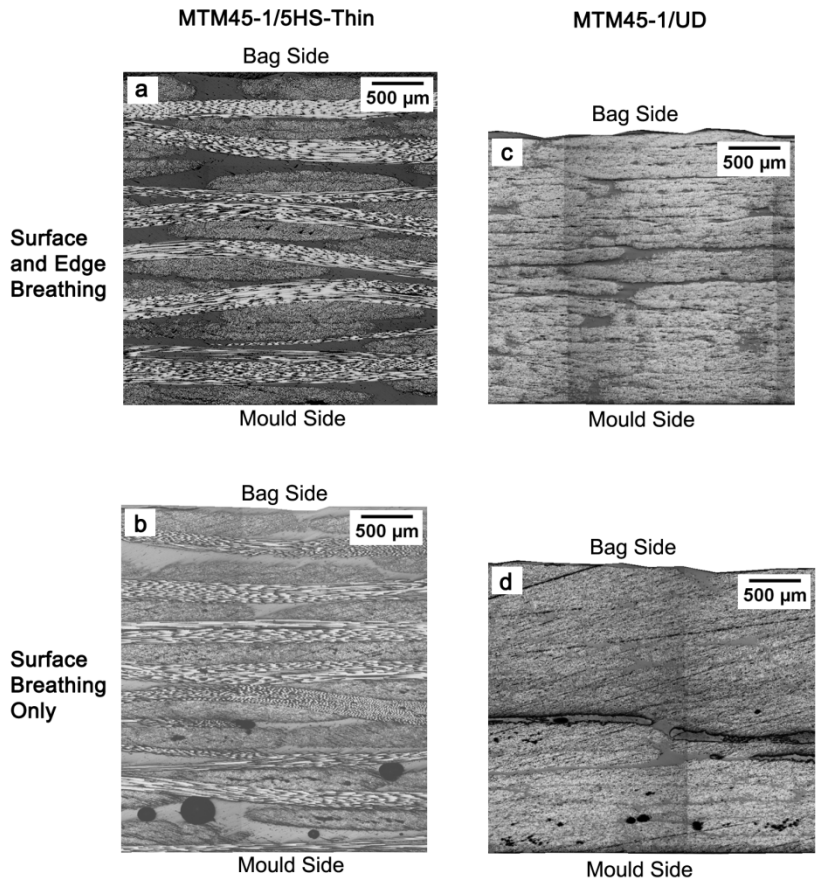

Figure 7-3 Cross sectional optical microscopy images of samples presented in Figure 7-2: (a) 5HS-Thin – Surface and Edge Breathing (no porosity gradient); (b) 5HS-Thin – Surface Breathing Only (porosity gradient); (c) UD – Surface and Edge Breathing (no porosity gradient); (d) UD – Surface Breathing Only (porosity gradient).

7.3.2 Time Scales for Gas Transport during Processing of Small Flat Laminates

Approximate time scales associated with molecular diffusion and Darcy flow of dry air during room temperature debulk, heat-up and cure are determined for the manufactured 127 mm × 127 mm × 8 layers (≈ 4 mm) laminates made of 5HS-Thick prepreg. Determination of approximate time scales for different transport mechanisms during the process elucidates the effectiveness of

different transport mechanisms in achieving a low porosity laminate. Time scales are determined based on standard one dimensional Darcy flow and Fickian diffusion.

Gas advection in porous medium is widely analyzed using Darcy's law [44], which states that the superficial gas velocity (*v)* is directly proportional to the gas permeability of the porous medium and the pressure gradient of the gas phase in the direction of the flow. In one dimension, this can be expressed

$$v = -\frac{K}{\mu}\frac{dP}{dx} \tag{7-1}$$

Where K (m^2): gas permeability, μ (Pa.s): gas dynamic viscosity, P (Pa): gas pressure, x (m): distance.

For Darcy's law to be applicable, the gas flow needs to be laminar. The Reynolds number (Re) is generally used to determine the transition from turbulent to laminar flow regimes in the high permeability range and the "Klinkenberg effect" is used to study the boundary between laminar and molecular flow in the low permeability range. The permeability related Reynolds number is defined as follows [44]

$$Re = \frac{\rho v\sqrt{K}}{\mu} \tag{7-2}$$

Where ρ (kg/m^3): gas density, v (m/s): gas velocity, K (m^2): gas permeability and μ (Pa.s): gas viscosity.

The transition from laminar to turbulent flow regime occurs in the Reynolds number range of 1 to 10 [45]. The Reynolds number for the current flow conditions is of the order of 10^{-4} using

equation (7-2) with the input values listed in Table 7-2, indicating that the flow is laminar. The air viscosity is assumed to be constant at 1.82×10^{-5} Pa.s and the slight variation within the temperature range of this study (≈ 20 °C - 80 °C) is considered [45]. The air flow velocity is approximately 0.01 m/s for a one atmosphere pressure gradient over the short 0.064 meter flow distance in this study (Figure 7-4).

Table 7-2 Input parameters for calculation of the Reynolds number and time scales for Darcy flow and diffusion.

Parameter	Symbol	Value
Density	ρ_{air}	1.2 kg/m^3 (T = 20 °C, P = 1 atm)
		1.1 kg/m^3 (20 < T (°C) < 80, P = 1 atm)[1]
Permeability	K_{air}	1.5×10^{-13} m^2 [section 5.3.2.2]
Viscosity	μ_{air}	1.82×10^{-5} Pa.s
Air velocity	v_{air}	0.01 m/s
Diffusion Coefficient	$D_{N2 \text{ in epoxy}}$	10^{-11} - 5×10^{-10} m^2/s [42] (20 < T (°C) < 80, P = 1 atm)
Henry's Constant	$K_{H\ (N2 \text{ in epoxy})}$	4.83 MPa.m^3/kg [42] (T = 40 °C, P = 1 atm)

[1] Average density in the temperature range.

In Darcy flow it is assumed that the flow velocity is zero at the interface between the fluid and the porous medium. However, in low permeability medium or at very low gas pressures, slip phenomenon occurs, which is due to free molecular flow (Knudsen diffusion) and results in higher velocity and permeability than predicted by Darcy's law [44, 46]. This phenomenon is known as the "Klinkenberg effect". Klinkenberg derived an expression relating the effective permeability of gas (K) in the Knudsen regime to the liquid permeability (K_l) or permeability for the no slippage condition [44]:

$$K = K_l\left(1 + \frac{b}{\bar{P}}\right) \quad (7\text{-}3)$$

Where, $\bar{P}$ (Pa) is the average gas pressure and b is the Klinkenberg coefficient. The Klinkenberg coefficient is specific to each gas, temperature and porous medium. Heid et al. [44] developed the following correlation (7-5) for the Klinkenberg coefficient of air at 25 °C in a low permeability porous medium ($10^{-12} – 10^{-17}$ m^2), which is representative of the current conditions.

$$b = 0.11K_l^{-0.39} \tag{7-4}$$

Where K_l is in m^2 and b is in Pascals.

Equations (7-3) and (7-4) are used to evaluate the presence of slip conditions in this study. The minimum permeability measured in this study is of the order of 10^{-17} m^2, and the pressure varies in the range of zero to one atmosphere. Under current conditions the slip effect can increase effective air permeability of this system by a factor of five at most. As the majority of gas transport will occur at much higher permeability under Darcy conditions, the "Klinkenberg effect" is not included in the following time scale calculations.

Considering the geometry of the simple flat laminate in Figure 7-4, the time scale for Darcy flow can be approximated as

$$t \approx \frac{\Delta x}{v} \tag{7-5}$$

where Δx is the distance traveled and *v* the average velocity.

By substituting the velocity from equation (7-1) into equation (7-5) we get the following expression for the time scale of Darcy flow in the x-direction, under a constant pressure gradient of ΔP over the flow distance Δx

$$t_{Darcy} \approx \frac{\mu}{K}\frac{\Delta x^2}{\Delta P} \quad (7\text{-}6)$$

Equation 7-6 will be used to estimate the Darcy flow time scale in the in-plane (IP) and through thickness (TT) directions during a long room temperature debulk and during a heated cure cycle (Figure 7-5). The permeability K required in eq. (7-6) is taken from permeability evolution study on the same prepreg system where the permeability was measured as a function of time during a long temperature debulk and heat up, see section 5.3.2.2 (Table 7-3).

Table 7-3 In-plane and through thickness permeability of MTM45-1/5HS – Thick during the process.

Processing Stage		Processing Time (hr)	Temperature (°C)	In-plane Permeability (m^2)	Through thickness Permeability (m^2)
Long Debulk		0	20	1.56×10^{-13}	2.26×10^{-16}
		0.23	20	9.61×10^{-14}	8.67×10^{-17}
		4	20	$5.96\times10^{-14(1)}$	$5.38\times10^{-17(1)}$
		13.5	20	$5.82\times10^{-14(1)}$	$5.27\times10^{-17(1)}$
Cure Cycle	Debulk	0	20	1.56×10^{-13}	2.26×10^{-16}
		0.23	20	9.61×10^{-14}	8.67×10^{-17}
	Ramp	0.73	35	5.66×10^{-14}	4.89×10^{-17}
		1.23	50	1.07×10^{-14}	1.98×10^{-17}
		1.73	65	3.87×10^{-15}	1.96×10^{-17}
		2.23	80	2.63×10^{-15}	1.95×10^{-17}
	Hold	3.23	80	0^2	2.20×10^{-16}
		4.23	80	0^2	4.05×10^{-16}
		5.23	80	0^2	7.49×10^{-18}
		6.23	80	0^2	0^2
		22.23	80	0^2	0^2

[1] Data from [11]
[2]At this level of permeability, the gas flow rate is below the detectable limit (< 6 mL/min).

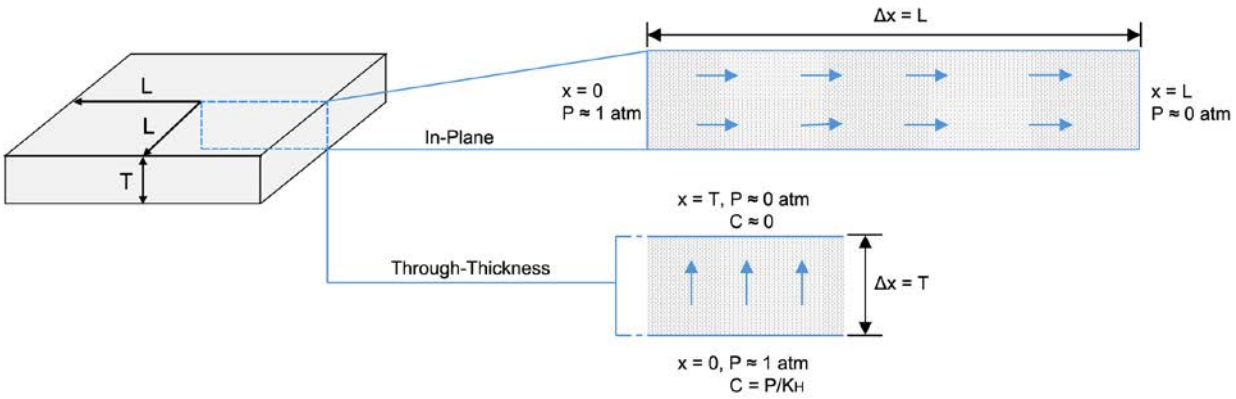

Figure 7-4 Geometry, flow distance, pressure and concentration boundary conditions used in the time scale study.

Another potential means of gas transport in this system is the molecular flow or diffusion of gaseous species under concentration gradient through the epoxy matrix. Fick's first law of diffusion in the x direction is written as [40]

$$J = -D\frac{dC}{dx} \tag{7-7}$$

Where J (kg/m^{2}s): diffusion mass flux, D (m^2/s): diffusion coefficient, C (kg/m^3): concentration and x (m): distance. The average velocity is

$$v_x = \frac{J}{\rho} \tag{7-8}$$

Where ρ (kg/m3) is the density of diffusing gas.

Having the diffusion velocity (v_x), the time scale for gas diffusion in the x-direction, under a constant concentration gradient ΔC over the diffusion distance of Δx can be approximated as

$$t_{Diff} \approx \frac{\rho}{D}\frac{\Delta x^2}{\Delta C} \tag{7-9}$$

At gas-liquid interfaces, Henry's law relates the concentration of the dissolved gas in the liquid phase to its partial pressure, when the concentration of the diffusing gas is low in the liquid phase [40]

$$C = \frac{P}{K_H} \tag{7-10}$$

Where P (Pa): partial pressure of the gas at the interface, C (kg/m^3): concentration of gas in resin at the interface, K_H (Pa.m^3/kg): Henry's constant (a temperature-dependent empirical constant).

In this study it is assumed that the gaseous phase is air and the presence of other constituents such as water vapor is neglected. The equilibrium concentration of air dissolved in the resin at the interface with the gaseous phase adjacent to it can be estimated using Henry's law. Substitution of C from equation (7-10) into equation (7-9) gives the following expression for the diffusion time scale

$$t_{Diffusion} \approx \frac{\rho K_H}{D}\frac{\Delta x^2}{\Delta P} \tag{7-11}$$

We can now use the developed expressions for Darcy flow and diffusion, eqns. (7-6) and (7-11), to calculate the approximate mass transport time scales for the laminates made in this study. We will evaluate gas transport in two directions, in-plane $\Delta x = L$ and through-thickness $\Delta x = T$ (Figure 7-4). It is assumed that the gas pressure inside the laminate is equal to resin pressure and constant at one atmosphere and that the pressure is zero atmospheres at the laminate boundaries, giving a constant ΔP of one atmosphere in the time scale calculations, which defines a lower bound for the time scale. In general, the applied pressure (one atmosphere) is shared by resin and fiber bed. Xin et al. [104] monitored resin pressure during the processing of a net resin prepreg

system under atmospheric compaction pressure and showed that resin pressure stays constant and about 0.5 atmosphere throughout the process. The gas permeability of the laminate is varying during room temperature debulk and cure, according to direct gas permeability measurements on the laminate (Table 7-3). In calculating the diffusional time scale, Henry's constant is taken as 4.83 MPa.m^3/kg [42] and the diffusivity of nitrogen (as the main constituent of air) in the epoxy resin as 10^{-11} – 10^{-10} m^2/s [42]. The input data for the calculations are summarized in Table 7-2. The diffusional time scale was only calculated for diffusion through the thickness of the laminate as this gives the shortest time scale. For diffusion, the laminates were simply treated as being composed of homogenous resin with the same diffusivity in all directions. For Darcy flow, time scales were calculated both for in-plane and through-thickness gas transport as they are very different. The results of these calculations during an extended room temperature debulk and during heat up and cure are shown in Figure 7-5.

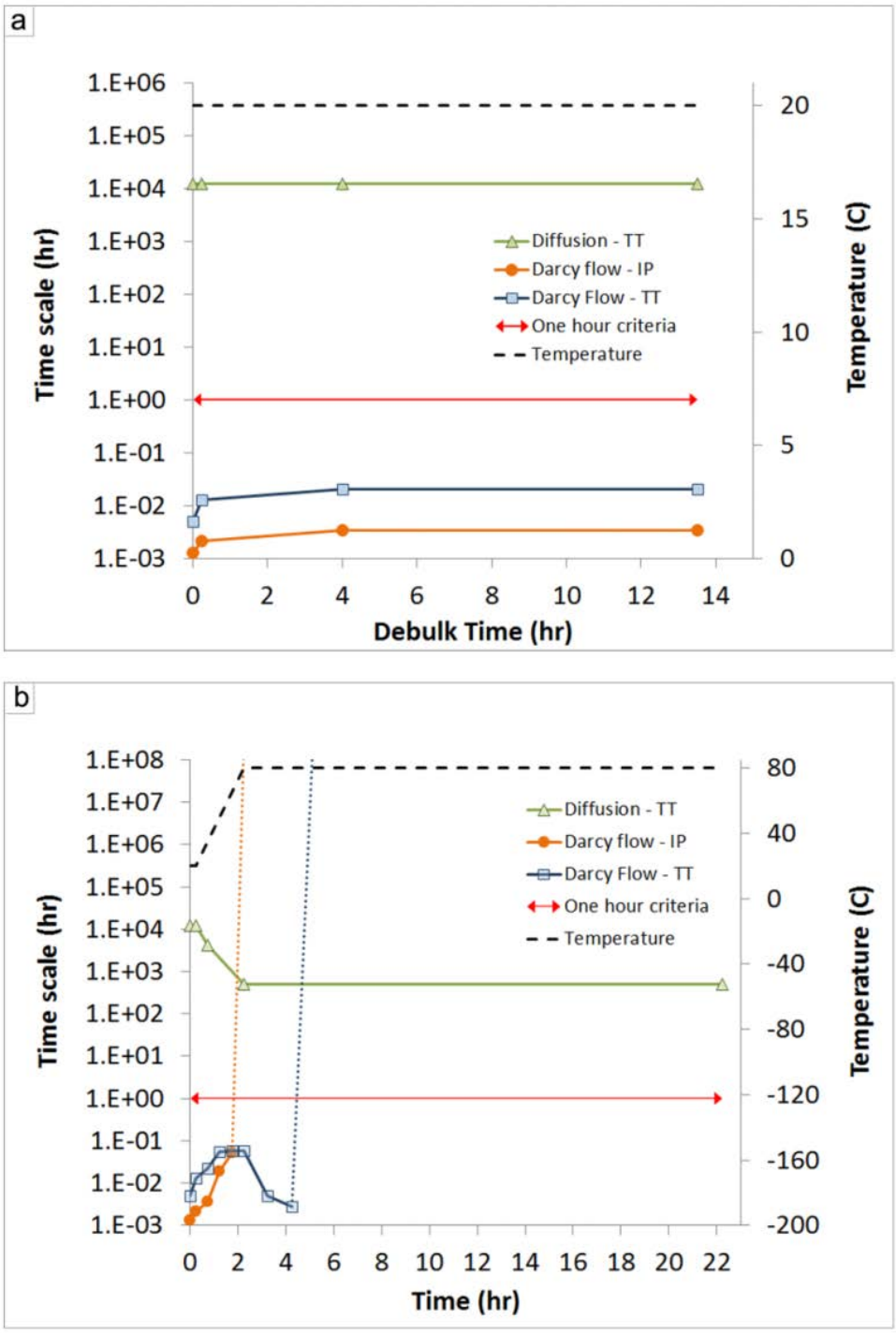

Figure 7-5 Time scales for gas transport via Darcy flow and diffusion during a) Long room temperature debulk; b) 80 °C cure cycle. The calculations were made for laminates with L ≈ 64 mm, T ≈ 4 mm (Figure 7-4). The red line represents a reference time of one hour. TT = Through-Thickness, IP = In-Plane.

Figure 7-5 a shows that during the long room temperature debulk the time scale associated with diffusion through the thickness of the laminate is of the order of 10^4 hours. Diffusion is therefore not an effective means of air removal during the room temperature debulk stage. The time scales associated with air transport via Darcy flow is 10^{-3} hours in the in-plane direction and 10^{-2} hours in the through-thickness direction. This shows that Darcy flow is a viable gas transport mechanism during room temperature debulk and that for the laminate size in this study, in-plane Darcy flow is the main gas removal mechanism during room temperature debulk. The time scale for diffusion is constant in Figure 7-5 a because all properties in eq. (7-11) are assumed constant during the debulk phase. The time scales for Darcy flow however are increasing with debulk time as the gas permeability is reduced due to a compaction of the laminate during debulk [21].

Figure 7-5 b shows the approximate time scales for gas transport during a heated cure cycle. The time scale for diffusion through the thickness of the laminate decreases from 10^4 hours at room temperature to 10^2 hours at 80°C due to the temperature dependence of the diffusivity D [42]. Despite this decrease, diffusion does not provide an effective means of air transport given the timescale of the cure cycle. The time scales for Darcy flow, both in-plane and through thickness, start at the same level as for the room temperature debulk but increases with temperature as the resin heats up and flows into the pore spaces of the laminate, reducing the gas permeability. At the end of the heat-up ramp the time scale for in-plane Darcy flow becomes infinite as the gas permeability in-plane becomes effectively zero (section 5.3.2.2). However, Darcy flow in the through thickness direction is still possible due to the increased through thickness gas permeability at this stage of the process (5.3.2.2). Through-thickness Darcy flow will cease to be

effective at about 5 hours, when the through thickness gas permeability becomes zero (Table 7-3).

Figure 7-5 suggests that under the conditions of this study, gas transport occurs mainly via Darcy flow as the time needed for diffusion of air through the laminate is too long given the time scale of this process. During the room temperature debulk and the temperature ramp section of the heated cycle, Darcy flow in both in-plane and through thickness are viable transport mechanisms. In the early stages of the hold period (2.23 – 5.23 hours) the only viable air transport mechanism is Darcy flow in the thickness direction and after that period no effective air transport mechanism is available (5.3.2.2). It should be noted that the long time scales associated with gas diffusion in this study are specific to diffusion of air in epoxy. The time scale of diffusion of other species may have shorter or longer time scales depending on their solubility and diffusivity in epoxy. Water, for example, has higher solubility in epoxy than air, which results in higher concentration gradients and shorter diffusional time scales. Grunenfelder et al. [7] and Kay et al [13] both have shown that the moisture content of the laminate can have a pronounced effect on the porosity of OOA laminates, and that moisture transport in these systems are important. Another point that needs to be emphasized is the importance of diffusion distance. While diffusion of air through the whole thickness of laminate ($T \approx 4$ mm) is evaluated to be infeasible due to long time scales, air diffusion can be feasible over short distances such as through a thin resin film. An example is the time scale of air diffusion from a resin void towards a low pressure interconnected porous network ($\Delta x \approx 200$ μm), which is about an hour and can be considered as a viable gas transport mechanism during the hold stage.

The time scale analysis presented in Figure 7-5 is applicable for the small laminate geometry shown in Figure 7-4 (L ≈ 64 mm, T ≈ 4 mm). In section 5.3.1.3 it is shown that the final porosity of samples with this geometry, subject to the described processing conditions, is less than 0.3 %. However, the sample geometry has a significant effect on the timescale for gas transport. Equations 7-6 and 7-11 show that the time scale for gas transport increases quadratically with transport distance, suggesting that much longer times must be allowed for gas removal when processing large laminates. In the following section the effect of sample size on gas transport in flat, square laminates is investigated.

7.3.3 Effect of Size on Time Scales for Gas Transport

Part geometry and part complexity play an important role for the effectiveness of gas transport during the process. In a complex layup with ply-drops and gaps, caul-sheets and complex bagging, the pathways through which gas transport occur are more tortuous and complex than for simple flat laminates. A critical aspect is the distance any trapped or generated gas has to travel to escape the laminate [13]. The longer the transport distance the slower the transport process. Consequently, it is challenging to remove the gas out of large complex parts and produce void free structures as the critical transport distances typically scale with part size for these material systems [105, 106, 107].

The samples analyzed in the previous section were very small, lab scale specimens. In this section, the effect of length and thickness on the time scales of gas transport via diffusion and Darcy flow during three different stages of the process is evaluated: long room temperature

debulk, heat up ramp, and 80 °C hold. The Darcy and diffusion time scales (equations 7-6 and 7-11) are written in terms of sample length L and thickness T in Table 7-4.

Table 7-4 Time scale approximations with respect to laminate size (L: half of total in-plane length, T: thickness).

Time scales		
Darcy Flow		Diffusion
In-Plane	Through-Thickness	Through-Thickness
$\frac{\mu}{K_{IP}}\frac{L^2}{\Delta P}$	$\frac{\mu}{K_{TT}}\frac{\mathrm{T}^2}{\Delta P}$	$\frac{\rho K_H}{\mathrm{D}}\frac{\mathrm{T}^2}{\Delta P}$

K_{IP} = In-plane permeability, K_{TT} = Through-thickness permeability.

The average input parameters used for each stage of the process are listed in Table 7-5. All calculations are done based on the presence of a one atmosphere pressure difference over the transport distance.

Table 7-5 Average input parameters for each processing stage used in the scale up study

Parameter	Symbol	Long debulk 13.5 hours at 20 °C	Heat up ramp 20 °C to 80 °C at 0.5 °C/min	Hold at 80 °C 2 – 5 hours
Diffusion Coefficient [42]	$D_{N2\ in\ epoxy}$ (m^2/s)	2×10^{-11}	1.2×10^{-10}	5×10^{-10}
In-Plane Permeability [section 5.3.2.2]	K_{IP} (m^2)	9.3×10^{-14}	2.38×10^{-14}	2.59×10^{-15}
Through-Thickness Permeability [5.3.2.2]	K_{TT} (m^2)	1.2×10^{-16}	2.9×10^{-17}	1.32×10^{-16}

Figure 7-6 shows the effect of laminate length (L) and thickness (T) on the time scales for the different transport mechanisms during the three stages of the process: long debulk, heat up ramp, and 80°C hold. In the length study (Figure 7-6 a, c and e), the thickness of the laminate is fixed at 10 millimeters and the length varies from 0.1 to 1 meter and in the thickness study (Figure 7-6 b, d, f), the length of the laminate is fixed at one meter and the thickness varies from 10 to 50

millimeters. Note that L represents the transport length which is half of the total in-plane length (Figure 7-4).

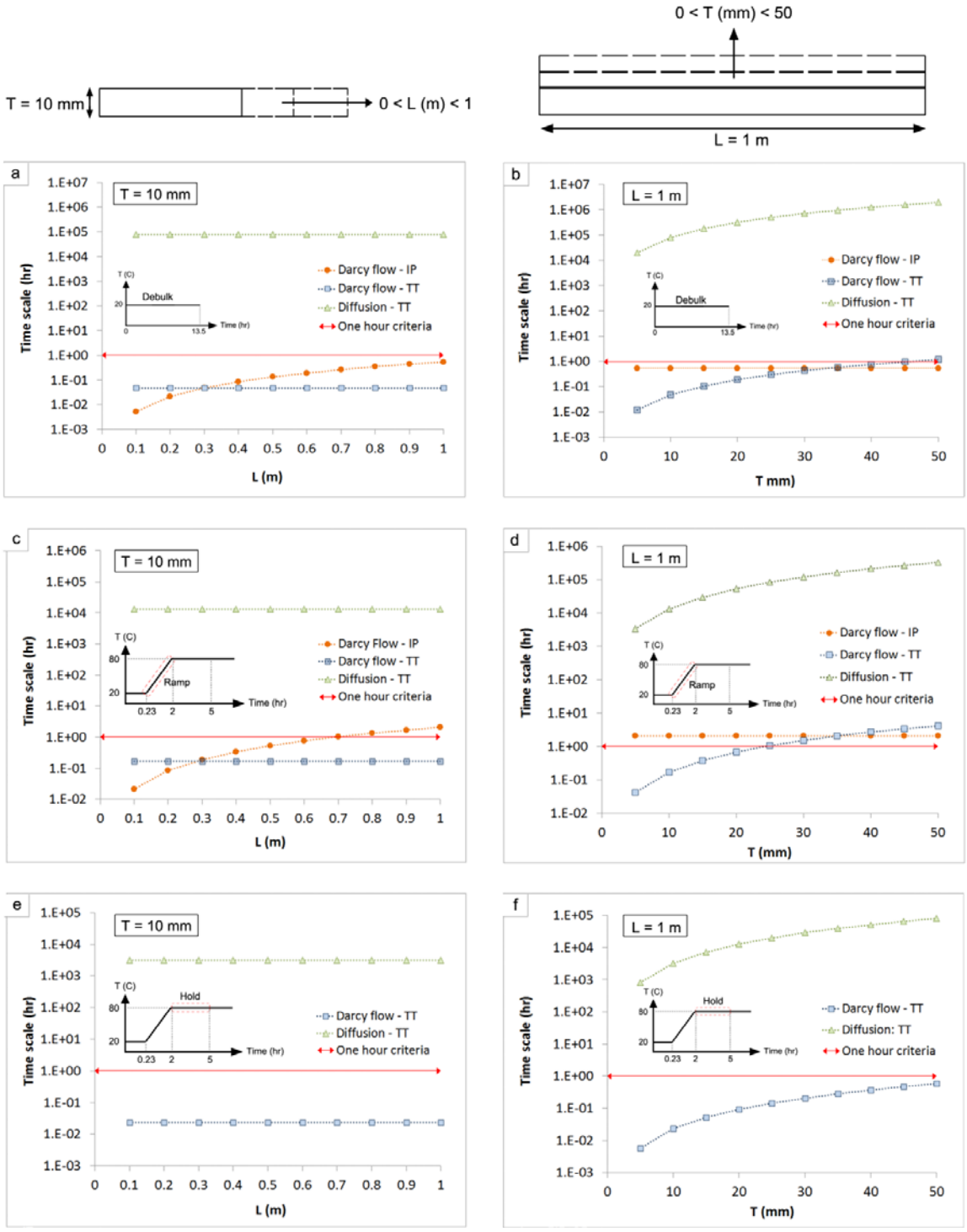

Figure 7-6 Effect of laminate geometry, length L and thickness T, on time scales for gas transport at different stages of the process a, b) debulk, b, d) ramp and e, f) early temperature hold. IP = In-Plane, TT = Through-Thickness.

The feasibility criteria for effective gas transport is defined to be a time scale of less than one hour as indicated with a red line in Figure 7-6. During the debulk stage (Figure 7-6 a,b), Darcy flow is feasible over the entire size range ($L \leq 1m$, $T \leq 50$ mm). However, the dominant flow direction changes from in-plane to through thickness for laminates longer than 0.3 m ($T = 10$ mm). The opposite change in the preferred flow direction occurs as the thickness passes 35 mm ($L = 1$ m). Similar trends can be seen during the heat up ramp (Figure 7-6 c, d). During the heat up ramp, the average permeability decreases in both directions, which results in longer time scales than during the debulk stage. Consequently, in-plane Darcy flow is only feasible for laminates shorter than 0.7 m ($T = 10$ mm) and through- thickness Darcy flow is only feasible for laminates thinner than 25 mm. During the early hold stage, Darcy flow in the in-plane direction is not viable and the only feasible means of gas transport is Darcy flow in the thickness direction. Figure 7-6 shows that regardless of the processing stage, Darcy flow is the only feasible gas transport mechanism in this size range ($L \leq 1$ m, $T \leq 50$ mm) as the required time scale for air diffusion is too long.

7.3.4 Guidelines for the Required Debulk Time to Achieve a Defined Porosity Level

Having established the importance of Darcy flow for gas transport in this material system we will now develop guidelines for the required debulk time to achieve a defined porosity level. The analysis in the previous section focused on approximate velocities and time scales for gas transport but did not account for the decrease in gas pressure and increase in transport time as the gas is progressively removed from the laminate. A more comprehensive study of gas transport in prepreg systems has been performed previously [34]. The study considered one-dimensional Darcy flow of an ideal gas through a medium with constant porosity, which is a good

approximation of the current material system during a room temperature debulk. By performing an empirical fit to a numerical solution of the resulting non-linear differential equation, an explicit relationship between debulk time t and mass of gas m remaining in the laminate can be established [34, 108]

$$t \approx \left(\frac{\mu}{K}\frac{\Delta x^2}{\Delta P}\right)\varphi_0\left[1.11 * ln\left(\frac{m_0}{m}\right)\right]^{\frac{5}{3}} \quad (7\text{-}12)$$

Where: t: time, φ_0 (-): initial volume fraction of porosity, μ (Pa.s): gas viscosity, Δx (m): distance to vacuum port, P (Pa): gas pressure, K (m^2): prepreg permeability, m (kg): mass of gas in laminate, m_0 (kg): initial mass of gas in laminate.

Note the similarity of eq. (7-12) with the simplified time scale equation for Darcy flow, eq. (7-6). As gas is removed via Darcy flow, the pressure drops and the rate of gas removal decreases, which is reflected by the logarithmic term in eq. (7-12). The remaining mass m of gas in the laminate is proportional to the integral of the gas pressure over the transport length and is therefore a measure of the average gas pressure at that time [34]. We can use eq. (7-12) to make a conservative estimate of the final porosity in the laminate. By assuming that the gas permeability is constant during the vacuum debulk, the porosity (volume fraction of pore space in the laminate) is the same at the end of the debulk as it was at the start. The difference is that the gas pressure p inside the pore space is now significantly lower than the one atmosphere at the start. If it is assumed that no more gas evacuation occurs after the end of the room temperature debulk and the resin when heated up flows into the partially evacuated pore space until the resin pressure equilibrates with the gas pressure in the pores we get the following relationship between gas mass (m) and porosity (φ) using the ideal gas law:

$$\frac{\varphi}{\varphi_0} = \frac{m}{m_0} \tag{7-13}$$

Substituting into eq (7-12) we have

$$t \approx \left(\frac{\mu}{K}\frac{\Delta x^2}{\Delta P}\right)\varphi_0\left[1.11 * ln\left(\frac{\varphi_0}{\varphi}\right)\right]^{\frac{5}{3}} \tag{7-14}$$

This expression can be used for one dimensional Darcy flow of gas in a porous medium at constant permeability and temperature. The measured permeability after a room temperature debulk (Table 7-5 and Table 7-6) gives us a lower bound on the permeability and a conservative estimate of gas remaining in the laminate after a specified debulk time t.

Equation 7-14 can be used to create simple debulk time maps that can aid the practitioner in selecting the appropriate debulk time for achieving a specific target porosity (φ) based on part geometry (L, T), prepreg permeability (in-plane and through-thickness) and initial porosity (φ_0). A debulk map that indicates the maximum sample geometry (L^*, T^*) that can be made with a target porosity of less than 2% for different debulk times is shown in Figure 7-1. To achieve a conservative map that is valid for all prepregs used in this study, the minimum permeability and maximum initial porosity measured for the prepregs are used in creating this map (
Table 7-1 and Table 7-6). The map for each debulk time consists of a horizontal line that represents the maximum laminate thickness T^* that can be evacuated in the through-thickness direction to the extent that a final porosity of less than 2% is achieved and a vertical line that represents maximum laminate length L^* that can be evacuated in-plane to achieve a porosity level of less than 2%. The maximum allowable laminate size L^*, T^* increases as the debulk time

increases in Figure 7-7. With the current simplified one-dimensional gas transport model, no coupling between in-plane and through-thickness transport is considered. Figure 7-7 shows that a 0.5 hour debulk is sufficient to evacuate any laminate that is 3.7 mm or thinner via through-thickness gas transport and shorter than 0.21 m (2L ≈ 0.42 m) via in-plane gas transport. In most practical cases, the laminate can breathe both in-plane and through-thickness and it is sufficient that only one laminate dimension is less than the critical dimensions L^*, T^* to achieve a low porosity laminate.

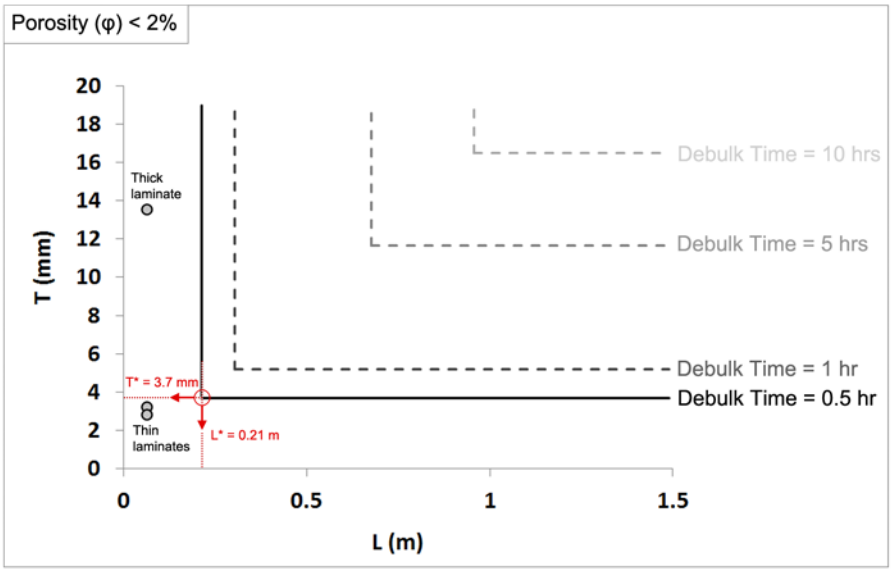

Figure 7-7 Debulk maps showing the maximum part size (L^*, T^*) for achieving a porosity level of less than 2% for a specific debulk time based on eq. (7-14).

Also plotted on the debulk map are the experimental porosity results from the samples made with different breathing conditions and prepregs presented in Figure 7-2, which all were debulked for 0.5 hours and had a porosity level of less than 2%. These samples are represented as three groups which had the same length L but different thicknesses, T = 2.8 mm, 3.2 mm and 13.5 mm. All

thin laminates presented in Figure 7-2 (T = 3.2 or 2.8 mm) fall in the lower left corner of the map, and have dimensions that are smaller than both L^* and T^* for a 0.5 hour debulk. The laminate with higher thickness (13.5 mm) have an in-plane length less than L^* but thickness greater than T^*. As this laminate was allowed to breathe in-plane the expected porosity level is less than 2% which was confirmed experimentally. All samples are expected to have porosity less than 2% according to the debulk map (equation 7-14) which is in agreement with the measured porosity of these laminates (Figure 7-2). This is not a particularly discriminating validation of the debulk map and the predictive capabilities of eq. (7-14) given the limited range of sample dimensions in this study, but it serves as a starting point for a more knowledge-based approach to processing of OOA laminates.

Table 7-6 Prepreg permeabilities after room temperature debulk[1]

Fabric Name	K_{IP} (m^2)	K_{TT} (m^2)
MTM45-1/5HS - Thin [39]	3.1×10^{-14}	2.97×10^{-18}
MTM45-1/5HS - Thick [section 5.3.2.2]	9.61×10^{-14}	8.67×10^{-17}
MTM45-1/GA045 - UD [34]	10^{-14}	10^{-17}

[1] After 7 minutes debulk for each four layers

7.4 Summary

Time scales for air transport via diffusion and Darcy flow were investigated during room temperature vacuum debulk and heat up for laminates made of MTM45-1/5HS OOA prepreg. It was shown that diffusion of air in epoxy, through the laminate thickness, is not an effective means of air transport in order to remove porosity for these material systems and process conditions due to the large time scales associated with molecular diffusion. On the other hand, air transport via Darcy flow is highly feasible and can occur both in-plane and through-thickness,

generally with shorter time scales in the in-plane direction. Experiments with laminates that were sealed at the edges so that gas transport was restricted showed that low porosity laminates can be achieved even if in-plane air transport is prevented and the laminated can only breathe through-thickness.

The effect of laminate size on the time scales of gas transport was examined and it was shown that the time scales for both diffusion and Darcy flow increases quadratically with distance to the vacuum source. Consequently, by changing laminate geometry, the time scale for in-plane and through-thickness air transport is strongly affected and larger laminates require much longer debulks to achieve low porosity.

To aid the practitioner in selecting appropriate room temperature debulk times to achieve low porosity laminates, a simple debulk map based on one-dimensional Darcy flow and measured gas permeability of the prepreg laminates were developed. The debulk maps guides the user in determining the minimum required debulk time to achieve a low porosity laminate for a given length, thickness and material system. The created debulk map confirmed the low porosity levels found in the samples made in this study but further validation is required to determine the applicability of these simple maps for larger and more complex laminates.

Chapter 8: Summary, Conclusions, Contributions and Future Work

The main objective of this work was to study the evolution of voids during OOA prepreg processing. The majority of the study was done on MTM45-1/5HS prepreg from the ACG Company (now Cytec) and optical microscopy was used as the main void characterization method. Gas transport during the process was measured via permeability testing. The following sections present a summary, main conclusions and contributions from this study as well as limitations and potential areas for future studies.

8.1 Summary

This is a summary of our current understanding of void evolution and gas transport in OOA processing of MTM45-1/5HS laminates. Multiple phenomena including gas transport, resin infiltration and fiber bed compaction control porosity reduction. Figure 8-1 shows the potential void sources and sinks in a vacuum bagged laminate. Void sources include entrapped air, off-gassing and leaks, and void sinks include gas removal and void shrinkage or dissolution. The focus of this study was on entrapped air as a void source and gas removal as the predominant void sink. The insert in Figure 8-1 shows the void morphology of laminate on the micro-scale. Voids are categorized into three groups:

1- Fiber tow voids: The un-impregnated sections of the fiber bed that form the interconnected porous network in the in-plane direction. OOA prepregs are intentionally made partially impregnated format to give an interconnected porous network that facilitates gas removal and void reduction during the process.
2- Inter-laminar voids: The entrapped air between the plies during lay-up.
3- Resin Voids: These voids are formed in resin during resin mixing stage of prepreging

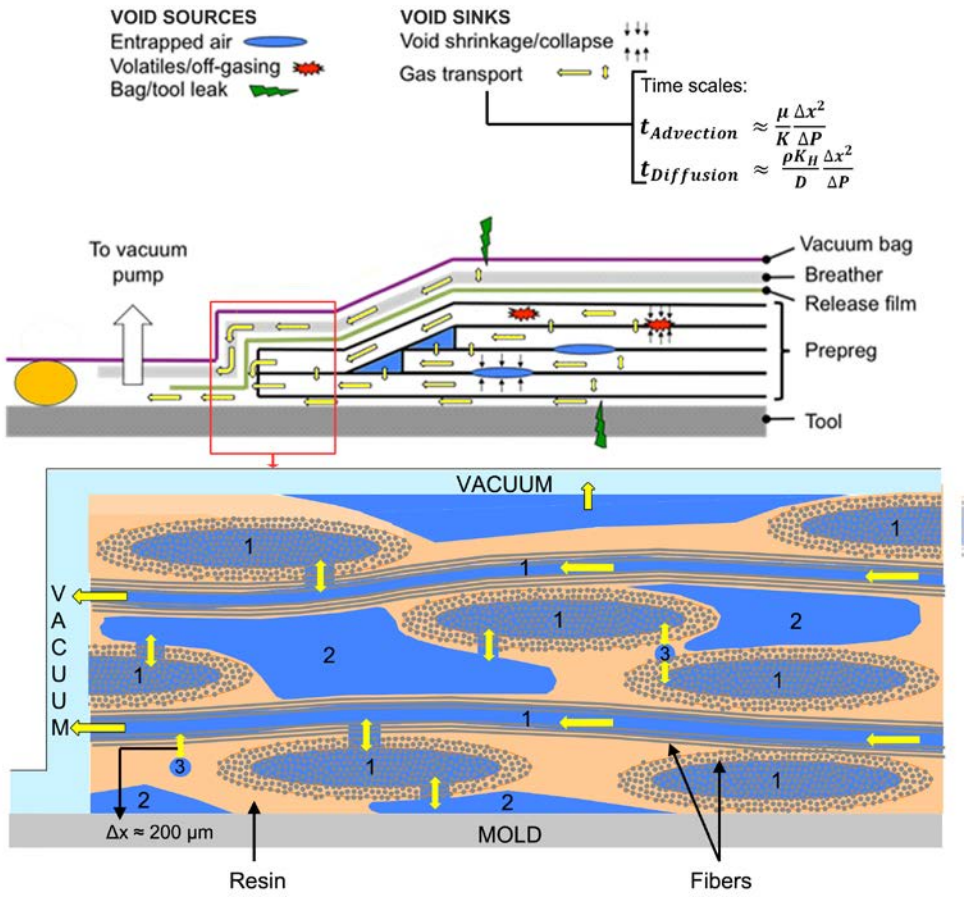

Figure 8-1 Void sources and sinks in a vacuum bagged laminate. Void morphology of a laminate before processing, 1) fiber tow voids, 2) inter-laminar voids and 3) resin voids. Note that void morphology changes during the process.

To reduce porosity the gases inside the voids should be removed. Gas transport occurs through advection or diffusion mechanisms (see section 7.3.2). Pressure gradient provides the required driving force for gas transport, under which gas flows towards the closest point with minimum pressure.

The gas inside the fiber tow voids can be removed via advection as this type of void is part of the interconnected porous network through which advection occurs. Inter-laminar voids are adjacent

to the fiber tows and can potentially connect to their inter-connected porous network through the dry un-impregnated zones between them (see Figure 5-6 a) or coalescence [49]. Resin voids can be evacuated only through diffusion as they are surrounded with resin, unless they coalesce with interconnected porous network [49]. Note that these statements are based on the morphology of the prepreg studied.

Figure 8-2 shows the relative changes of the three types of porosity at different points in the cure cycle and Table 8-1 presents a summary of the corresponding void reduction mechanisms.

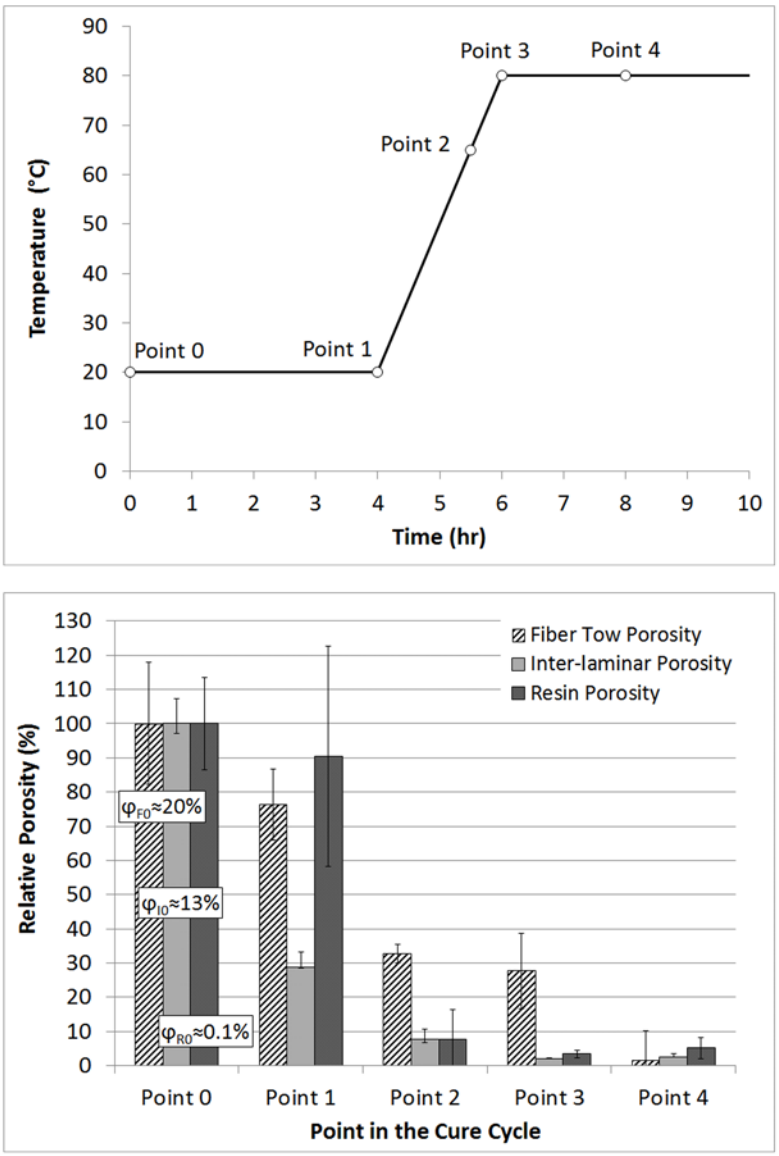

Figure 8-2 Relative porosity at different points in the cure cycle. This graph is created based on the data in Figure 5-7 from the void evolution study on MTM45-1/5HS laminates (127 mm × 127 mm × 8 layers).

Table 8-1 Summary of porosity reduction mechanisms in Figure 8-2. Note: Pressure state is assumed, not measured.

Long Debulk		Point in the cycle		Comment
		"0"	"1"	
Fiber Tow Voids	Pressure (atm)	≈ 1[1]	≈ 0	Air Darcy flow reduces pressure inside fiber tows which leads to fiber tow compaction.
	Relative Porosity (%)	≈ 100	≈ 75	Reduction due to fiber bed compaction. No significant resin flow due to high viscosity (see section 5.3.3).
Inter-laminar Voids	Pressure (atm)	≈ 1	≈ 0	Air Darcy flow reduces pressure inside inter-laminar voids as they are connected to fiber tow voids because of patchy resin film application (see Figure 5-6 a).
	Relative Porosity (%)	≈ 100	≈ 30	Same mechanism as fiber tow voids. Inter-laminar voids reduce faster than fiber tow voids because of low resistance to collapse from fibre bed.
Resin Voids	Pressure (atm)	≈ 1	≈ 1	Pressure inside resin voids does not change. Resin voids are isolated and their pressure can only be reduced through diffusion, which is a slow process at room temperature (see section 7.3.2).
	Relative Porosity (%)	≈ 100	≈ 90	Resin voids stay almost constant.
Hold		Point in the cycle		
		"1"	"4"	
Fiber Tow Voids	Pressure (atm)	≈ 0	≈ 0	Darcy flow further reduces the pressure inside fiber tows (if not already fully evacuated). Pressure reduction continues as long as fiber tow void network is interconnected[2] and connected to vacuum source. Increased temperature lowers resin viscosity and promotes resin infiltration into fiber tows. Resin infiltration continues until void pressure equilibrates with resin pressure[3] and surface tension.
	Relative Porosity (%)	≈ 75	≈ 1.5	Reduction due to both fiber bed compaction and resin viscosity drop and infiltration of fiber tows (see section 7.3.2).
Inter-laminar Voids	Pressure (atm)	≈ 0	≈ 0	Pressure continues to drop as long as inter-laminar voids are connected to interconnected porous network and voids not fully evacuated. After that, void pressure equilibrates with resin pressure[3].
	Relative Porosity (%)	≈ 30	≈ 2.5	Reduction due to the same reasons as fiber tow voids, with the difference that they do not benefit from capillary forces for resin infiltration.
Resin Voids	Pressure (atm)	≈ 1	≈ 0.5 – 1[3]	Pressure inside voids equilibrates with resin pressure[3].
	Relative Porosity (%)	≈ 90	≈ 5	Reduction due to diffusion of gases from resin void towards interconnected porous network or coalescence with it [49]. At the heated portion of the process, the diffusion coefficient is increased an order of magnitude due to temperature increase with facilitates porosity reduction.

[1] It is assumed that at initial state the whole system is equilibrated at one atmosphere pressure.

[2] Gas permeability measurements show that the in-plane interconnected porous network is open during 0 to 2 hours of process and through-thickness network is open from 0 to 5 hours (see Figure 5-15).

[3] Resin pressure depends on the distribution of applied pressured between resin and fiber bed. Xin et al. [104] monitored resin pressure during the processing of a net resin prepreg system under atmospheric compaction pressure and showed that resin pressure stays constant and about 0.5 atmospheres throughout the process.

Feasibility of gas removal using advection and diffusion mechanisms can be evaluated by comparison of their corresponding time scales. In chapter 7, simplified time scales associated with these two mechanisms were developed (see section 7.3.2):

$$t_{Advection} \approx \frac{\mu}{K}\frac{\Delta x^2}{\Delta P} \tag{7-6}$$

$$t_{Diffusion} \approx \frac{\rho K_H}{D}\frac{\Delta x^2}{\Delta P} \tag{7-11}$$

Where μ: gas dynamic viscosity, K: gas permeability, ρ: density of diffusing gas, D: gas diffusion coefficient, K_H: Henry's constant, x: distance, P: gas pressure.

Gas transport distance, permeability, diffusion coefficient and solubility (K_H) affect the time scale. These parameters change during the process as the microstructure of the material evolves (e.g., porous network, cure reaction). In Chapter 7 (section 7.3.2) the time scales associated with air advection and diffusion in flat laminates were investigated. In summary, time scales for air diffusion through the whole laminate thickness are large and it is not an effective gas transport mechanism, while air transport via Darcy flow has short time scales and is highly feasible. However, diffusion over shorter distances such as between a resin void and a dry fiber tow (~ 200 micron) has a much smaller time scale and is viable mechanism, particularly when the resin is heated and diffusivity is increased.

Most of the experimental results presented in this thesis are based on small flat laminates (127 mm × 127 mm × 4 mm) made from MTM45-1/5HS prepreg. As it is mentioned in Future work (section 8.3) it would be interesting to study the effect of part complexities (length, tight curvatures, pad ups, etc) as well as prepreg characteristics (fiber bed architecture, resin

chemistry, etc) on the generality of the results of present study. In this thesis an understanding of the underlying mechanisms that control porosity evolution has been developed as well as tailored methods for measurement of porosity and permeability applicable to any prepreg material. Factors such as pressure distribution in resin and gas phases, gas permeability and resin infiltration are known to be the key parameters in void evolution and their role is discussed in this thesis. By understanding the effect of geometrical complexities, material characteristics and other variables on these three underlying key factors, a basic knowledge of the porosity evolution under each specific condition can be established.

8.2 Conclusions and Contributions

Below is a brief summary of the main conclusions and contributions of this work.

a. Void Characterization of Partially Cured Laminates

Sample preparation techniques were developed to enable the use of optical microscopy and density methods for porosity determination in uncured and partially cured prepreg samples. In the optical microscopy method, partially cured samples were infiltrated with a low viscosity mounting resin to support the soft matrix during cutting and surface preparation steps. In density tests the surface of partially cured samples was coated with a thin polyurethane coat to prevent the penetration of water into the exposed areas. The porosity results from these methods are in good agreement with each other, with deviations of less than 1% absolute for partially cured samples.

It was also shown that laminate thickness can be used for approximate calculations of porosity in no-bleed prepreg systems. The porosity results from this non-destructive and robust method deviate less than 5% absolute compared to porosity measurements from optical microscopy and density methods.

b. Porosity Evolution during the Process and Effect of Processing Parameters

The void morphology of prepreg laminates was examined in detail using optical microscopy. Three distinct groups of voids were identified in the studied material system: inter-laminar, fiber tow and resin voids, and their evolution during different processing conditions was investigated. The 80 °C MRCC cure cycle was chosen as the baseline of this study and the effect of vacuum time during debulk, heating cycle, gas evacuation direction, hold temperature and relative humidity on porosity evolution was studied. The baseline, 80˚C cure cycle, consists of a 0.23 hour room temperature debulk and heated cycle at 80 °C. In this cycle, the initial porosity was 33% but decreased to less than 0.3 % after four hours, well ahead of the gellation time. It was shown that increasing the vacuum debulk time decreases porosity to a limited extent and further debulking does not reduce the porosity of the uncured prepreg at the end of debulk. The effect of vacuum time was also studied during the heated section of the processing cycle and it was shown that porosity decreases as the duration of vacuum application increases. It was shown that releasing the vacuum in the early stages of the process (< 6 hours) results in high porosity samples (20% - 28%), whereas, releasing the vacuum after 6 hours into the cure cycle does not affect the void content. Investigation of the effect of gas evacuation direction (in-plane versus through-thickness) revealed that gas

evacuation can be achieved in both cases and void free laminates can be obtained regardless of gas evacuation direction.

Increasing the hold temperature from 80˚C to 120˚C did not affect the porosity evolution for this prepreg system. Increasing the relative humidity of the laminates from 23% (ambient) to 75% resulted in an increase in porosity during the cycle but the final porosity was zero in both cases. However, increasing the relative humidity to 98% increased final porosity to about 6%.

c. Main Mechanisms Controlling Void Evolution during Processing of MTM45-1 OOA Prepregs

Porosity evolution under different processing conditions was investigated. Laminate permeability, fiber bed compaction and resin infiltration were shown to play important roles in porosity evolution in the MTM45-1 prepreg system. Fiber bed compaction is the main mechanism that controls the evolution of fiber tow voids when resin viscosity is high such as during a room temperature debulk. During the cure cycle, both fiber bed compaction and resin infiltration affect evolution of fiber tow voids. It was shown that gas permeability in both in-plane and through-thickness affect void evolution and that it is possible to obtain low porosity laminates even when the in-plane air transport is prevented and the laminate can only breathe in the through-thickness direction.

d. Permeability Evolution and Relationship with Porosity

Permeability evolution during processing was studied in-plane and through-thickness. It was shown that in-plane permeability is about three orders of magnitude higher than through-thickness permeability at its maximum. Permeability in both directions changes during the process. The majority of gas transport occurs in-plane during debulk, whereas later in the process during heat up, in-plane permeability becomes effectively zero and leaves through-thickness as the main gas transport direction.

A direct relationship between in-plane gas permeability and fiber tow voids, i.e. the non-impregnated core of the fiber tows was identified. This observation confirms the concept of Engineered Vacuum Channels (EVACs) in OOA prepregs. Partially impregnated tows act as vacuum channels and facilitate gas removal in this prepreg system. The vacuum channels are open and permeable until they are closed off by the flow off low viscosity resin at a porosity level of about 5%.

The effect of through-thickness gas transport on void removal was demonstrated by manufacturing low porosity laminates where gas transport was restricted to the thickness direction and the formation of a void gradient in the thickness direction was observed.

e. Permeability Testing

Continuous measurement of permeability in the low viscosity region of the resin changes the porous structure and consequently permeability of the tested sample. This influence can be

lowered by interrupted and discrete measurement of permeability, which is a better representative of permeability during actual processing conditions.

f. Importance of Darcy Flow in Gas Evacuation

Due to the importance of gas transport in void removal, time scales of gas transport via Darcy flow and diffusion mechanisms during vacuum debulk and heat up was studied for MTM45-1/5HS prepreg. It was shown that time scales for air diffusion through the laminate thickness are large and that air diffusion is not an effective gas transport mechanism for this material system and process condition. Air transport via Darcy flow however has short time scales and is highly feasible. Gas transport via Darcy flow occurs in both in-plane and through-thickness directions, generally with shorter time scales in the in-plane direction. It is also shown that laminate size (length and thickness) affects the gas transport time and the dominant gas transport direction. The time scale increases quadratically with distance to the vacuum source.

Permeability measurements and time scale calculations showed that gas evacuation via Darcy flow during the room temperature debulk has the shortest time scale for gas removal. Thus in order to achieve low porosity it is critical to remove the gases from the laminate during this step of the process. To aid the end user in selecting an appropriate required debulk time to obtain a low porosity laminate for a given size and prepreg system, simple debulk maps based on one-dimensional Darcy flow and measured gas permeability of the prepreg laminates were developed.

g. Batch to Batch Variably of Prepreg

Two different rolls of MTM45-1/5HS prepreg was used in this study. The initial ply thickness, porosity, surface morphology and permeability of these prepregs are different from each other, whereas the final cured ply thickness is the same. These differences can be a source of uncertainty and variability in porosity control of large complex parts.

8.3 Future Work

a. Scale up to Industrially Relevant Structures

The experimental results presented in this study were from lab scale flat laminates (127 mm × 127 mm × 4 mm). These results provide a basic fundamental understanding of the void evolution process. However they may not be directly applicable to industrial cases due to the extra complications such as distance to vacuum (part size), ply drop offs, pad-ups, gaps, caul sheet, inserts, sandwich cores, moisture, tight radii and bridging which can affect gas transport, consolidation phenomena and consequently porosity.

b. Investigation of The Effect of Prepreg Characteristics on Porosity

The primary prepreg used in this study was MTMT45-1/5HS prepreg from ACG Company (now Cytec) and some experiments were done on MTM45-1/Unidirectional prepreg. It is necessary to evaluate of the generality of the results of this study by performing tests on a wider range of prepreg systems. Parameters of interest include fiber bed geometry, resin viscosity, resin content

and prepreg impregnation level and pattern. Evaluation of differences between performance of autoclave and out of autoclave prepregs is another field of interest.

c. Through-Thickness Gas Evacuation

This study showed the viability of gas evacuation in the through-thickness direction. Through thickness permeability of prepregs is in general a few orders of magnitude less than in-plane permeability because of the resin film method used when making prepregs. However gas evacuation in the through thickness direction is more scale independent and offers two important advantages, shorter distance to the vacuum source and larger flow area. Through-thickness evacuation is also of special interest in gas evacuation of honeycomb core structures. Thus it is beneficial to study enhancement of gas evacuation in the thickness direction by use of breathable consumables on top and bottom surfaces of the parts or design of prepregs with high through thickness permeability.

8.4 Broader Implications

This study showed that achieving low porosity in OOA laminates is mainly about mass transport. First, removal of entrapped air within and between plies, and second, infiltration of the evacuated void space by resin. Without removing the entrapped air, sufficient resin infiltration will not occur to achieve low porosity laminates. Both air and resin transport is predominantly driven by Darcy flow. To achieve complete removal of entrapped air it is important that a continuous porous gas transport network remains open until gas evacuation is complete. This requires that the prepreg is partially impregnated and that the resin viscosity is high enough that it does not

flow into the evacuated voids space until gas removal is complete. There is a trade-off in terms of the degree of resin impregnation of the prepreg. A low degree of resin impregnation gives higher permeability and better gas transport but a higher bulk factor which causes problems with wrinkling and bridging in curved laminate areas. To achieve low porosity laminates it is important to ensure that there are continuous path ways for gas transport all the way out to the vacuum system, which emphasizes the importance of lay-up details such as ply drops and the details of the bagging system. By using the developed understanding of gas transport and porosity, and quantifying the laminate gas permeability and porosity with the methods proposed in this thesis, the gas evacuation and porosity reduction process of complex laminates is amenable to analysis and numerical prediction. This work will serve as a foundation for a predictive capability of porosity in configured composite structures.

References

1. Ashby, M.F.J., *Materials and Design: The Art and Science of Material Selection in Product Design,* 2009, Butterworth-Heinemann, San Diego.

2. C. Red. , *"The market for OOA aero-composites (2013-2022)"*, High-Performance Composites, 2014.

3. Campbell, F.C., *Manufacturing Processes for Advanced Composites,* 2004, Elsevier, New York.

4. Repecka, L. & Boyd, J., *Vacuum-Bag-Only-Curable Prepregs that Produce Void-Free Parts.* SAMPE International Symposium, 2002, Long Beach, CA.

5. Ridgard, C., *Out of Autoclave Composite Technology for Aerospace, Defense and Space Structures,* SAMPE International Symposium, 2009, Baltimore, MD.

6. Thomas, S., Bongiovanni, C. & Nutt, S.R., *In Situ Estimation of through-Thickness Resin Flow using Ultrasound,* Composites Science and Technology, 2008, vol. 68, no. 15–16, pp. 3093-3098.

7. Grunenfelder, L. & Nutt, S.R., *Void Formation in Composite Prepregs – Effect of Dissolved Moisture,* Composites Science and Technology, 2010, vol. 70, no. 16, pp. 2304-2309.

8. Tavares. S., S., Caillet-Bois, N., Michaud, V. & Månson, J.-.E., *Non-Autoclave Processing of Honeycomb Sandwich Structures: Skin through Thickness Air Permeability during Cure,* Composites Part A: Applied Science and Manufacturing, 2010, vol. 41, no. 5, pp. 646-652.

9. Centea, T. & Hubert, P., *Modelling the Effect of Material Properties and Process Parameters on Tow Impregnation in Out-of-Autoclave Prepregs,* Composites Part A: Applied Science and Manufacturing, 2012, vol. 43, no. 9, pp. 1505-1513.

10. Kratz, J. & Hubert, P., *Anisotropic Air Permeability in Out-of-Autoclave Prepregs: Effect on Honeycomb Panel Evacuation Prior to Cure,* Composites Part A, 2013, vol. 49, pp. 179-191.

11. Louis, B., Hsiao, K. & Fernlund, G., *Gas Permeability Measurements of Out of Autoclave Prepreg MTM45-1/CF2426A,* International SAMPE Symposium, 2010, Seattle, WA.

12. Hsiao, K., Kay, J. & Fernlund, G., *Gas Transport and Water Evaporation in Out-of-Autoclave Prepregs,* 2nd Joint ASC-CANCOM Conference, 2011, Montreal, Canada.

13. Kay, J. & Fernlund, G., *Processing Conditions and Voids in Out of Autoclave Prepregs,* International SAMPE Symposium, 2012, Baltimore, MD.

14. Helmus, R., Centea, T., Hubert, P. & Hinterholzl, R., *An Integrated Process Model for Air Evacuation and Tow Impregnation in Out-of-Autoclave Prepreg Consolidation,* American Society for Composites 2013 - 28th Technical Conference, 2013, Pennsylvania, USA.

15. Callister, W.D., *Materials Science and Engineering :An Introduction,* 2005, John Wiley & Sons, New York, NY.

16. Ghiorse, S.R., *A Comparison of Void Measurement Methods for Carbon/Epoxy Composites,* 1991, Army Lab Command Watertown Material Technology Lab.

17. Adanur, S. & Arumugham, Y., *Characteristics of Ultraviolet Cured Glass–Epoxy Textile Composites: Part 1: Experimental Procedures and Testing,* Journal of Industrial Textiles, 2002, vol. 32, no. 2, pp. 93-106.

18. Kumar, P.K., Raghavendra, N.V. & Sridhara, B.K., *Optimization of Infrared Radiation Cure Process Parameters for Glass Fiber Reinforced Polymer Composites,* Materials & Design, 2011, vol. 32, no. 3, pp. 1129-1137.

19. *RAVEN*, http://www.convergent.ca/products/raven-simulation-software, Convergent Manufacturing Technologies Inc., 2014.

20. Gutowski, T.G.P., *Advanced Composites Manufacturing,* 1997, John Wiley & Sons, New York.

21. Louis, B., *Gas Transport in Out-of-Autoclave Prepreg Laminates,* M.Sc. Thesis, 2010, University of British Columbia (UBC), Vancouver, Canada.

22. Ridgard, C., *Next Generation Out of Autoclave Systems,* International SAMPE Symposium, 2010, Seattle, WA.

23. Boyd, J , *Tutorial: Vacuum Bag Only Composite Part Manufacturing,* International SAMPE Symposium, 2003, Dayton, OH.

24. Steele, M. & Corden, T., *New Prepregs for Cost Effective, Out-of-Autoclave Tool and Component Manufacture,* SAMPE Journal, 2004, vol. 40, no. 2, pp. 30-34.

25. Thomas, S. & Nutt, S.R., *Temperature Dependence of Resin Flow in a Resin Film Infusion (RFI) Process by Ultrasound Imaging,* Applied Composite Materials, 2009, vol. 16, no. 3, pp. 183-196.

26. Xu, G.F., Repecka, L., Mortimer, S., et al., *Manufacture of Void-Free Laminates and use Thereof,* US. Pat.#6,391,436 B1, 2002.

27. Hartness, J.T. & Xu, G.F., *Resin Composition, a Fiber Reinforced Material having a Partially Impregnated Resin and Composites made Therefrom.* US. Pat.#6,565,944 B1, 2003.

28. Thorfinnson, B. & Biermann, T.F., *Production of Void Free Composite Parts without Debulking*, International SAMPE Symposium, 1986, Las Vegas, Nevada.

29. Thorfinnson, B. & Biermann, T.F., *Degree of Impregnation of Prepregs: Effects on Porosity*, International SAMPE Symposium, 1987, Anaheim, California.

30. Liu, L., Zhang, B., Wang, D. & Wu, Z., *Effects of Cure Cycles on Void Content and Mechanical Properties of Composite Laminates*, Composite Structures, 2006, vol. 73, no. 3, pp. 303-309.

31. Guo, Z., Liu, L., Zhang, B. & Du, S., *Critical Void Content for Thermoset Composite Laminates,* Journal of Composite Materials, 2009, vol. 43, no. 17, pp. 1775-1790.

32. Harper, B.D., Staab, G.H. & Chen, R.S., *Properties of AS4/3502 Graphite/Epoxy A Note on the Effects of Voids upon the Hygral and Mechanical,* Journal of Composite Materials, 1986, vol. 21, pp. 280-289.

33. Ghiorse, S., *Effect of Void Content on the Mechanical-Properties of Carbon Epoxy Laminates,* SAMPE Quarterly, 1993, vol. 24, no. 2, pp. 54-59.

34. Arafath, A.R.A., Fernlund, G. & Poursartip, A., *Gas Transport in Prepregs:Model and Permeability Experiments*, ICCM-17, 2009, Edinburgh, UK.

35. Kardos, J.L., *"Void Growth and Dissolution"* in Processing of Composites, Edited by R.S. Dave & A.C. Loos, 2000, Hanser publishers, Munich, pp. 182-206.

36. Brown, G., McKague, E. & Brand RA, *Processing Science of Epoxy Resin Composites,* 1984, Materials Laboratory, Air Force Wright Aeronautical Laboratories.

37. Campbell, F.C., Mallow, A.R. & Browning, C.E., *Porosity in Carbon Fiber Composites an Overview of Causes,* Journal of Advanced Materials, 1995, vol. 26, no. 4, pp. 18-33.

38. Zingraff, L. , *Void Formation and Transport during Liquid Moulding and Forming of Reactive Thermoplastic Composites,* PhD Thesis, 2004, École polytechnique fédérale de Lausanne (EPFL), Lausanne, Switzerland.

39. Farhang, L. & Fernlund, G., *Void Evolution and Gas Transport in Out-of-Autoclave Prepregs,* 2nd Joint ASC-CANCOM Conference, 2011, Montreal, Canada.

40. Lienhard IV, J.H. & Lienhard V, J.H., *A Heat Transfer Textbook,* 2006, Phlogiston Press, Cambridge, Massachusetts, USA.

41. Wood, J.R. & Bader, M.G., *Modelling the Behaviour of Gas Bubbles in an Epoxy Resin: Evaluating the Input Parameters for a Diffusion Model using a Free-Volume Approach,* Journal of Materials Science, 1995, vol. 30, no. 4, pp. 916-922.

42. Wood, J.R. & Bader, M.G., *Void Control for Polymer - Matrix Composites (1): Theoritical and Experimental Methods for Determining the Growth and Collapse of Gas Bubbles,* Composites Manufacturing, 1994, vol. 5, no. 3, pp. 139-147.

43. Ledru, Y., Bernhart, G., Piquet, R., Schmidt, F. & Michel, L., *Coupled Visco-Mechanical and Diffusion Void Growth Modelling during Composite Curing,* Composites Science and Technology, 2010, vol. 70, no. 15, pp. 2139-2145.

44. Webb, S.W. & Ho, C.K. (eds) 2006, *Gas Transport in Porous Media,* Springer Netherlands, Netherlands.

45. Gaskell, D.R., *An Introduction to Transport Phenomena in Materials Engineering,* 1992, Macmillan Publishing Company, USA.

46. Civan, F. , *Porous Media Transport Phenomena,* 2011, John Wiley & Sons, Canada.

47. Arbter, R., Beraud, J.M., Binetruy, C., Bizet, L., Bréard, J., Comas-Cardona, S., Demaria, C., Endruweit, A., Ermanni, P., Gommer, F., Hasanovic, S., Henrat, P., Klunker, F., Laine, B., Lavanchy, S., Lomov, S.V., Long, A., Michaud, V., Morren, G., Ruiz, E., Sol, H., Trochu, F., Verleye, B., Wietgrefe, M., Wu, W. & Ziegmann, G., *Experimental Determination of the Permeability of Textiles: A Benchmark Exercise,* Composites Part A: Applied Science and Manufacturing, 2011, vol. 42, no. 9, pp. 1157-1168.

48. Chhabra, R.P., *Bubbles, Drops, and Particles in Non-Newtonian Liquids,* 2007, Taylor and Francis (CRC), USA.

49. Cender, T.A., Gangloff Jr. J. J., Simacek, P. & Advani, S.G., *Void Reduction during Out-of-Autoclave Thermoset Prepreg Composite Processing,* SAMPE International Symposium, 2014, Seattle, Washington.

50. Ahn, K.J., Seferis, J.C. & Berg, J.C., *Simultaneous Measurements of Permeability and Capillary Pressure of Thermosetting Matrices in Woven Fabric Reinforcements,* Polymer Composites, 1991, vol. 12, pp. 146–152.

51. Tavares, S.S., Michaud, V. & Manson, J.-.E., *Through Thickness Air Permeability of Prepregs during Cure,* Composites Part A: Applied Science and Manufacturing, 2009, vol. 40, no. 10, pp. 1587-1596.

52. *MTM45-1 Matrix Resin Product Data Sheet,* Advanced Composites Group (ACG Inc.) , 2012.

53. Putnam, J.W. & Seferis, J.C., *Prepreg Gas Permeation as a Function of Fiber Orientation and Aging Time,* Journal of Advanced Materials, 1995, vol. 26, no. 3, pp. 35-41.

54. Xin, C., Li, M., Gu, Y., Li, Y. & Zhang, Z., *Measurement and Analysis on in-Plane and through-Thickness Air Permeation of Fiber/Resin Prepreg,* Journal of Reinforced Plastics and Composites, 2011, vol. 30, no. 17, pp. 1467-1479.

55. Bescond, C., Wong, R. & Desrosiers, P., *Porosity Assessment in Large Composite Components: Realization and Challenges,* SAE International, 2013, Detroit, Michigan, USA.

56. Georgeson, G.E., Hafenrichter, J., Lilienthal, D. A., Kennedy, J.C., et al., *Reference Standard for Ultrasonic Measurement of Porosity and Related Method,* US. Pat.#US 7,617,715 B2, 2009.

57. Jeong, H. , *Effects of Voids on the Mechanical Strength and Ultrasonic Attenuation of Laminated Composites,* Journal of Composite Materials, 1997, vol. 31, no. 3, pp. 276-292.

58. Cobbs, S.D. & Bond, G.G., *Development of Porosity Standards for Cycom®5320-1 Out-of-Autoclave Composite Laminates,* SAMPE International Symposium, 2012, Baltimore, US.

59. Ray, B.C., Hasan, S.T. & Clegg, D.W., *Evaluation of Defects in FRP Composites by NDT Techniques,* Journal of Reinforced Plastics and Composites, 2007, vol. 26, no. 12, pp. 1187-1192.

60. Thomas, M.M., Joseph, B. & Kardos, J.L., *Experimental Characterization of Autoclave-Cured Glass-Epoxy Composite Laminates: Cure Cycle Effects upon Thickness, Void Content, and Related Phenomena,* Polymer Composites, 1997, vol. 18, no. 3, pp. 283-299.

61. Centea, T. & Hubert, P., *Measuring the Impregnation of an Out-of-Autoclave Prepreg by Micro-CT,* Composites Science and Technology, 2011, vol. 71, no. 5, pp. 593.

62. Schilling, P.J., Karedla, B.R., Tatiparthi, A.K., Verges, M.A. & Herrington, P.D., *X-Ray Computed Microtomography of Internal Damage in Fiber Reinforced Polymer Matrix Composites,* Composites Science and Technology, 2005, vol. 65, no. 14, pp. 2071-2078.

63. Schell, J.S.U., Deleglise, M., Binetruy, C., Krawczak, P. & Ermanni, P., *Numerical Prediction and Experimental Characterisation of Meso-Scale-Voids in Liquid Composite Moulding,* Composites Part A: Applied Science and Manufacturing, 2007, vol. 38, no. 12, pp. 2460-2470.

64. Kosek, M. & Sejak, P., *Visualization of Voids in Actual C/C Woven Composite Structure,* Composites Science and Technology, 2009, vol. 69, no. 9, pp. 1465-1469.

65. S. Paciornik & J.R.M. D'Almeida, *Measurement of Void Content and Distribution in Composite Materials through Digital Microscopy,* Journal of Composite Materials, 2009, vol. 43, no. 2, pp. 101-112.

66. *Military Handbook - MIL-HDBK-17-1F: Composite Materials Handbook, Volume 1 - Polymer Matrix Composites Guidelines for Characterization of Structural Materials,* 2002, U.S. Department of Defense, USA.

67. Dunkers, J.P., Sanders, D.P., Hunston, D.L., Everett, M.J. & Green, W.H., *Comparison of Optical Coherence Tomography, X-Ray Computed Tomography, and Confocal Microscopy Results from an Impact Damaged Epoxy/E-Glass Composite,* Journal of Adhesion, 2002, vol. 78, no. 2, pp. 129-154.

68. ASTM E2533 – 09 , *Standard Guide for Nondestructive Testing of Polymer Matrix Composites used in Aerospace Applications1,* 2009, ASTM International, West Conshohocken, PA.

69. Schell, J.S.U., Renggli, M., van Lenthe, G.H., Müller, R. & Ermanni, P., *Micro-Computed Tomography Determination of Glass Fibre Reinforced Polymer Meso-Structure,* Composites Science and Technology, 2006, vol. 66, no. 13, pp. 2016-2022.

70. ASTM D2734-09, *Standard Test Methods for Void Content of Reinforced Plastics,* 2009, ASTM International, West Conshohocken, PA.

71. Centea, T. & Hubert, P., *Out-of-Autoclave Prepreg Consolidation Under Deficient Pressure Conditions,* Journal of Composite Materials, 2013, pp. 1-13.

72. Grunenfelder, L.K., Centea, T., Hubert, P. & Nutt, S.R., *Effect of Room-Temperature Out-Time on Tow Impregnation in an Out-of-Autoclave Prepreg,* Composites Part A, 2013, vol. 45, pp. 119-126.

73. Nam, J.-. & Seferis, J.C., *Gas Permeation and Viscoelastic Deformation of Prepregs in Composite Manufacturing Processes,* Polymer Composites, 1995, vol. 16, no. 5, pp. 370-377.

74. Hsiao, K. , *Gas Transport and Water Vapourization in Out-of-Autoclave Prepreg Laminates,* M.Sc. Thesis, 2012, University of British Columbia (UBC), Vancouver, Canada.

75. Gangloff Jr., J.J., Hwang, W.R. & Advani, S.G., *Characterization of Bubble Mobility in Channel Flow with Fibrous Porous Media Walls,* International Journal of Multiphase Flow, 2014, vol. 60, no. 0, pp. 76-86.

76. Cender, T.A., Simacek, P. & Advani, S.G., *Resin Film Impregnation in Fabric Prepregs with Dual Length Scale Permeability,* Composites Part A: Applied Science and Manufacturing, 2013, vol. 53, no. 0, pp. 118-128.

77. Cender, T.A., Abu-Obaid, A., Simacek, P. & Advani, S.G., *Experimental Characterization of a Partially Pre-Impregnated Fabric for Out-of-Autoclave Processing,* SAMPE, 2011, Long Beach, CA.

78. Martin, C.J., Putnam, J.W., Hayes, B.S., Seferis, J.C., Turner, M.J. & Green, G.E., *Effect of Impregnation Conditions on Prepreg Properties and Honeycomb Core Crush,* Polymer Composites, 1997, vol. 18, no. 1, pp. 90-99.

79. Shim, S. & Seferis, J.C., *Thermal and Air Permeation Properties of a Carbon Fiber/Toughened Epoxy Based Prepreg System,* Journal of Applied Polymer Science, 1997, vol. 65, no. 1, pp. 5-16.

80. Gonon, P., Sylvestre, A., Teysseyre, J. & Prior, C., *Combined Effects of Humidity and Thermal Stress on the Dielectric Properties of Epoxy-Silica Composites,* Materials Science and Engineering: B, 2001, vol. 83, no. 1–3, pp. 158-164.

81. Gueribiz, D., Jacquemin, F. & Fréour, S., *A Moisture Diffusion Coupled Model for Composite Materials,* European Journal of Mechanics - A/Solids, 2013, vol. 42, no. 0, pp. 81-89.

82. van der Wel, G.K. & Adan, O.C.G., *Moisture in Organic Coatings — a Review,* Progress in Organic Coatings, 1999, vol. 37, no. 1–2, pp. 1-14.

83. E2015-04, *Standard Guide for Preparation of Plastics and Polymeric Specimens for Microstructural Examination,* 2004, ASTM International, West Conshohocken, PA.

84. Dillon, G.P., *Influence of Prepreg Microstructures on Structural Performance of Polymer Matrix Composites,* 2005, Air Force Office of Scientific Research (AFOSR).

85. *Image Processing and Analysis in Java (ImageJ),* http://rsbweb.nih.gov/ij/index.html, 2014.

86. *HTS40 E13 6K 400tex Product Data Sheet,* Toho Tenax America (Inc.) , 2008.

87. *D792-08 Standard Test Methods for Density and Specific Gravity (Relative Density) of Plastics by Displacement,* 2008, ASTM International, West Conshohocken, PA.

88. *M-Coat A Product Data Sheet,* Vishay Micro Measurements, 2010.

89. Hull, D. & Clyne, T.W., *An Introduction to Composite Materials,* 1996, Cambridge University Press, UK.

90. Garstka, T., Ersoy, N., Potter, K.D. & Wisnom, M.R., *In Situ Measurements of through-the-Thickness Strains during Processing of AS4/8552 Composite,* Composites Part A: Applied Science and Manufacturing, 2007, vol. 38, no. 12, pp. 2517-2526.

91. Wang, X., Hu, Y., Song, L., Xing, W. & Lu, H., *Thermal Degradation Mechanism of Flame Retarded Epoxy Resins with a DOPO-Substitued Organophosphorus Oligomer by TG-FTIR and DP-MS,* Journal of Analytical and Applied Pyrolysis, 2011, vol. 92, no. 1, pp. 164-170.

92. Hickey, C.M.D., *The Influence of Variation in Process Parameters on the Manufacturing of Advanced Fiber Composites,* 2013, The University of Auckland, Auckland, New Zealand.

93. Leclerc, J.S. & Ruiz, E., *Porosity Reduction using Optimized Flow Velocity in Resin Transfer Molding,* Composites Part A: Applied Science and Manufacturing, 2008, vol. 39, no. 12, pp. 1859-1868.

94. Park, C.H., Lebel, A., Saouab, A., Bréard, J. & Lee, W.I., *Modeling and Simulation of Voids and Saturation in Liquid Composite Molding Processes,* Composites Part A: Applied Science and Manufacturing, 2011, vol. 42, no. 6, pp. 658-668.

95. Ridgard, C. , *Aerospace Out of Autoclave Prepreg Technology,* SEICO - 32nd International Conference, 2011, Paris, France.

96. Farhang, L. & Fernlund, G., *Void Evolution and Gas Transport during Cure in Out-of-Autoclave Prepreg Laminates,* International SAMPE Symposium, 2011, Long Beach, CA.

97. *CYCOM®5320 Product Data Sheet,* Cytec Engineered Materials, 2012.

98. Gangloff Jr., J.J., Daniel, C. & Advani, S.G., *A Model of Two-Phase Resin and Void Flowduring Composites Processing,* International Journal of Multiphase Flow, no. 0, .

99. Hartness, J.T. & Xu, G.F., *Resin Composition, a Fiber Reinforced Material having a Partially Impregnated Resin and Composites made Therefrom,* US. Pat.#6565944 B1, 2003.

100. Zhou, J. & Lucas, J.P., *Hygrothermal Effects of Epoxy Resin. Part I: The Nature of Water in Epoxy,* Polymer, 1999, vol. 40, no. 20, pp. 5505-5512.

101. Dullien, F.A.L., *Porous Media: Fluid Transport and Pore Structure,* 1992, Academic Press, USA.

102. Ahn, K.J., Seferis, J.C., Price, J.O. & Berg, A.J., *Permeation Measurements through Prepreg Laminates,* SAMPE Journal, 1991, vol. 27, no. 6, pp. 19-26.

103. Gangloff Jr., J.J., Simacek, P., Sinha, S. & Advani, S.G., *A Process Model for the Compaction and Saturation of Partially Impregnated Thermoset Prepreg Tapes,* Composites Part A: Applied Science and Manufacturing, no. 0, .

104. Xin, C., Gu, Y., Li, M., Li, Y. & Zhang, Z., *Online Monitoring and Analysis of Resin Pressure Inside Composite Laminate during Zero-Bleeding Autoclave Process,* Polymer Composites, 2011, vol. 32, no. 2, pp. 314-323.

105. Quinlan, E. & et al., *Evaluation of Laminate Quality for Out of Autoclave Manufacturing for a Complex Shaped Crew Door,* AHS 70th Annual Forum and Technology Display, 2014, Montreal, Canada.

106. Brillant, M. & Hubert, P., *Out-of-Autoclave Processing of Complex Shape Laminates,* SAMPE International Symposium, 2010, Seattle, WA.

107. Cauberghs, Julien, H. & Pascal, *Effect of Tight Corners and Ply Terminations on Quality in Out-of-Autoclave Parts,* SAMPE International Symposium, 2011, Long Beach, CA.

108. Arafath, A.R.A, Private Communication.

109. Caston, T.B., Murphy, A.R. & Harris, T.A.L., *Effect of Weave Tightness and Structure on the in-Plane and through-Plane Air Permeability of Woven Carbon Fibers for Gas Diffusion Layers,* Journal of Power Sources, 2011, vol. 196, no. 2, pp. 709-716.

110. *GA045 Carbon Fabrics Product Data,* Hexcel Schwebel, 2013.

111. Dykeman, D., *Minimizing Uncertainty in Cure Modeling for Composites Manufacturing,* PhD Thesis, 2008, University of British Columbia, Vancouver, Canada.

112. Gebart, B.R., *Permeability of Unidirectional Reinforcements for RTM,* Journal of Composite Materials, 1992, vol. 26, no. 8, pp. 1100-1133.

Appendices

Appendix A Gas Permeability Measurements

A.1 Introduction

The ability for gas transport in prepregs can be evaluated by measuring gas permeability of a laminate throughout the process. In permeability measurement the sample is typically subjected to forced air flow. This forced air flow can change the microstructure of the sample by displacing the resin when the viscosity is low and the resin is mobile. The change in porous microstructure can affect the permeability measurements, meaning that the test measurements can be influenced by the testing technique itself. Tavares et al. [51] reported an increase in prepreg permeability when the measurements are taken frequently during the low viscosity range. Louis [11] and Hsiao [74] also measured a sudden increase in permeability during heated permeability tests which is attributed to test artifacts. To determine if permeability measurements are representative of actual processing conditions, a clear understanding of the potential detrimental testing effects is required.

In this study the effect of test technique on microstructure and permeability of the test sample is studied. Permeability measurements in continuous and interrupted modes are performed and the void morphology of the test samples is characterized using optical microscopy. For determination of the potential detrimental test effects, the results of these tests are compared to a sample cured under manufacturer recommended cure cycle (MRCC), in the absence of any forced air flow. This study is done in both in-plane and through thickness.

A.2 Methods

A.2.1 Material

MTM45-1/5HS-Thick prepreg was used in this study (see section 4.2.1).

A.2.2 Permeability Measurements

Interrupted permeability measurements were done according to the procedures described in section 5.2.5. Continuous permeability tests were performed using the same test set up as the interrupted permeability test (section 5.2.5). In this test the air flow required for permeability measurements is generated by venting one side of the sample to the atmosphere, while the other end is held under vacuum. In the interrupted tests the sample was vented only at measurement times until the air flow reached a steady state condition (≈ 8 minutes) and was then put back under vacuum again. However in the continuous test, one side of the sample was continuously vented during the entire test and flow measurements were being recorded continuously. In this test a quasi-steady state assumption is made for air flow at each measurement time ($\Delta t = 0.25$ s).

A.2.3 Void Characterization (Optical Microscopy)

Void characterization and porosity measurement is done using optical microscopy and area fraction measurement (section 5.2.4).

A.2.4 Viscosity

The resin viscosity during the cure cycle was calculated using the Raven software (version 3). The software uses cure kinetics equations based on extensive calorimetric testing [19].

A.3 Results and Discussion

A.3.1 Continuous versus Interrupted Permeability Measurements

Figure A-1b shows the measured gas permeability in the two test modes, continuous and interrupted, in both in-plane and through thickness directions. The detailed discussion of permeability measurement in the interrupted mode is presented in section 5.3.2.2. In this section the focus is on the results of "continuous tests" and the comparison with "interrupted tests". It can be seen that in-plane and through-thickness permeability decrease during the ramp in both interrupted and continuous tests. Permeability reduction during the first heat up ramp has been reported by other researchers [21, 51, 73, 74]. This reduction is believed to be due to infiltration of gas transport pathways in the porous prepreg with resin, as resin viscosity decreases during the ramp (Figure A-1a). Deviation of "continuous" from "interrupted" permeability starts at the beginning of the 80 °C hold, when the resin viscosity reaches its minimum. At this time, both in-plane and through thickness "continuous" permeability sharply increase to values slightly higher than their room temperature values and stay constant to the end of cure cycle. This sharp increase in permeability during the minimum viscosity regime has also been observed by other researchers [21, 51, 74]. The increased permeability may be a result of the creation a connected network for gas transport in the sample. This network is created by continuous forced air flow through the sample during the low viscosity resin regime, when the resin is mobile. The final

microstructures of samples cured under continuous and interrupted flow were examined to confirm this (Figure A-3 and Figure A-4). In contrary to "continuous test", in "interrupted test" the final permeability of the samples is effectively zero. This is because in this test samples are under forced air flow for short periods of time for each measurement (8 min), as the flow measurements are taken discretely with minimum 30 minutes time intervals. Consequently the microstructure of tested sample is influenced to a lesser extent with this measurement method (Figures A-2 and A-3).

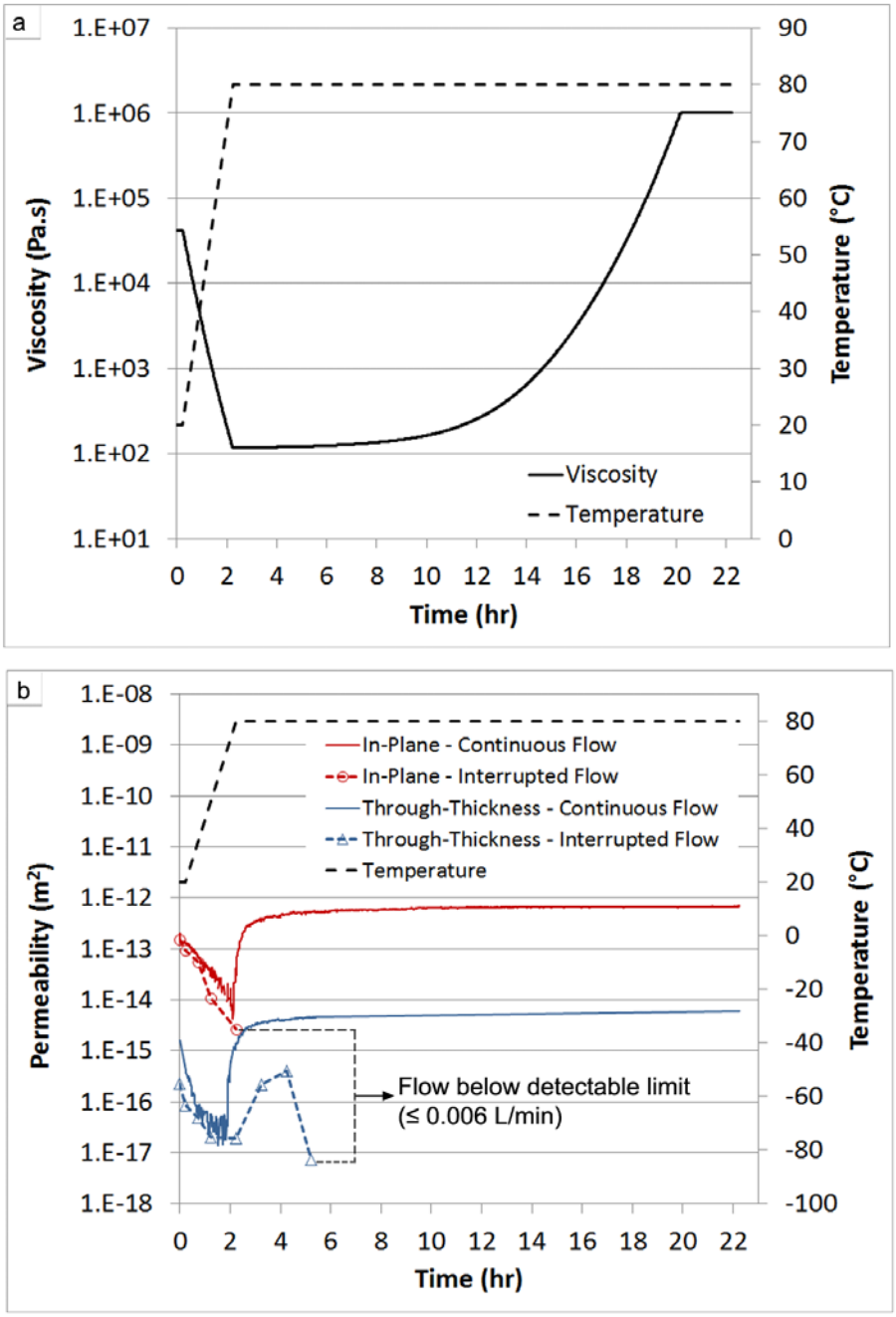

Figure A-1 a) Resin viscosity profile in 80 °C cure cycle, b) Continuous and interrupted permeability in in-plane and through-thickness directions. Flow and permeability values below detectable limit (Q ≈ 0.006 L/min, K (In-Plane) ≈ 10^{-15} m^2, K (Through-Thickness) ≈ 10^{-17} m^2) are considered to be zero.

Void morphology of samples cured under "continuous" and "interrupted" forced air flow is studied by optical microscopy. The porosity and void morphology of these samples in both through-thickness and in-plane tests are shown in Figures A-2 to A-4.

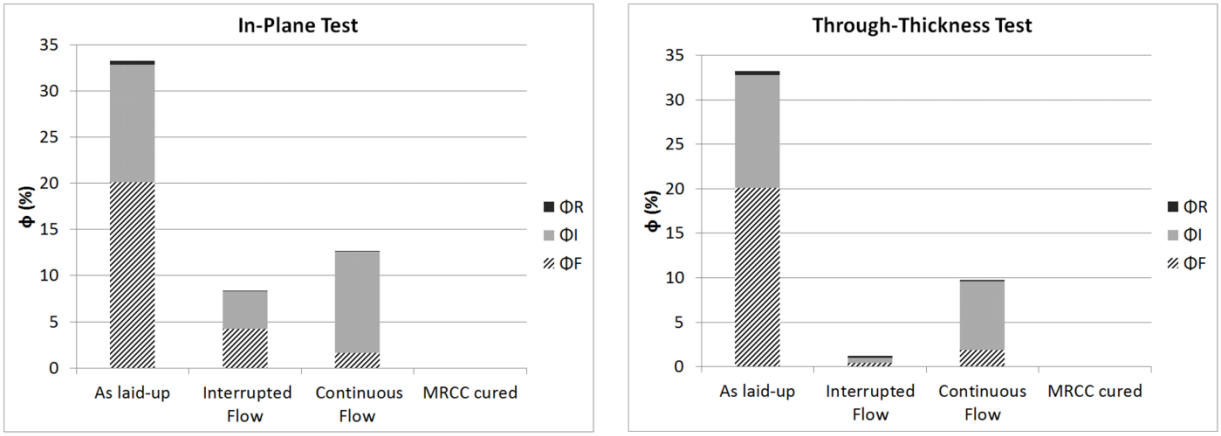

Figure A-2 Comparison of porosity of samples that have undergone interrupted and continuous permeability measurements with as laid-up and MRCC cured samples. The as laid-up sample is not cured whereas the other three samples are fully cured.

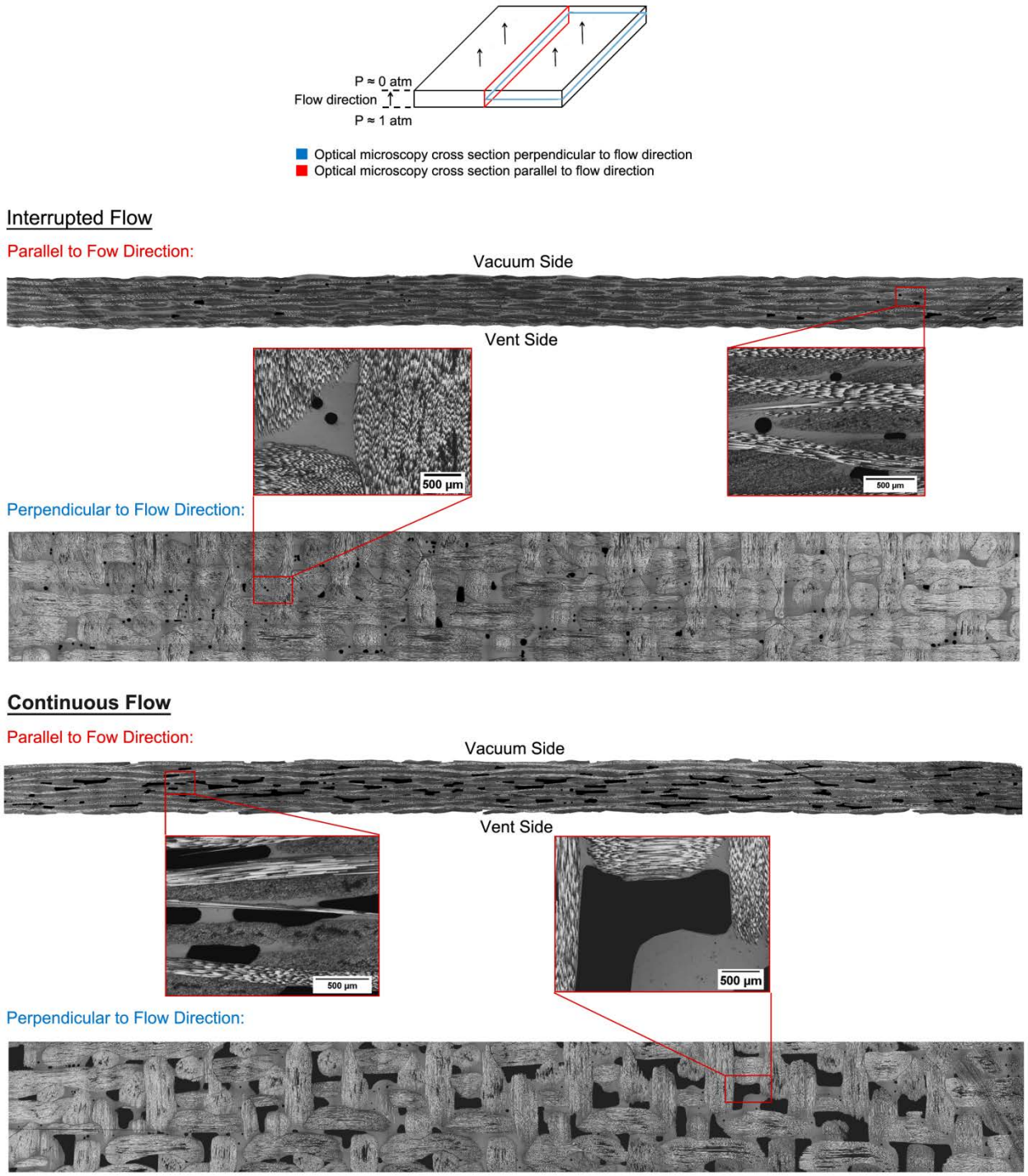

Figure A-3 Cross sectional optical micrograph of through-thickness permeability sample under "continuous" and "interrupted" measurement methods. Cross sections perpendicular and parallel to flow are considered.

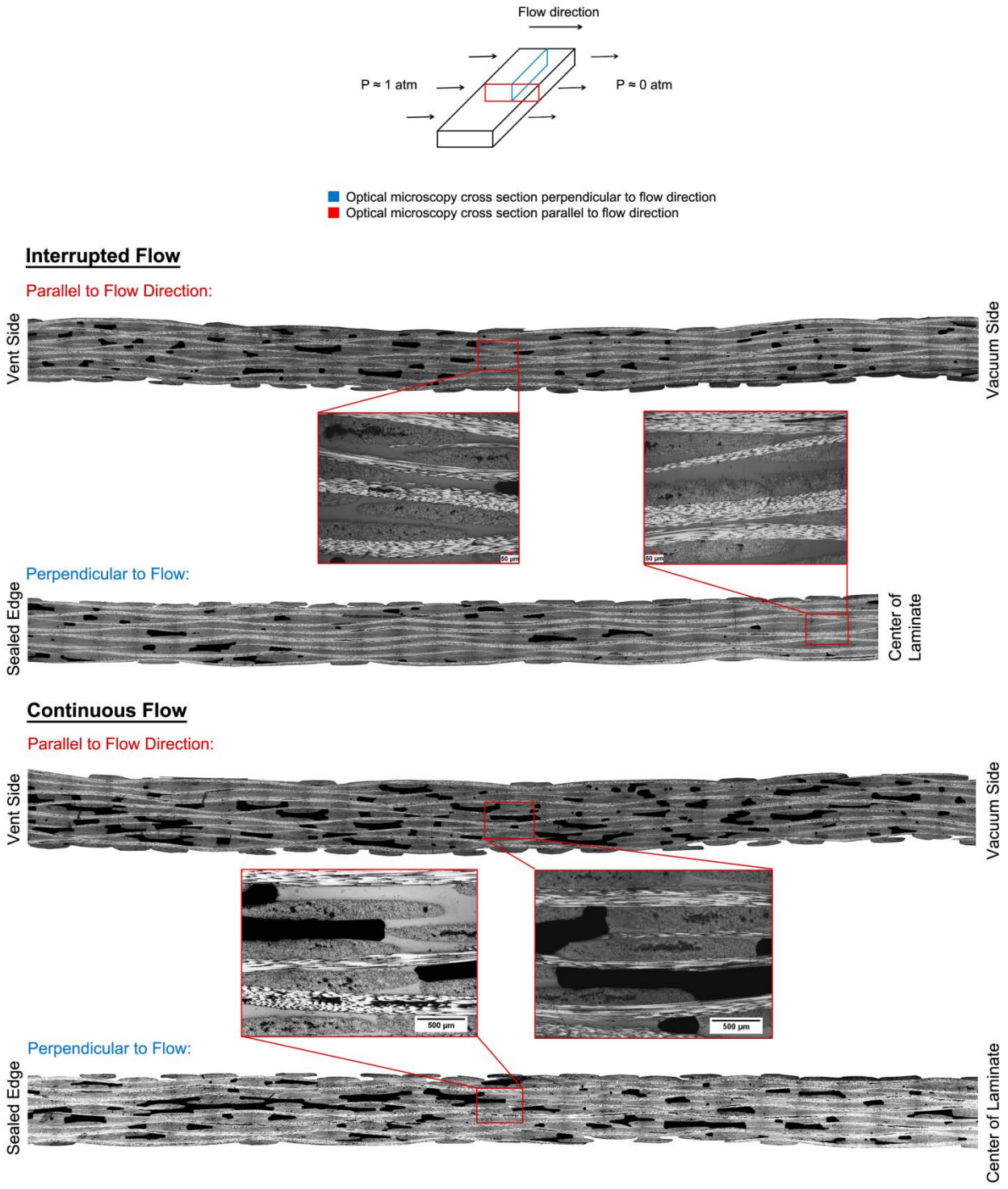

Figure A-4 Cross sectional optical micrograph of in-plane permeability sample under "continuous" and "interrupted" measurement methods. Cross sections perpendicular and parallel to flow are considered.

It can be seen that after both continuous and interrupted tests, the final porosity is higher than a sample that is cured under the manufacturer's recommended cure cycle (MRCC) without any air being forced through it during cure (Table A-1). This indicates that both these test methods increase the void content of test samples by pushing air through them, which is the requirement of permeability measurement. However the "continuous test" method affects the microstructure and permeability of tested samples more than the "interrupted test". "Continuous test" results in higher final porosity and permeability values compared to "interrupted test". Comparison of the optical micrographs of samples from these two tests shows that the continuous sample has a more porous microstructure than the interrupted sample (Figures A-3 and A-4). This observation is in agreement with the high final permeability values of continuous samples compared to the "zero" permeability in interrupted samples.

Table A-1 Porosity and permeability of as laid up, continuous, interrupted and MRCC samples

Sample	φ (%)	K_{In-Pl} (m^2)	K_{T-T} (m^2)
As-laid up	33.24	1.56×10^{-13}	2.26×10^{-16}
Continuous (In-Pl)	12.65	6.9×10^{-13}	NA
Continuous (T-T)	9.81	NA	6.15×10^{-15}
Interrupted (In-Pl)	8.34	0	NA
Interrupted (T-T)	1.25	NA	0
MRCC cured	0.3	0	0

Despite that the final porosity of continuous samples is about one third of as-laid up samples, their permeability is higher than them (Table A-1). Figure A-2 shows that in as laid up samples the porous microstructure mainly consists of fiber tow voids while in the continuous test inter-laminar voids are in majority. This observation shows that the inter-connected network of inter-laminar voids is more efficient in gas transport than fiber tow voids. The reason behind this is that permeability does not only depend on porosity but also on tortuosity, pore size distribution,

connectivity of pores, and specific surface [45, 46]. The lower efficiency of fiber tow void network is likely due to factors such as smaller pore size, higher tortuosity and specific surface than a network of inter-laminar voids.

A.3.2 Spatial Variation of Porosity in Samples Subjected to Permeability Testing

The porosity of all samples in this study was investigated at cross-sections perpendicular and parallel with respect to the gas flow direction in the permeability test. The primary goal is determine if there is a spatial or directional effect on the porous structure (Figures A-3 and A-4). Figure A-5 shows that porosity in parallel and perpendicular cross-sections with respect to the gas flow are in close agreement for all samples.

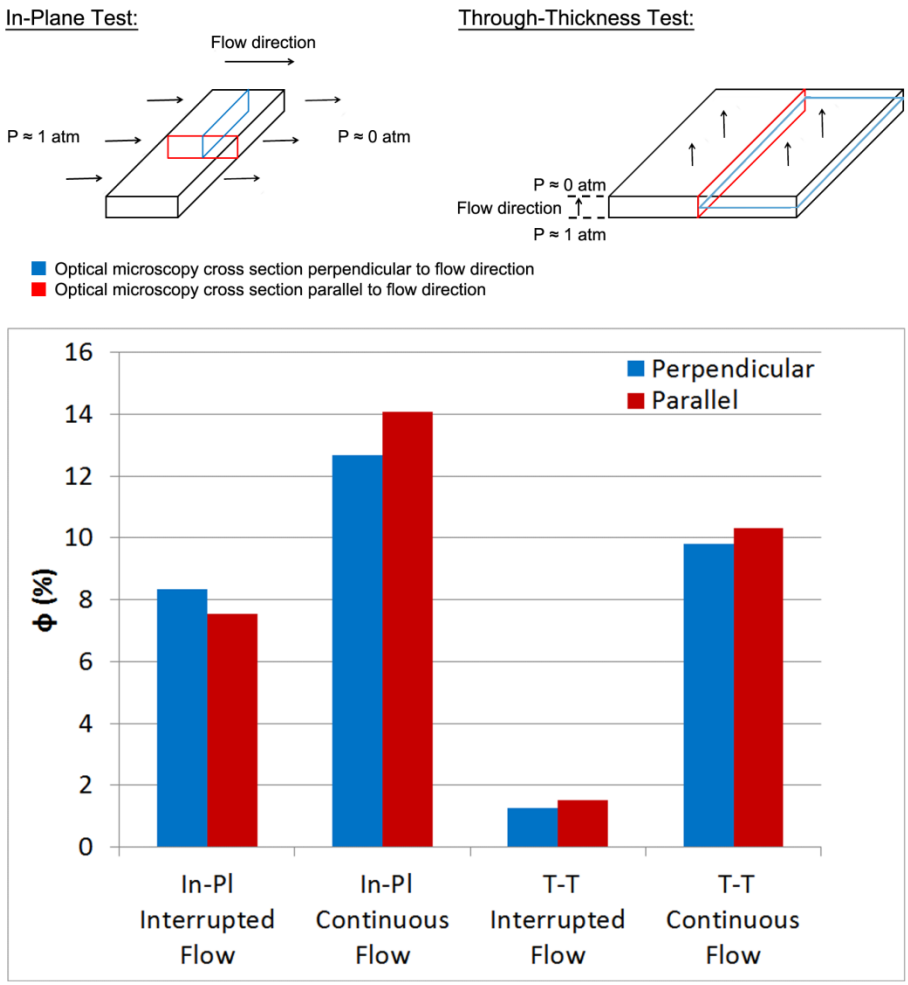

Figure A-5 Comparison of sample porosity in perpendicular and parallel directions to the gas flow for samples subjected to permeability testing.

A.4 Summary

- The porous structure and the permeability of a sample is influenced by permeability measurement when taken continuously during the low viscosity region. This influence can be reduced by interrupted and discrete measurements of permeability. Interrupted measurement of permeability is more representative of the permeability during actual processing conditions.

- Continuous application of air flow during permeability test forms an interconnected network of inter-laminar voids. This is true for both in-plane and through-thickness directions.
- A sample with a lower porosity can have a higher gas permeability due to a less tortuous porous network.

Appendix B Modified Through-Thickness Permeability Test Set-up and Comparison of MTM45-1/5HS Thin and Thick Prepregs Permeability

B.1 Modified Through-Thickness Permeability Test Set-up

The through-thickness permeability test set-up is described in detail in section 5.2.5. This set-up is a slight modification with respect to the original test set-up used in previous work in our research group [11, 12]. This modification was performed to prevent excessive resin bleed from laminate into adjacent consumables (Figure B-1). Excessive resin bleed during the cure cycle can alter sample microstructure by creation of resin starved regions and thus affect the permeability test results. In the modified test set up a perforated release film layer was placed between the sample surfaces (top and bottom) and the adjacent consumables (glass fabric and brick) to minimize resin bleed (Figure B-1).

The through thickness permeability of laminates made of 5HS-Thin prepreg were measured with the original test set-up (one repeat) and the permeability of 5HS-Thick made laminates (section 5.3.2.2) were measured using the modified set-up (three repeats).

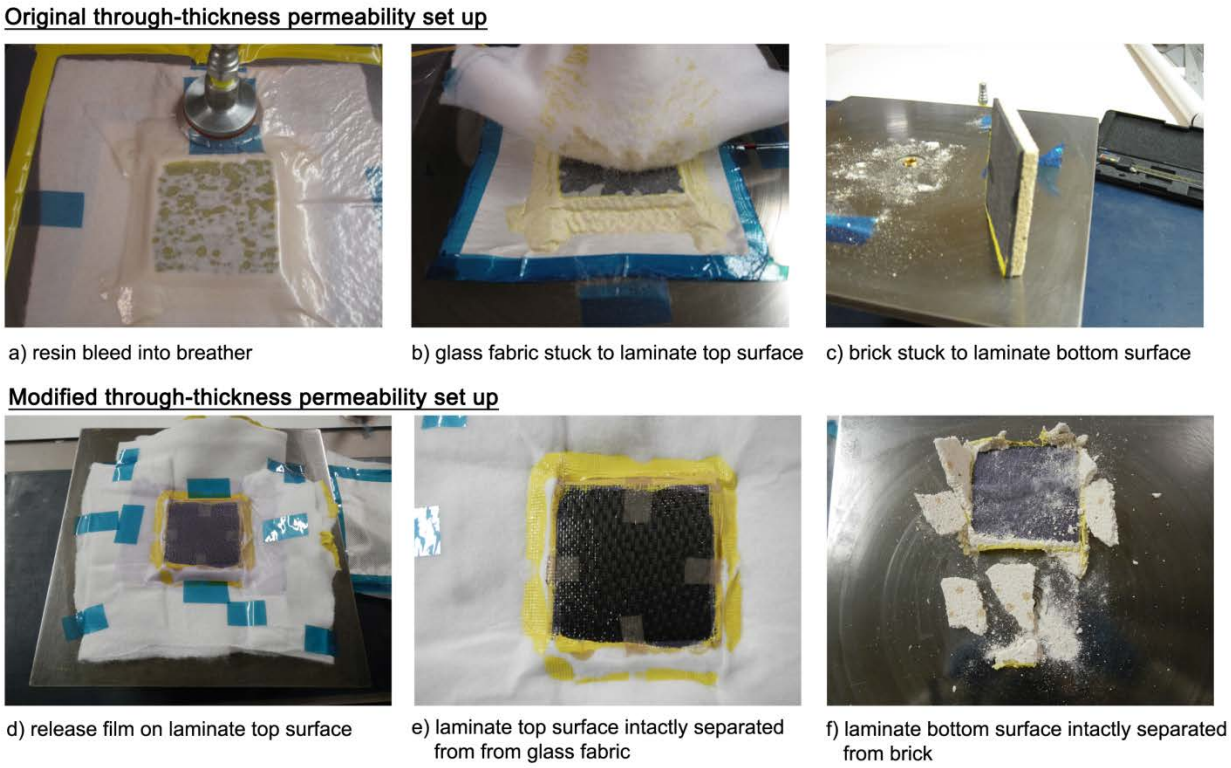

Figure B-1 Through-thickness permeability test set-up. a to c) original set-up, d to f) modified set-up.

B.2 Results and Discussion

Permeability evolution during processing of MTM45-1/5HS-Thick laminates is studied in section 5.3.2.2. Figure B-2 compares the permeability of 5HS-Thick and Thin laminates during the cure cycle. The in-plane permeability of both prepregs is measured using the same test set-up. Through-thickness permeability of 5HS-Thin prepreg is measured with the original test set-up and the 5HS-Thick prepreg is measured with the modified test set-up.

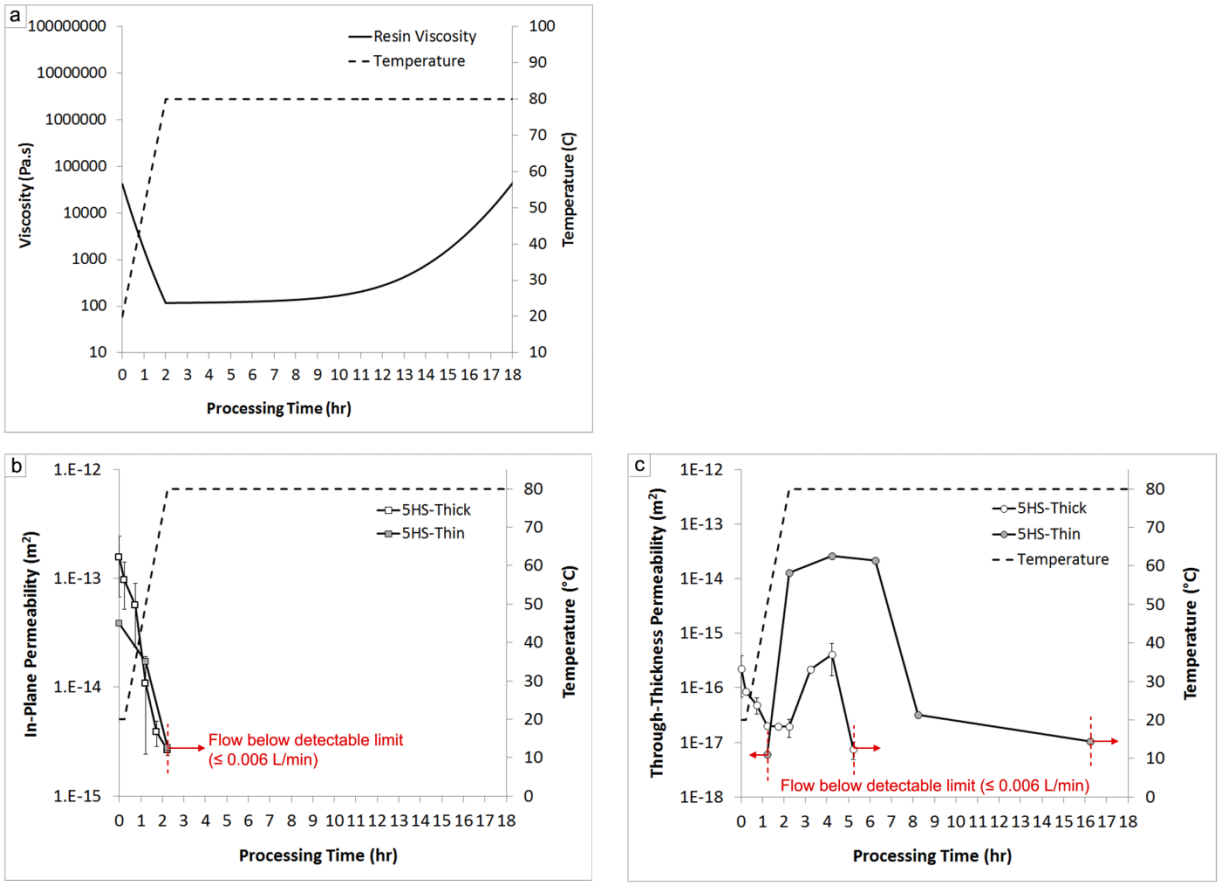

Figure B-2 Permeability of 5HS–Thick and 5HS–Thin prepregs during 80 °C cure cycle.

The initial in-plane permeability of the 5HS-Thin prepreg is about half an order of magnitude less than for the 5HS-Thick prepreg. The lower permeability of the 5HS-Thin prepreg can be due to the higher degree of resin impregnation, which reduces the available dry fraction of the fiber tows that facilitate in-plane permeability. The resin and fiber contents of 5HS-Thick and Thin prepregs are equal but their initial per ply thickness is different (0.53 mm vs. 0.46 mm). This suggests that the Thin prepreg has a higher resin impregnation factor than the Thick prepreg. The in-plane permeability of both prepregs decreases and becomes effectively zero after two hours of processing.

The initial through-thickness permeability of 5HS-Thick prepreg is on the order of 10^{-16} m^2, while 5HS-Thin prepreg has effectively zero permeability. The reason behind this difference may be that 5HS-Thin has a tighter weave and lower number of pinholes than 5HS-Thick prepreg (Figure B-3). The through-thickness permeability of both prepregs increases as the cure cycle gets close to the hold temperature and the minimum viscosity resin region and then reduces back to small values later during the hold stage. The through-thickness permeability of 5HS-Thin prepreg is at its maximum about two orders of magnitude higher than 5HS-Thick prepreg. The increased permeability of 5HS-Thin prepreg may be due to creation of large resin starved regions as a result of excessive resin bleeding in the original test set-up and consequently facilitation of gas transport.

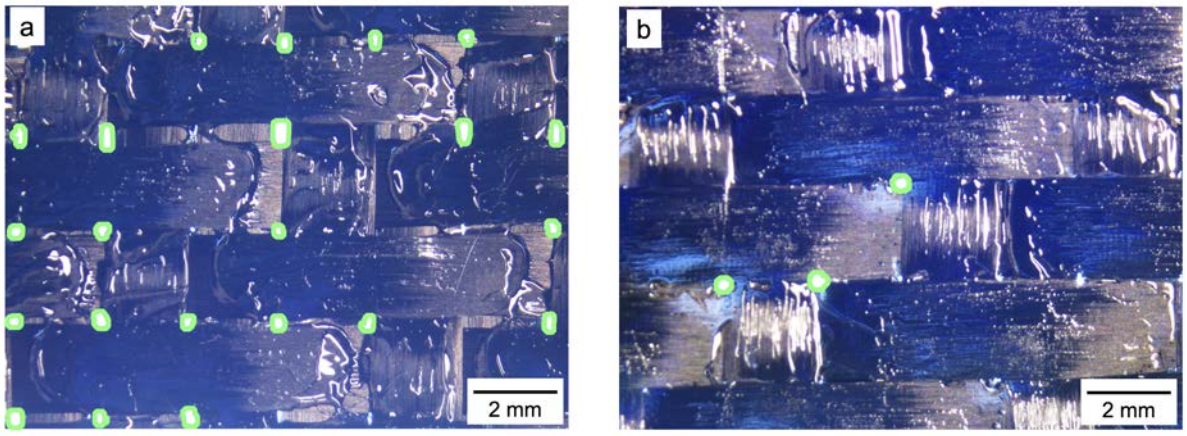

Figure B-3 Pinholes in a) 5HS-Thick prepreg, b) 5HS-Thin prepreg. Pinholes are marked with green border.

Appendix C Prepreg Surface Morphology

Three OOA prepregs were used in this study MTM45-1/5HS-Thick, MTM45-1/5HS-Thin and MTM45-1/UD (see section 7.2.1). The surface morphology of the un-cured prepregs were investigated with Nikon Stereo Microscope (SMZ745T) and Keyence digital microscope (VHX1000) in reflection and transmission light modes (Figure C-1).

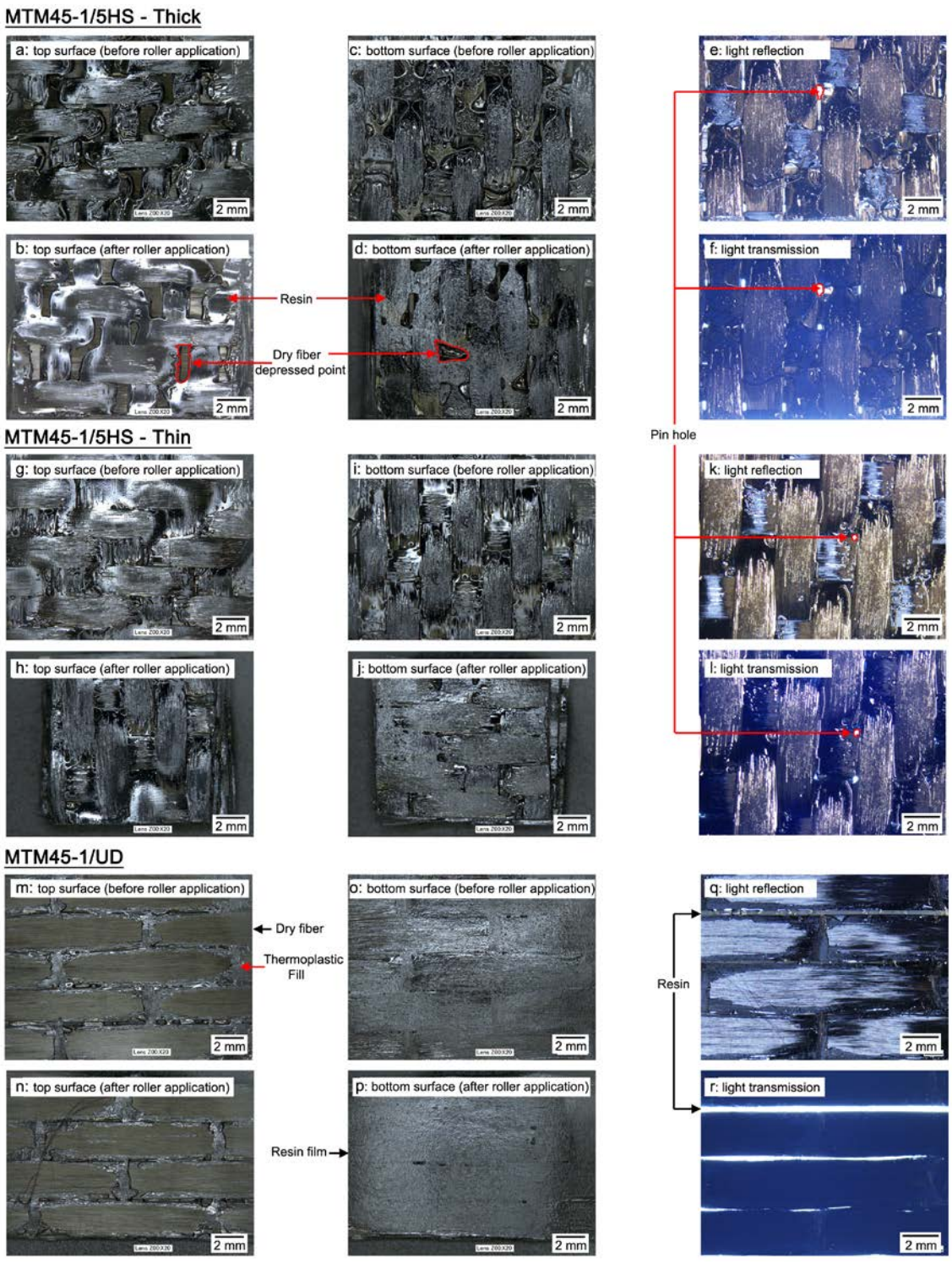

Figure C-1 Surface morphology of prepregs used in this study, a to f) MTM45-1/5HS – Thick, g to l) MTM45-1/5HS – Thin, m to r) MTM45-1/UD. Top and bottom surface of prepregs before and after roller application (a - d, g – j, m – p). Prepreg layer under light reflection and transmission modes (e – f, k – l, q – r).

Out of autoclave prepreg manufacturers employ different impregnation strategies, however they all impregnate the fiber preforms partially [23, 24]. Some prepregs are impregnated with resin on both sides while others are impregnated on one side or with a perforated pattern [23, 24]. The un-impregnated zones of these prepregs are dry pathways through which entrapped gases can be evacuated from the prepreg resulting in low porosity [28, 29]. In Figure C-1, images of both top and bottom surfaces of the prepregs are shown. Visual examination of these images suggests that resin distribution and content is different on both sides of the prepreg and the bottom side has higher resin content. This observation is more clear in the case of one sided tacky UD prepreg which is dry on the top surface and has a uniform resin film on the bottom surface. The fabrics are two sided tacky with a non-uniform and patchy distribution of resin that leaves the depressed regions of prepreg surface dry. The images before and after application of roller to prepreg surface are shown in Figure C-1. The depressed sites after roller application are the potential locations for air entrapment and formation of inter-laminar voids during the lay-up. It can be seen that MTM45-1/5HS - Thick prepreg has the highest number of depressed sites and the MTM45-1/UD prepreg has almost none of them. MTM45-1/5HS – Thick and Thin prepregs have same resin content of 36wt%. Comparison of the images after roller application suggests that Thick prepreg has a lower fiber impregnation factor as it seems to have more resin content on the surface. This observation is in agreement with the higher initial thickness per ply of MTM45-1/5HS – Thick (0.53 mm) compared to MTM45-1/5HS – Thin (0.46 mm) (measured after 7 minutes of debulk for every four layers).

Light reflection and transmission images of the prepreg surfaces are shown in Figure C-1. In fabrics, the bright points located at intersections of warp and fill tows are pinholes. It can be seen

that MTM45-1/5HS –Thick has a more open structure and higher number of pinholes compared to MTM45-1/5HS – Thin. A prepreg with more open microstructure has likely higher through-thickness permeability [109]. The bright lines that appear in the light transmission image of the uni-directional prepreg are spaces between carbon fiber tows that are filled with resin. The fill fibers in the uni-directional prepreg are proprietary thermoplastic fibers that are intended to hold the prepreg together during lay-up and handling [110].

Appendix D Autoclave Prepreg vs. Out-of-Autoclave Prepreg

D.1 Introduction

It is generally believed that OOA prepregs have design features such as partial impregnation of the fiber bed, low volatile content and modified resin viscosity that enable them to give low porosity under atmospheric compaction pressure [26]. Autoclave prepregs that are commonly cured under high compaction pressures (e. g., 6 atm) are expected to give higher porosity than their OOA counterparts, if cured under atmospheric compaction pressure. In this study an autoclave prepreg (3900-2/T800H) is cured under atmospheric compaction pressure to investigate its performance in terms of porosity.

D.2 Methods

D.2.1 Material

The prepreg used in this study is 3900-2/T800H (BMS8-276) from Toray composites. This fabric prepreg has a plain weave with 35wt% resin content [111].

D.2.2 Sample Preparation

Two laminates were made in this study. The first was only debulked at room temperature and the second was cured. The laminates were made of 8 layers of 127 mm × 127 mm prepreg and were bagged and debulked with the same procedure used for the MTM45-1/5HS laminates (section 4.2.2). The second laminate was cured under full vacuum (absolute pressure < 4.0 kPa) with the cure cycle shown in Table D-1.

Table D-1 3900-2/T800H cure cycle [111]

Heat up ramp (°C/min)	Hold		Cool down ramp (°C/min)
	Temperature (°C)	Time (min)	
1.5	180	130	2

D.2.3 Optical Microscopy Imaging and Void Characterization

The porosity of the laminates was quantified by measuring the void area fraction of sectioned laminates using optical microscopy. Both laminates were cut and their whole cross section was prepared for optical microscopy using the procedures described in section 4.2.3. A mosaic image was taken from the entire cross section at 100X magnification using a Nikon optical microscope (EPIPHOT 300) and the Clemex software (vision PE 6.0). The Image J software [85] was used for measurement of the area fraction of the voids from the mosaic images.

D.2.4 Thickness Measurement

The thickness of the samples was measured with a Pro-Max digital caliper from the Fowler company (accuracy: 0.02 mm). The reported thickness of each laminate is the average of twelve measurements. Measurement points were located 25.4 mm away from the laminate edges.

D.3 Results and Discussion

Figure D-1 shows the microstructure of the laminate before and after cure. The debulked laminate is highly porous ($\varphi \approx 18\%$, based on thickness measurements), however it gave zero porosity after the cure. The initial and final thickness of the laminates is listed in Table D-2. This result is somewhat surprising and contrary to the expectations from AC prepregs. However, this study was limited to small flat laminates and it is possible that in the case of more complex

geometries, OOA prepregs show superior performance over their AC counterparts under vacuum bag only and atmospheric compaction cure.

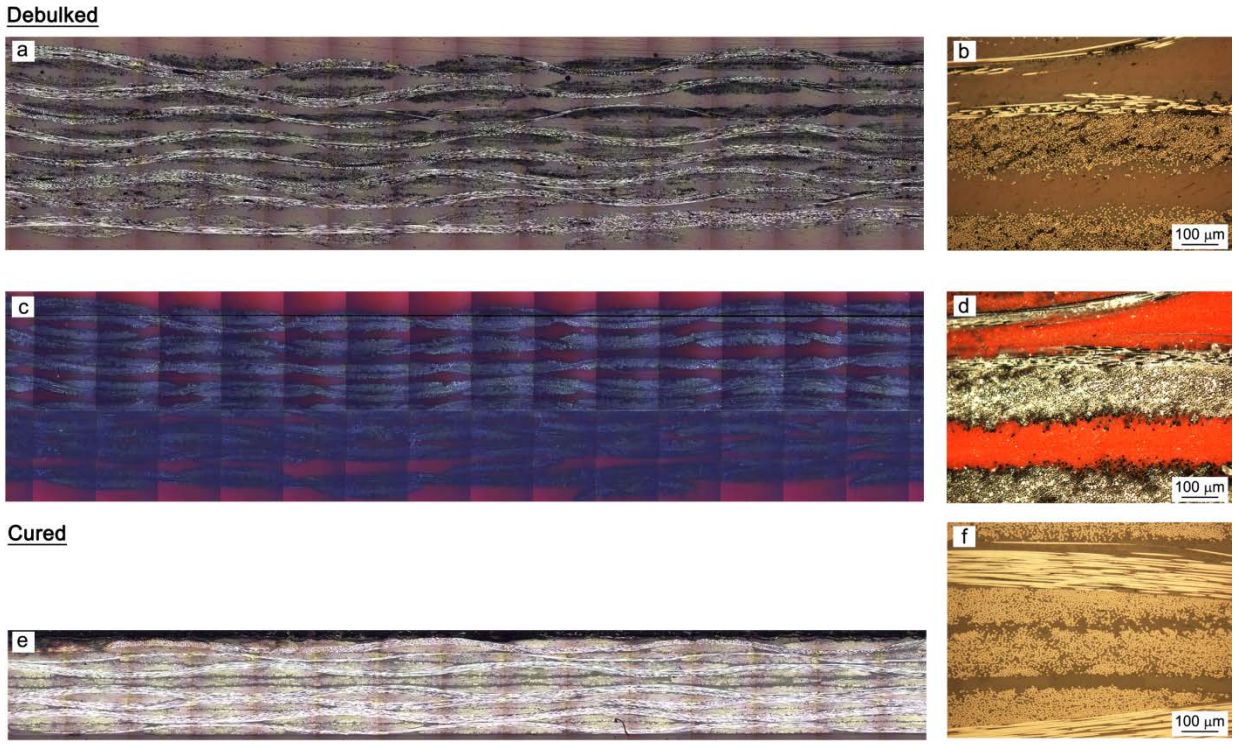

Figure D-1 Optical micrograph of a 3900-2/T800H laminate after debulk (a, b: bright-field and c, d: dark-field) and after cure (e, f: bright-field).

Table D-2 Laminate thickness before and after cure

		Debulked	Cured
Thickness (mm)	Average	2.18	1.78
	STDEVA	0.02	0.01

Appendix E Theoretical Estimation of Laminate Permeability

In this section the theoretical in-plane permeability of the laminates in this study is estimated based on models available in the literature and compared to experimental measurements (Figure 5-15).

The in-plane permeability of the laminate can be assumed equal to the permeability of its dry section (Figure E-1 and equation E-1). In OOA prepregs the fiber tows are partially impregnated and thus have a dry and permeable core. The parameter β is used to describe the impregnated fraction of tows (section 5.3.3).

$$K_{IP-LAM} = \frac{A_{TOW}(1-\beta)}{A_{TOTAL}} \times K_{IP-TOW} \qquad \text{(E-1)}$$

Where $K_{IP\text{-}LAM}$ (m^2): laminate in-plane permeability, $K_{IP\text{-}TOW}$ (m^2): permeability of dry tow along the fibers, A_{TOTAL}: total cross-section area A_{TOW}: area of fiber tows in the laminate cross section, , β: tow impregnation factor ($0 \leq \beta \leq 1$), β = 0: no impregnation, β = 1: fully impregnated tow.

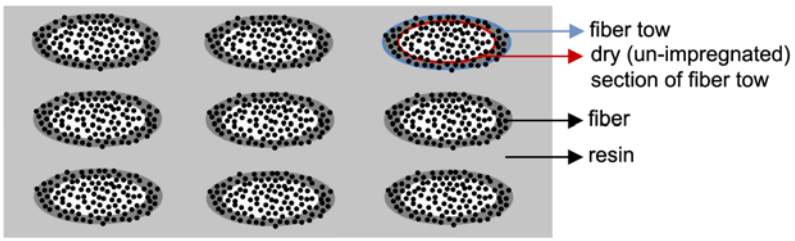

Figure E-1 Schematic of laminate cross-section.

The permeability of an array of aligned cylindrical fibers for flow along the fibers can be estimated from the analytical equation proposed by Gebart [112]:

$$K_{IP-TOW} = \frac{8R_f^2}{c}\frac{(1-V_f)^3}{V_f^2} \quad \text{(E-2)}$$

Where $K_{IP\text{-}TOW}$ (m^2): permeability of dry tow along the fibers, R_f (m): fiber diameter, V_f: volume fraction of fibers in the tow, c: shape factor (depends on fiber arrangement, e.g., quadratic (c = 0.57), hexagonal (c = 53)).

Table E-1 Input parameters used for $K_{IP\text{-}LAM}$ estimation

R_f (μm) [86]	V_f	A_{TOW}/A_{TOTAL}	β_0 [1]
7	0.74	0.27	0.2

[1]Initial β at ambient condition [9]

Assuming quadratic fiber arrangement and the input parameters listed in Table E-1, the in-plane permeability of a dry tow in our system is about 2.2×10^{-13} m^2. The input parameters in Table E-1 are taken from another study on the same prepreg system [9]. The area fraction of fiber tows is assumed to be half of the prepreg fiber volume fraction (0.54) as half of the tows are perpendicular to flow direction and do not contribute to the in-plane permeability [52]. Using equations E-1 and E-2 and the input parameters listed in Table E-1, the in-plane permeability of laminate at ambient condition is estimated to be 4.7×10^{-14} m^2. This value is close to the experimental measurements for laminate in-plane permeability at ambient condition for MTM45-1/5HS-Thin (3.83×10^{-14} m^2), but is lower than the MTM45-1/5HS-Thick (1.56×10^{-13} m^2) roll.

Appendix F Mass Flow Sensor Calibration and Detection Limit

F.1 Mass Flow Sensor Calibration

Flow rate data was measured using electronic mass flow sensors in this thesis. However the original data is in the form of a voltage. The voltage data is converted to flow rate using a calibration curve provided by Convergent Manufacturing Technologies (Figure F-1). The mass flow sensor used in this study was on loan from Convergent Manufacturing Technologies (CMT).

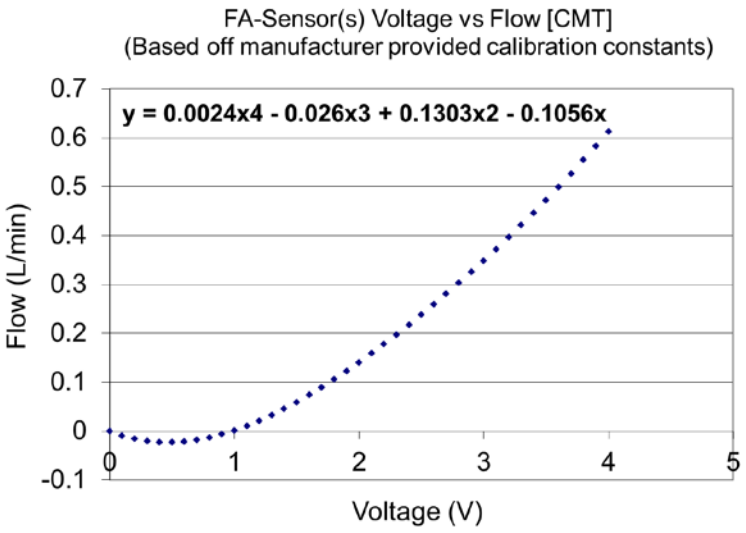

Figure F-1 Digital mass flow sensor calibration curve provided by Convergent.

In order to ensure the validity of the calibration curve, the flow rate from the mass flow sensor was compared with flow rate readings from rotameter. This test was done by putting the rotameter in series with two mass flow sensors and measuring the flow rate by both devices. Different flow rate levels were achieved by a flow regulator valve, placed between two mass

flow sensors (Figure F-2). The mass flow sensor on the vent side of the valve was named “vent” and the one on the vacuum side was named “vacuum”. The rotameter was placed on the vent side as it can only be used at ambient pressure. The voltage readings of the mass flow sensors were recorded by a DAQ system (NI 9205) and lab view software. The voltage readings were then converted to flow rate using the calibration curve in Figure F-1. Rotameter readings are done visually by reading the scale at which the rotameter glass ball is located at each flow rate. The corresponding flow rates for each scale were determined using the calibration curve provided by the manufacturer, Figure F-3. A small glass ball rotameter (17190) is used for low flow rates (maximum flow rate = 300 mL/min) and a large glass ball rotameter (37288) is used for higher flow rates (maximum flow rate = 14 L/min). The measurement range of the mass flow sensor is zero to one liter per minute.

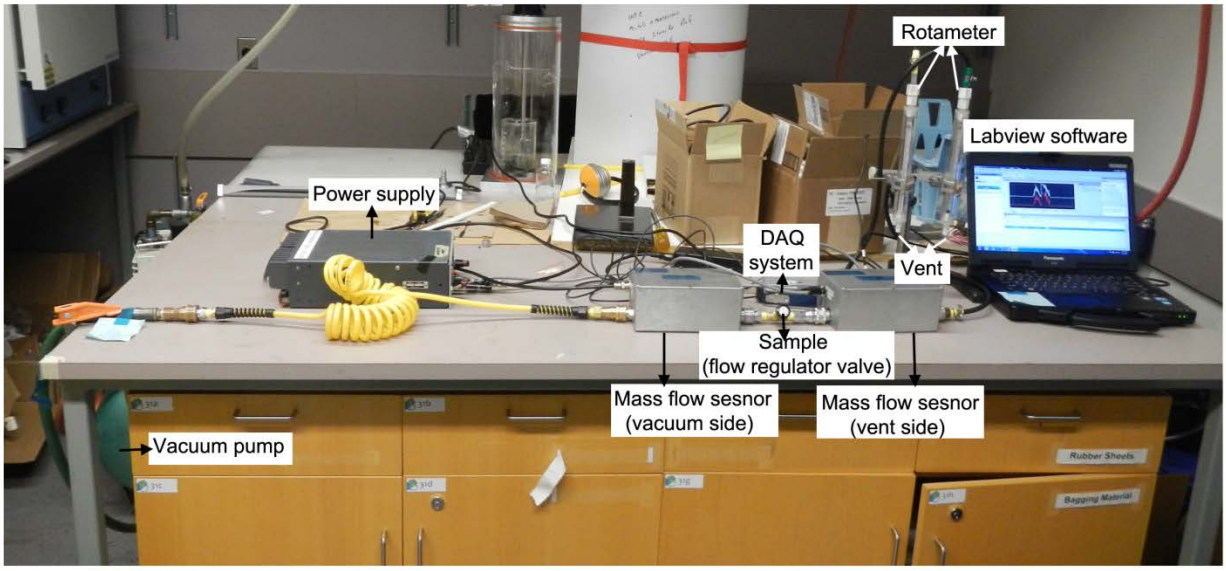

Figure F-2 Flow rate measurement set-up.

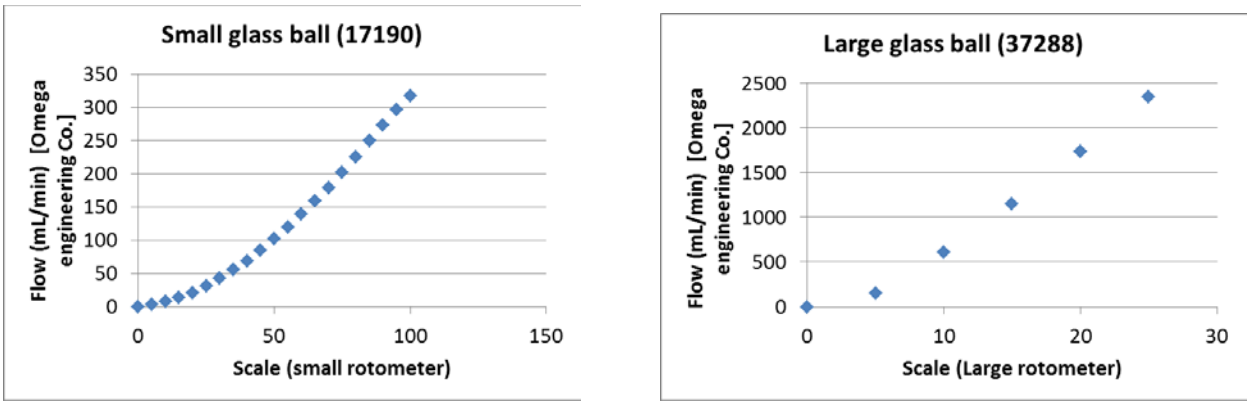

Figure F-3 Rotameter calibration curve (Omega engineering company).

The comparison of the flow rates from rotameter versus mass flow sensors are shown in Figure F-4. As mentioned earlier, in this test two mass flow sensors are used one on the vacuum side and the other on the vent side. The readings of these two sensors should be equal as they are mass flow sensor and thus their performance should not depend on pressure (vacuum vs. vent).

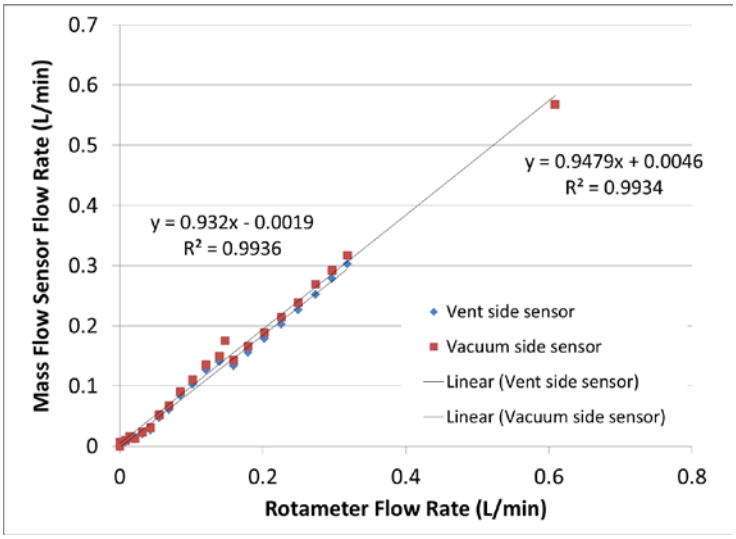

Figure F-4 Flow rate: mass flow sensor versus rotameter.

Figure F-4 shows that the flow rates obtained from the mass flow sensors are in close agreement with the rotameter, as the slope of the linear fit is close to one. Figure F-5 also shows close agreement between the flow rates recorded by mass flow sensors on vacuum and vent sides. In the current study the flow rate readings of the vent side sensor is used for calculation of permeability in all permeability measurement tests (laminate, consumables, in-plane and through thickness).

F.2 Mass Flow Sensor: Minimum Detectable Flow Rate

A minimum meaningful flow rate can be defined for the mass flow sensors. This is done by measuring the flow rate using the permeability test set-up with a "zero porosity cured laminate" and "closed valve" (flow regulator valve in Figure F-2) as samples. These two sample types are chosen because they are expected to give zero flow rates. The summary of these measurements are shown in Table F-1. The geometry of the cured samples is the same as the geometry of the laminates used in the permeability tests.

Table F-1 Mass flow sensor minimum flow readings

Sample	Test set-up/sample code	Q (mL/min)		
		Rotameter	Mass flow sensor (Vent) (mL/min)	
				average
Closed flow regulator valve	NA	0	1.139042	NA
Cured laminate	In-Plane Test			
	Test 1 (4/4/2013)	0	1.944765	1.797414
	Test 2 (28/3/2013)	0	2.002707	
	Test 3 (26/3/2013)	0	1.444769	
	Test 4 [74]	NA	2	
	Through-Thickness Test			
	Test 1 (12/3/2013)	0	6.652544	4.00543
	Test 2 (3/4/2013)	0	1.358316	
Release film (Teflon)	19/3/2013	0	6.514597	

Table F-1 shows that the minimum flow rates are slightly different based on the test set-up. It is about 2 mL/min for the in-plane set-up and 6 mL/min for the through thickness set-up. Based on these values flow rates lower than 6 mL/min are considered below the detectable limit of the mass flow sensors in this study. It is not known whether this minimum limit is due to device limitation or set-up issue, e.g. a micro leak. It has to be noted that even with the "closed valve", which is the simplest set-up without any tacky tape sealing involved; still a 1 mL/min flow is reported instead of zero flow. The rotameter reports no signal because of lack of sensitivity.

F.3 Summary

- The flow rate readings by mass flow sensors and rotameters are in agreement.
- The flow rate readings by mass flow sensors placed on the vacuum and vent sides are in agreement. In this study the flow readings on the vent side are used for permeability calculations.
- The minimum flow rate that can be detected by the mass flow sensor is approximately 6 mL/min. Flow rates lower than 6 mL/min are considered below the detectable limit of the mass flow sensors used in this study.

Appendix G Comparison of the Gas Removed during Debulk Test with the Expected Gas in the Laminate

In this section the mass of the gas removed during the long debulk test (see section 5.3.2.1) is compared with the amount of gas expected in the laminate. The mass of the gas in the as laid-up laminate is assumed to be equal to the mass of air residing in voids plus the mass of moisture and nitrogen dissolved in epoxy. The presence of other gases in resin is neglected as OOA resin systems are designed to have negligible volatile content [27]. The ideal gas law is used to calculate the mass of the air in the voids.

$$m_{air\ in\ voids} = \mathrm{n} \times \mathrm{M}_{air} \quad \text{(G-1)}$$

Where m (kg): mass of air, n (mol): number of air moles, M (Kg/mol): molar mass of air.

$$n = \frac{PV}{RT} \quad \text{(G-2)}$$

Where P (Pa): pressure, V (m^3): gas volume, R (J/Kmol): gas constant, T (K): temperature.

The initial volume of gas inside the voids is equal to void volume and can be calculated based on the porosity of an as-laid up laminate (section 5.3.1.2):

$$\mathrm{V} = \varphi_T \times \mathrm{V_L} \quad \text{(G-3)}$$

Where V (m^3): void volume, φ_T (%): total porosity, V_L (m^3): laminate volume.

Using equations G-1 to G-3 and input parameters in Table G-1 the mass of air in voids is estimated to be about 2.8×10^{-2} gr. The mass of dissolved moisture and nitrogen in the laminate is estimated based on the closest concentration data in the literature (C_{N2} and C_{H2O} in Table G-1). The total mass of gas in the as-laid up laminate is estimated to be about 4.9×10^{-2} gr (Table G-2).

The measured mass of the gas evacuated during debulk is about ten times greater than that estimated based on the initial mass of gas in laminate. This difference may be due to air entrapped in vacuum hoses, consumables etc.

Table G-1 Input parameters used in estimation of gas mass in an as laid-up laminate.

Volume of laminate (V_L) (m^3)	7.22×10^{-5}
Mass of laminate (m_L) (kg)	0.078
Porosity (φ) in as-laid up	0.33
Fiber volume fraction (V_F) [52]	0.54
Air molar mass (M_{air}) (kg/mol)	0.02897
Universal gas constant (R) (J/K.mol)	8.31446
Air density (ρ_{air}) (kg/m^3) (at T = 20 °C, P = 1 atm)	1.2
Nitrogen concentration in epoxy ($C_{N2\ in\ epoxy}$) (kg/m^3) (at T = 40 °C, P = 1 atm) [42]	0.0207
Moisture concentration in epoxy ($C_{H2O\ in\ laminate}$) (wt%) (at T = 21 °C, RH = 22%) [35]	0.027

Table G-2 Mass of gas in as laid-up laminate versus gas mass measured by flow sensor during long debulk.

Mass of gas (gr)	in as laid-up laminate (gr)	air in voids	2.8×10^{-2}
		N_2 in epoxy	6.87×10^{-4}
		moisture in laminate	2.10×10^{-2}
		total	4.90×10^{-2}
	measured by flow sensor during 10 hour debulk (gr)		$5.76\ 10^{-1}$

Appendix H Void Area Fraction Measurement: Effect of Surface Preparation and Image Acquisition Equipment

Void characterization via optical microscopy (OM) and area fraction measurement is a well-established method. However the required sample surface preparation for OM is laborious. In this study first porosity is measured with optical microscopy (see section 6.2.3) and then it is compared with porosity measured from images taken with a Nikon D100 camera from diamond saw cut cross-sections of the laminates.

H.1 Void Characterization Method

The laminates were cut with a diamond saw, using water coolant, along a line three centimeters from the laminate edge. Then the cross-sections were rinsed and dried. A Nikon D100 camera with 55-200 mm lens was used to take an image of the laminate cross-sections. The distance between sample cross-section and camera was 30 cm and the image was taken using a remote shutter (Figure H-1a).

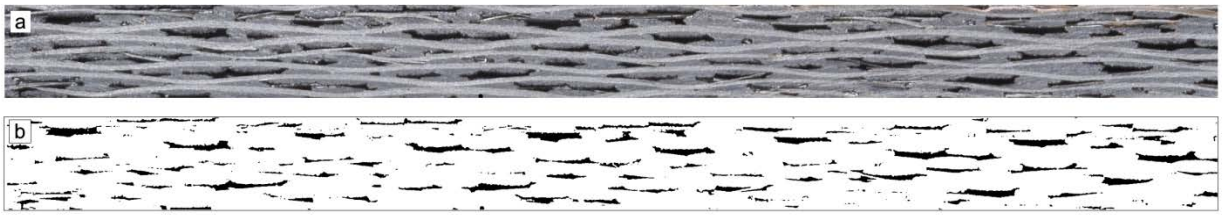

Figure H-1 Part of cross-section image (vent time = 0 hour), a) original image, b) binary image.

The Image J software was used for image analysis and area measurements. Three image analysis procedures listed in Table H-1 were used for creation of the binary image of each cross-section.

Different image analysis procedures were used to evaluate the sensitivity of the porosity results to image processing steps (contrast improvement, noise removal and threshold selection). The void area (black features in Figure H-1b) was measured using the "analyze particle" command.

Table H-1 Image analysis procedures used for creation of binary images using the Image J software.

Procedure #	Contrast	Noise Removal	Threshold
1	enhanced contrast	NA	50
2	sharpen & enhanced contrast	despeckle	48 - 52
3	enhanced contrast or manual contrast	NA	50 – 70

H.2 Results

The porosity results measured with Nikon camera are compared with optical microscopy measurements (see section 6.3.1) in Figure H-2a. Porosity measured from camera images is considerably lower than optical microscopy (up to 15%). Three different image analysis procedures, different contrast enhancement, noise removal and threshold selection, were used to evaluate their potential effect on camera porosity measurements. Porosity quantified by these three procedures are similar, and the large discrepancy between the optical microscopy and camera results are due to image capture, not image processing. The difference is likely due to the poorer surface preparation (diamond saw cut) and low magnification (3.5X vs. 50X) used in the camera method. The study shows that proper surface preparation and optical microscopy imaging is required for accurate porosity measurement.

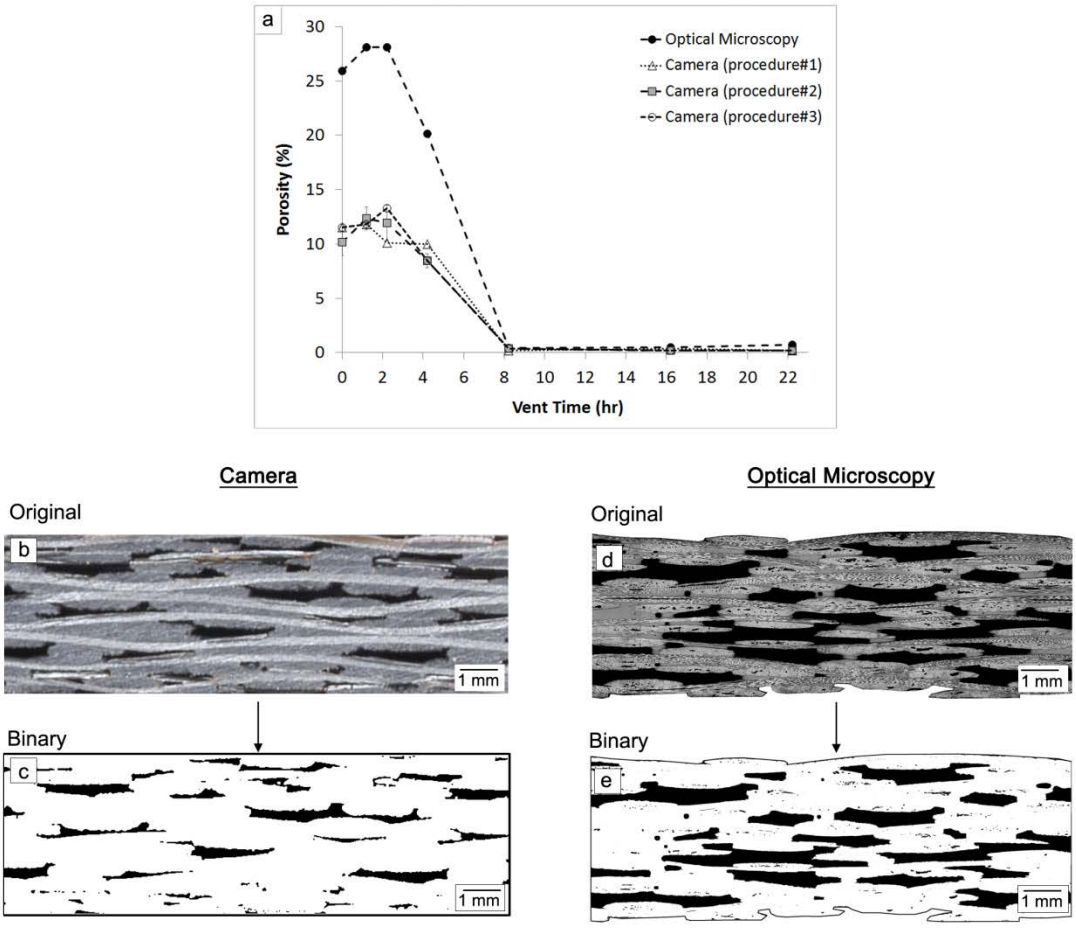

Figure H-2 a) Porosity from camera and OM images, b) original camera image, c) binary camera image, d) original OM image, e) binary OM image.

Appendix I Thickness Rebound of Un-cured and Partially Cured Laminates

As discussed in section 4.2.2, in order to determine the porosity of "partially cured" laminates throughout the cure process a series of laminates were made by stopping the cure cycle at different times during the process (Figure 4-2 a) and evaluating the void morphology and porosity at that time in the process. After stopping the cure cycle, the laminates were cooled down using a fan. Some rebounding with time occurred in the as-laid up and debulked samples. Thickness measurements suggest that rebound can increase porosity by a maximum of 5% in two months in these laminates (Figures I-1 and I-2). However, rebounding was negligible for partially cured laminates. The thickness of the laminates was measured with Calliper (details in section 4.2.5).

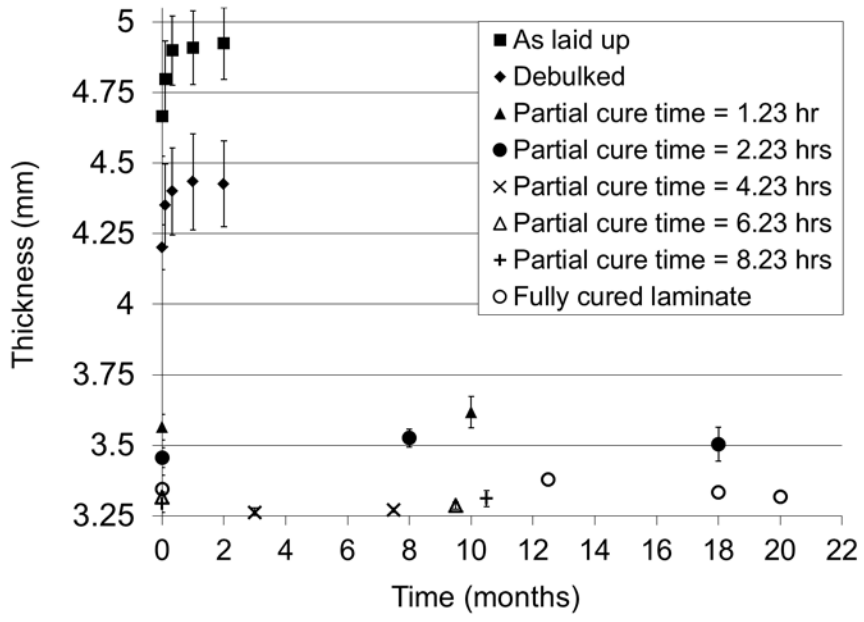

Figure I-1: Thickness rebound of uncured and partially cured laminates.

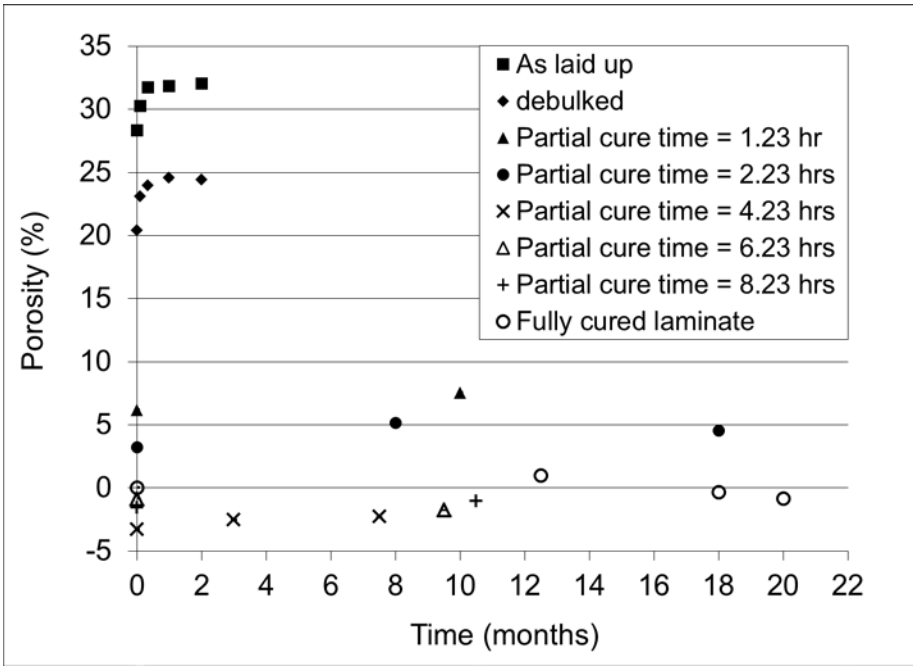

Figure I-2: Effect of thickness rebound of uncured and partially cured laminates on their porosity (porosity is estimated based on the thickness of the laminates (for calculation details refer to section 4.3.2)).